UNIVERSITY OF OKLAHOMA

GRADUATE COLLEGE

MOISTURE-INDUCED DAMAGE CHARACTERIZATION OF ASPHALT MIXES: A CHEMICAL, THERMODYNAMIC AND MECHANISTIC APPROACH

A DISSERTATION

SUBMITTED TO THE GRADUATE FACULTY

in partial fulfillment of the requirements for the

Degree of

DOCTOR OF PHILOSOPHY

By

SYED ASHIK ALI
Norman, Oklahoma
2021

MOISTURE-INDUCED DAMAGE CHARACTERIZATION OF ASPHALT MIXES:
A CHEMICAL, THERMODYNAMIC AND MECHANISTIC APPROACH

A DISSERTATION APPROVED FOR THE
SCHOOL OF CIVIL ENGINEERING AND ENVIRONMENTAL SCIENCE

BY THE COMMITTEE CONSISTING OF

Dr. Musharraf Zaman, Chair

Dr. Edgar A. O'Rear III

Dr. Gerald A. Miller

Dr. Kianoosh Hatami

Dr. Rouzbeh Ghabchi

Dedicated

to

My Mother, Wife and Daughter

Acknowledgements

At the beginning, I would like to express my gratitude to The Almighty God for His blessings in every step of my life. Then, I want to thank my parents, who have sacrificed their lives to fulfil my dreams. I am grateful to my wife, Syeda Abida Sultana, who was always beside me with her love, encouragement, support and prayers. Also, special thanks to my siblings for their significant support throughout my life.

I would like to express my deepest appreciation, sincere gratitude, and heartiest thanks to my advisor and chair of my dissertation committee, Dr. Musharraf Zaman, for his continued help, valuable guidance, constructive criticism, and active interest in my research work. His boundless energy, wide knowledge and effective mentorship shaped me into a researcher. Also, his direction and encouragement have been truly inspiring in my social, academic and professional endeavor.

I would like to acknowledge and thank Dr. Rouzbeh Ghabchi for his help in my research works in every way possible. Dr. Ghabchi was always there to help me in developing new ideas and to encourage me throughout my study. His valuable suggestions and comments helped improve my research work. Special thanks to Dr. Edgar O'Rear for serving in my committee and providing access to laboratory facilities that were crucial for the successful completion of this research work. I also want to express my sincere thanks to my other committee members, Dr. Gerald A. Miller and Dr. Kianoosh Hatami for offering their time and valuable input in completing this work.

I want to offer special thanks to Kenneth R. Hobson for his great help and cooperation throughout my research work. His assistance came in various forms: laboratory testing, interpreting results, and educating me on different aspects of asphalt

materials. I deeply appreciate his invaluable commitment to our research program. Also, I want to thank my friends and colleagues, Dr. Shivani Rani, Mohammed Ashiqur Rahman, Sagar Ghos, Matias Mendez, and Chris Sumter who helped me unselfishly throughout my research. I would like to express my sincere gratitude to all the staff of the School of Civil Engineering and Environmental Science and the Southern Plains Transportation Center (SPTC) for their help and support. I acknowledge and thank Richard Steger and Ingevity for their continuous support and assistance with laboratory works. Also, I am grateful to Dr. Keisha Walters and her research group for their help in conducting this research. The financial support provided by the Oklahoma Department of Transportation (ODOT), the Southern Plains Transportation Center (SPTC), and Accelerated Bridge Construction (ABC)-UTC at Florida International University are gratefully acknowledged. Thanks and appreciations are also extended to all the material suppliers for their help throughout this study.

Table of Contents

ACKNOWLEDGEMENTS ..... **V**
TABLE OF CONTENTS ..... **VII**
LIST OF TABLES ..... **IX**
LIST OF FIGURES ..... **XI**
ABSTRACT ..... **XIII**
CHAPTER 1. INTRODUCTION **1**
1.1 BACKGROUND 1
1.2 OBJECTIVES 4
1.3 OVERVIEW OF CURRENT LITERATURE 6
1.3.1 Theories Related to Moisture-induced Damage of Asphalt Pavements 6
1.3.2 Current Practices of Evaluating Moisture-induced Damage 7
1.3.3 Studies Related to Thermodynamic Approach 11
1.3.4 Effect of Chemical Compositions of Asphalt Binder and Aggregate on Moisture-induced Damage 14
1.3.5 Effect of Different Additives on the Moisture-induced Damage 17
1.4 SCOPE, ASSUMPTIONS AND LIMITATIONS OF THE CURRENT STUDY 20
1.5 DISSERTATION FORMAT AND CONTENT 22
CHAPTER 2. EFFECTS OF SURFACE FREE ENERGY ESTIMATION METHODS AND PROBE LIQUIDS ON THE MOISTURE-INDUCED DAMAGE POTENTIAL OF ASPHALT MIXES **24**
2.1 INTRODUCTION 25
2.2 OBJECTIVES 33
2.3 MATERIALS AND METHODS 34
2.4 RESULTS AND DISCUSSION 36
2.4.1 Contact Angles of Binders 36
2.4.2 Surface Free Energy of Binders 37
2.4.3 Comparison of Surface Free Energy Estimation Methods 49
2.5 CONCLUSIONS 50
CHAPTER 3. MICRO-STRUCTURAL EVALUATION OF THE EFFECTS OF AGGREGATE TYPE, AGING AND ADDITIVES ON THE MOISTURE SUSCEPTIBILITY OF BINDER-AGGREGATE SYSTEMS USING CHEMICAL AND THERMODYNAMIC APPROACHES **61**
3.1 INTRODUCTION 62
3.1.1 Effect of Aging 65
3.1.2 Effect of Additives and Modifiers 66
3.1.3 Surface Free Energy Technique 68
3.2 OBJECTIVES 70
3.3 MATERIALS AND METHODOLOGIES 71
3.3.1 Materials 71
3.3.2 Methods 73
3.4 RESULTS AND DISCUSSIONS 77
3.4.1 Asphalt Binder Test Results 77

3.4.2 Aggregate Test Results 87
3.4.3 Moisture-induced Damage Potential of Binder-Aggregate Systems 89
3.5 CONCLUSIONS 96
CHAPTER 4. EFFECT OF ADDITIVES AND AGING ON MOISTURE-INDUCED DAMAGE POTENTIAL OF ASPHALT MIXES USING SURFACE FREE ENERGY AND LABORATORY-BASED PERFORMANCE TESTS 110
4.1 INTRODUCTION 111
4.2 OBJECTIVES 115
4.3 THERMODYNAMIC APPROACH OF EVALUATING MOISTURE-INDUCED DAMAGE 116
4.4 MATERIALS AND METHODS 119
4.4.1 Materials 119
4.4.2 Test Methods 122
4.5 RESULTS AND DISCUSSIONS 127
4.5.1 Surface Free Energy Components of Binder Blends 127
4.5.2 Surface Free Energy Components of Aggregates 129
4.5.3 Energy Parameters from SFE Method 129
4.5.4 Indirect Tensile Strength Test 132
4.5.5 Illinois Semi-Circular Bend Test 133
4.5.6 Comparison of Moisture-induced Damage Parameters 134
4.6 CONCLUSIONS 135
CHAPTER 5. LABORATORY CHARACTERIZATION OF MOISTURE-INDUCED DAMAGE POTENTIAL OF ASPHALT MIXES USING CONVENTIONAL AND UNCONVENTIONAL PERFORMANCE-BASED TESTS 145
5.1 INTRODUCTION 146
5.2 OBJECTIVES 152
5.3 MATERIALS AND METHODS 153
5.3.1 Materials 153
5.3.2 Sample Preparation 154
5.3.3 Moisture Conditioning of Compacted Samples 154
5.3.4 Test Methods 155
5.4 RESULTS AND DISCUSSIONS 159
5.4.1 HWT Results 159
5.4.2 Indirect Tensile Strength (ITS) Test 162
5.4.3 Louisiana Semi-Circular Bend (LA-SCB) Test 164
5.4.4 Surface Free Energy Method 165
5.4.5 Comparison of Different Parameters 168
5.5 CONCLUSIONS 170
CHAPTER 6. CONCLUSIONS AND RECOMMENDATIONS 180
6.1 CONCLUSIONS 180
6.2 RECOMMENDATIONS 184
REFERENCES 186

List of Tables

Table 2.1 Surface Free Energy Components of the Probe Liquids at 20°C (Hefer et al., 2006) 52
Table 2.2 Contact Angles of Binders with Different Probe Liquids 52
Table 2.3 Surface Free Energy Components of S1 and S4 Binders from GvOC Method 52
Table 2.4 Condition Number of Different Probe Liquid Sets 53
Table 2.5 Surface Free Energy Components of Limestone aggregate 53
Table 2.6 Energy Parameters of Binder-Aggregate Systems from GvOC Methods 53
Table 2.7 Surface Free Energy Components of S1 and S4 Binders from Owens-Wendt Method 54
Table 2.8 Energy Parameters of Binder-Aggregate Systems from Owens-Wendt Method 55
Table 2.9 Surface Free Energy Components of S1 and S4 Binders from Wu Method 56
Table 2.10 Energy Parameters of Binder-Aggregate Systems from Wu Method 57
Table 2.11 Surface Free Energy of Binders using Neumann Method 57
Table 2.12 Differences in Measured and Predicted Contact Angles from Neumann Method 57
Table 2.13 Energy Ratios of Binder-Aggregate Systems from Neumann Method 58
Table 2.14 %Difference in Γ_A SFE component with Respect to Neumann's Method 58
Table 2.15 Susceptibility to Moisture-Induced Damage by Different SFE Method (Least = 1, Most = 4) 58
Table 3.1 Elemental compositions of PG 64-22 and PG 76-28 binder blends from XRF tests 99
Table 3.2 Contact angles of PG 64-22 and PG 76-28 binder blends with probe liquids 99
Table 3.3 SFE components of PG 64-22 and PG 76-28 binder blends at different aging conditions 100

Table 3.4 Mineralogical composition of aggregates from XRF test.....101
Table 3.5 Surface free energy components of different aggregates from USD test 101
Table 3.6 The W_{AR} and W^{wet}_{ARW} of PG 64-22 and PG 76-28 binder blends with different aggregates 102
Table 3.7 Energy ratios (ER_1 and ER_2) of PG 64-22 and PG 76-28 binder blends with different aggregates 103
Table 4.1 Contact Angles of the Binder Blends with Different Solvents 137
Table 4.2 SFE Components of the Binder Blends and Aggregate.....137
Table 5.1 Test Matrix for Laboratory Performance Tests on Asphalt Mixes.....173
Table 5.2 Different Parameters Obtained from HWT Test.....173
Table 5.3 Ranking of Asphalt Mixes based on Different Laboratory-based Performance Parameters 174

List of Figures

Figure 2.1 Contact angle measurement using DWP test: (a) asphalt binder used for testing; (b) binder coated glass plates; and (c) DWP test setup.....59
Figure 2.2 The ΓL versus $\Gamma Lcos\theta$ plot for WGFDE probe liquid set.....59
Figure 2.3 The ΓL versus $\Gamma Lcos\theta$ plot of binders using Neumann model.....60
Figure 3.1 Work-flow diagram for the study.....104
Figure 3.2 Setup for (a) DWP test on binder coated glass plates, (b) FTIR test on binder, and (c) USD test on aggregate.....104
Figure 3.3 FTIR Spectra of unaged PG 64-22 and PG 76-28 binders.....105
Figure 3.4 FTIR Spectra for PG 64-22 and PG 76-28 binders with WMA additives at different aging conditions.....105
Figure 3.5 FTIR Spectra for PG 64-22 and PG 76-28 binders with ASA additives at different aging conditions.....106
Figure 3.6 FTIR Spectra for PG 64-22 and PG 76-28 binders with 20% RAP binder at different aging conditions.....106
Figure 3.7 FTIR Spectra for PG 64-22 binder with 1.5% PPA at different aging conditions.....107
Figure 3.8 I_{CO} based on peak heights at 1695 and 1740 cm^{-1} for (a) PG 64-22 and (b) PG 76-28 binders.....108
Figure 3.9 I_{SO} based on peak height at 1030 cm^{-1} for (a) PG 64-22 and (b) PG 76-28 binders.....109
Figure 4.1 Work-flow diagram for the present study.....138
Figure 4.2 Gradation curve for the mixes.....138
Figure 4.3 The (a) $S_{A/S}$, (b) $W_{A/S}$ and (c) W^{wet}_{ASW} of RTFO-aged PG 64-22 binder containing different additives with rhyolite aggregate.....139
Figure 4.4 The (a) $S_{A/S}$, (b) $W_{A/S}$ and (c) W^{wet}_{ASW} of PAV-aged PG 64-22 binder containing different additives with rhyolite aggregate.....140
Figure 4.5 The ER_1 and ER_2 of (a) RTFO-aged and (b) PAV-aged PG 64-22 containing different additives with rhyolite aggregate.....141

Figure 4.6 (a) Indirect tensile strength (*ITS*) and (b) tensile strength ratio (*TSR*) of the tested asphalt mixes 142
Figure 4.7 (a) Fracture energy (G_f) and (b) fracture energy ratio (G_f *ratio*) of tested asphalt mixes 143
Figure 4.8 Comparison of moisture-induced damage parameters: (a) *TSR* vs. ER_1 and (b) G_f *ratio* vs. ER_1 144
Figure 5.1 Workflow diagram for the study 174
Figure 5.2 Rut depths vs. wheel passes from HWT test 175
Figure 5.3 (a) Indirect tensile strength (ITS_{dry} and ITS_{wet}) and *TSR* values; (b) toughness index (TI_{dry} and TI_{wet}) and *TI ratios* of asphalt mixes from ITS test 176
Figure 5.4 $J_{c\text{-}dry}$ and $J_{c\text{-}MIST}$ values and J_c *ratio* of asphalt mixes from LA-SCB test 177
Figure 5.5 Work of adhesion (W_{AS}), work of debonding ($WASWwet$) and energy ratio (ER_1) of binder blends with rhyolite aggregate 178
Figure 5.6 Comparison of different laboratory performance parameters with SFE parameter; (a) *SIP vs* ER_1, (b) LC_{SN} *vs* ER_1; (c)*TSR vs* ER_1; (d) *TI ratio vs* ER_1 and (e) J_c *ratio vs* ER_1 179

Abstract

Moisture-induced damage is one of the major distresses which leads to the deterioration of mechanical properties of asphalt mixes and failure of asphalt pavements. Evaluation of the moisture-induced damage potential is a challenging task because a number of factors including physical and chemical properties of aggregates and binders, aging, additives/polymers and other environmental and traffic conditions can significantly influence the adhesion and/or cohesion mechanisms of an asphalt mix. Previous studies have reported inadequacies of the current moisture-induced damage evaluation methods on their ability to address mechanisms that lead to failure of asphalt pavements. There is a need to identify relatively simple, reliable, and mechanistic methods for evaluating moisture-induced damage potential of asphalt mixes.

In this study, mechanistic approaches based on the thermodynamic theory, chemical characterization and laboratory-based performance tests were used to investigate the effects of different factors on the moisture-induced damage potential of asphalt mixes. Specifically, the thermodynamic theory using surface free energy (SFE) of constituent materials was used to mechanistically quantify the bonding strength of binder-aggregate systems. Attempts were made to study the effect of probe liquid sets and different SFE estimation methods on the calculation of moisture-induced damage of binder-aggregate systems. Suitable probe liquid sets to produce accurate and consistent energy parameters for binder-aggregate systems were identified. The changes in the bonding characteristics of an unmodified PG 64-22 and a polymer-modified PG 76-28 binders with the addition of different additives, namely warm mix asphalt (WMA) additive, anti-stripping agent (ASA), polyphosphoric acid (PPA) and reclaimed asphalt

pavement (RAP) were determined using the SFE method. Also, the compatibility of these binders with commonly available aggregates under different aging conditions was investigated. Fourier transform infrared (FTIR) spectroscopy and X-ray fluorescence (XRF) tests were conducted on the binders to examine the effects of chemical compositions on the moisture-induced damage potential of asphalt mixes. The elemental compositions of aggregates were determined using the XRF results. Asphalt mixes containing different additives were produced in the laboratory for the evaluation of moisture-induced damage using Hamburg wheel tracking (HWT), indirect tensile strength (ITS) and two different semi-circular bend (SCB) tests, namely Louisiana SCB (LA-SCB) and Illinois SCB (IL-SCB) tests. Correlations between different laboratory-based moisture-induced damage parameters and the SFE parameters were investigated. The results of the SFE parameters and chemical analyses indicated that the properties of aggregates have significantly higher influence on the moisture-induced damage potential of a mix than the properties of binder. Also, asphalt mixes, in general, were found to become more prone to moisture-induced damage with in-service aging. The presence of amine group in both WMA and ASA was found to reduce the moisture susceptibility of asphalt mixes. However, the modification of binder with PPA is expected to increase the moisture-induced damage potential of a mix. Unconventional laboratory-based parameters from conventional tests, namely stripping number (LC_{SN}) from HWT test and toughness index ratio (*TI ratio)* from ITS test exhibited potential to adequately characterize mixes for moisture-induced damage. Also, SCB test-based parameters, namely J-integral ratio (J_c *ratio*) from LA-SCB and fracture energy ratio (G_f

ratio) from Illinois-SCB showed promises for use as alternate moisture-induced damage parameters for asphalt mixes.

CHAPTER

1

INTRODUCTION

1.1 BACKGROUND

The loss of strength and durability of asphalt mixes in presence of moisture is defined as the moisture-induced damage of asphalt pavement (Harvey and Lu, 2005; Masad et al., 2006; Bhasin et al., 2007b). The moisture-induced damage phenomena for asphalt pavements was first recognized in the early 1930s. One of the earlier efforts to evaluate moisture-induced damage was reported in the late 1960s through visual inspection (Caro et al., 2008a; Abuawad et al., 2015). Although, moisture-induced damage is not a failure mode by itself, it can lead to other distresses such as rutting and cracking, particle degradation and disintegration, potholes, and shoving (Wasiuddin et al., 2007c; Caro et al., 2008b). A large portion of the state's pavement maintenance cost and vehicle user cost is directly related to the pavement damage related to moisture-induced damage (Caro et al., 2008a).

Evaluation of moisture-induced damage is a challenging task for transportation agencies (Wasiuddin et al., 2007c; Abuawad et al., 2015). This phenomenon starts with the transport of moisture into the pavement which subsequently leads to pavement deterioration (Wasiuddin et al., 2007c; Caro et al., 2008b). Typically, two types of failure can be associated with moisture intrusion in asphalt pavements: adhesive failure between binder and aggregate, and cohesive failure within the binder (Bhasin, 2007; Copeland et al., 2007; Wasiuddin et al., 2007c; Ghabchi, 2014). Therefore, the

evaluation of the bond strength between binder and aggregate is necessary to access moisture-induced damage potential of a mix (Harvey and Lu, 2005; Masad et al., 2006).

Several empirical test methods have been developed over the past few decades to evaluate moisture-induced damage potential of asphalt mixes (Kanitpong and Bahia, 2005; Caro et al., 2008a; Caro et al., 2008b). Researchers have used indirect tensile strength ratio (TSR), resilient modulus ratio, Marshall stability ratio, stripping inflection point (SIP) from Hamburg wheel tracking (HWT) test and fracture energy ratio for evaluating the moisture-induced damage potential of asphalt mixes (Bagampadde et al., 2006; Gorkem and Sengoz, 2009; Ghabchi et al., 2015; Mirzababaei, 2016). However, none of these test methods appeared to address the failure mechanisms governing the moisture-induced damage of asphalt pavements nor do these tests correlate well with field performance (Caro et al., 2008b). Also, there is no general agreement on a single test method among the state DOTs and the asphalt industry for evaluating moisture-induced damage. Recently, many DOTs are considering adopting a fatigue evaluation procedure using semi-circular bend (SCB) geometry in mix evaluation process (Kim et al., 2012; Al-Qadi et al., 2015; Mohammad et al., 2016; Ozer et al., 2016a; Ozer et al., 2016b). As the fatigue damage and healing in asphalt mixes are directly related to the cohesive and adhesive bonding of the binder-aggregate system, the incorporation of fracture mechanics through SCB test can better explain the mechanisms responsible for the moisture-induced damage phenomenon.

The thermodynamic adhesion theory has been successfully used by a number of studies to quantify the adhesive strength of a binder-aggregate system (Bhasin and Little, 2006; Bhasin et al., 2006; Hefer et al., 2006; Bhasin, 2007; Bhasin et al., 2007a;

Bhasin et al., 2007b; Wasiuddin et al., 2007c; Wasiuddin et al., 2008; Buddhala et al., 2011; Ghabchi et al., 2013; Esmaeili et al., 2019; Hossain et al., 2019). The thermodynamic quantities such as surface free energies of binder and aggregates were used to identify the compatible binder-aggregate combinations to reduce the potential of moisture-induced damage (Bhasin et al., 2006; Wasiuddin et al., 2007c; Moghadas Nejad et al., 2012; Arabani and Hamedi, 2014). A number of SFE estimation methods proposed by Fowkes (1964), Owens and Wendt (1969), Wu (Wu, 1971; Wu, 1973), Van Oss et al. (1988) and Neumann (Neumann et al., 1974; Li and Neumann, 1990; Li and Neumann, 1992) are currently available to calculate the SFE of a solid from contact angle measurements. However, differences in assumptions and mathematical formulations used by these methods are expected to influence the calculated values of the SFE. Also, the selection of probe liquids can affect the calculated SFE values of the binders which subsequently result in inaccuracies in bond energy calculations.

Previous studies have reported several factors that can influence the moisture-induced damage potential of asphalt mixes (Shu et al., 2012; Doyle and Howard, 2013; Tong et al., 2015). Among those, the physical and chemical characteristics of the binder and aggregate have been found to exhibit significant influence on the adhesive bond strength of asphalt mixes (Shu et al., 2012; Doyle and Howard, 2013; Tong et al., 2015). Also, with increasing use of different chemical additives and materials such as warm mix asphalt (WMA) additives, poly-phosphoric acid (PPA), anti-stripping agents (ASA) and reclaimed asphalt pavement (RAP) in asphalt mixes, the mechanistic evaluation of the moisture-induced damage potential becomes even more important. The interactions of the binder constituents and additives were found important in

determining the strength of the binder-aggregate interface (Hossain et al., 2012). The effectiveness of these additives under in-service aging conditions and with different aggregate types needs to be evaluated as well. Therefore, in addition to laboratory-based performance test and thermodynamic approaches, chemical interactions at the binder-aggregate interface need to be studied to better understand the moisture-induced damage phenomena of asphalt mixes. Several chemical analysis techniques are currently available that can provide important and useful information about the chemical properties of asphalt binder and aggregates in a relatively short period of time (Le Guern et al., 2010; Hossain et al., 2012; Hesp and Shurvell, 2013; Hofko et al., 2018; Ge et al., 2019).

1.2 OBJECTIVES

In this study, the effects of additives (WMA, ASA, RAP and PPA), aggregate types and aging (unaged, short-term and long-term) on the moisture-induced damage potential of asphalt mixes were studied by using the thermodynamic approaches, chemical analyses and laboratory-based performance tests. Attempts were made to identify suitable probe liquid sets for different SFE estimation methods. Compatible binder-aggregate combinations to obtain optimum resistance to moisture-induced damage were identified using the SFE technique and chemical analyses. The effect of the addition of different additives on the moisture-induced damage potential of asphalt mixes were investigated using conventional and unconventional laboratory-based performance parameters. Also, the moisture-induced damage parameters from different methods were compared to better understand the evaluation mechanisms used by the corresponding test methods. The overall objectives of this study are listed below:

i. To identify suitable probe liquid sets to obtain consistent energy parameters for different SFE estimation methods.

ii. To investigate the differences between different SFE estimation methods by comparing energy parameters of binder-aggregate systems.

iii. To evaluate the effects of different additives, namely WMA, ASA, RAP binder and PPA on the SFE components of commonly used unmodified and polymer-modified asphalt binders in Oklahoma. Also, evaluate the effect of aging on the moisture-induced damage potential of binder-aggregate system using the SFE method.

iv. To assess the effect of additives and aging on the chemical composition of binders using chemical analysis tools, namely XRF and FTIR spectroscopy. Also, determine the effects of the changes in chemical composition of binders on the moisture-induced damage potential binder-aggregate systems.

v. To investigate the contributions of the SFE components and elemental compositions of aggregates on the moisture susceptibility of a binder-aggregate system.

vi. To assess the effects of aging and additives on the moisture-induced damage potential of asphalt mixes using laboratory-based performance tests.

vii. To evaluate and compare the conventional and unconventional methods for analysis of HWT, ITS and SCB test results for characterizing moisture-induced damage potential of asphalt mixes And, to investigate the differences in mechanisms used to address moisture-induced damage by these laboratory-based parameters.

viii. To determine relationships between different laboratory-based moisture-induced damage parameters and the SFE parameters.

1.3 OVERVIEW OF CURRENT LITERATURE

1.3.1 Theories Related to Moisture-induced Damage of Asphalt Pavements

The deterioration of mechanical properties of asphalt mixes in presence of moisture is known as moisture-induced damage (Caro et al., 2008a). According to Caro et al. (2008a), moisture-induced damage is a two-step mechanism. First, the moisture (in liquid or vapor state) infiltrates into the binder-aggregate interface. Then the system responds to the infiltrated moisture either as adhesive and/or cohesive failures. Previous studies have reported three primary ways of transporting moisture into asphalt pavement, namely infiltration of surface water, capillary action of subsurface water and permeation or diffusion of water vapor (Masad et al., 2007; Caro et al., 2008a). Till now, five different adhesion theories have been proposed by different studies to quantify the bonding strength of a binder-aggregate system. These theories are: weak boundary layer theory, electrostatic theory, chemical bonding theory, mechanical bonding theory, and thermodynamic theory (Hefer et al., 2005; Caro et al., 2008a). The details of these theories can be found in literature (Hefer et al., 2005; Caro et al., 2008a; Guo et al., 2020). Adhesive failure in weak boundary layer theory is assumed to be associated with the presence of an interface of low cohesive strength. The presence of dust in the aggregate surface and/or dissolution of surface complexes in the presence of water are assumed to be responsible for the formation of this weak interface layer. According to the electrostatic theory, the presence of a liquid medium can result in the formation of an electric double layer at the interface. The interactions between

aggregate surface and the liquid media with dissolved ions were reported to be important to explain moisture-induced damage. According to this theory, the adhesive strength of an asphalt mix can be calculated using the coulombic forces at the binder and aggregate interface. The chemical bonding theory assumes that chemical reactions take place between alkalinity components in aggregate and carboxylic acid components in asphalt binder. The adhesive bonding can be quantified by considering these chemical reactions at the binder-aggregate interface. The mechanical bonding theory assumes that the asphalt binder will penetrate into the cavities, pores and asperities of the surface of the aggregate, resulting in a physical interlock between asphalt binder and aggregate. Aggregates with a rough and porous surface are expected to be more suitable for good interlock. According to Caro et al. (2008a), all these theories should be considered during modelling and characterizing moisture-induced damage of asphalt mixes. However, the thermodynamic theory using the surface free energy concept was reported to have the potential to quantify the adhesion of a binder-aggregate system (Bhasin et al., 2007b; Caro et al., 2008a).

1.3.2 Current Practices of Evaluating Moisture-induced Damage

Moisture-induced damage is a complex phenomenon and its evaluation is a challenging task for the transportation agencies (Abuawad et al., 2015). Several test methods have been developed by different researchers to evaluate the moisture-induced damage potential of asphalt mixes (Caro et al., 2008a; Caro et al., 2008b). However, inability to simulate field condition, dependency on moisture conditioning process, and poor correlations with field performance raise concerns about these methods (Caro et al., 2008b; Abuawad et al., 2015). Caro et al. (2008b) divided the moisture-induced

damage evaluation methods into three classes, namely subjective quantification, quantification using performance index, and ratio of a parameter for dry and moisture-conditioned specimens. Most state DOTs primarily use parametric ratio-based test methods to characterize moisture-induced damage of asphalt mixes. Laboratory-based moisture conditioning process is an inherent part of this type of testing to simulate the environment and moisture effect similar to that in the field.

Among all the moisture-induced damage evaluation methods, the tensile strength ratio (TSR) test using the AASHTO T 283 and HWT test under submerged condition are the most commonly used by the state DOTs (Abuawad et al., 2015). The TSR of an asphalt mix is calculated by comparing the average tensile strength of dry specimens to that of moisture-conditioned specimens from an indirect tensile strength (ITS) test. In this method (AASHTO T 283 test method), single freeze-thaw cycle is used for the moisture conditioning of asphalt specimens. For this purpose, a compacted asphalt mix specimen is first saturated with water with the level of saturation between 70% to 80%. The specimen is then kept at -18 °C for 16 hours followed by a thawing cycle by keeping it at 60 °C for 24 hours to simulate moisture conditioning. Generally, an asphalt mix with a TSR of 0.8 or above is expected to exhibit good moisture-induced damage resistance in the field.

Stripping inflection point (SIP) from HWT test is also commonly used for evaluating moisture-induced damage (Yin et al., 2014). The SIP represents the number of wheel passes on the rutting curve after which a significant increase in rut depth occurs due to the presence of water. A higher value of SIP for a mix corresponds to a lower moisture-induced damage potential and vice versa.

Previous studies have reported a number of other test procedures for evaluating moisture-induced damage of asphalt mixes (Gorkem and Sengoz, 2009; Liu et al., 2014; Tarefder and Ahmad, 2014; LaCroix et al., 2016). For example, the Nicholson stripping test and the modified Lottman test were used by Gorkem and Sengoz (2009) to evaluate the effect of the addition of hydrated lime and polymers on the moisture-induced damage potential of loose and compacted asphalt mixes, respectively. Liu et al. (2014) used the static immersion test, rolling bottle test, boiling water test, total water immersion test, and the ultrasonic method to evaluate the moisture-induced damage potential of aggregates and binders. The rolling bottle test and the boiling water test were observed to be the most sensitive to moisture-induced damage among the test methods. The AASHTO T 283 (AASHTO, 2014a), resilient modulus ratio, Marshall stability ratio, fracture energy ratio and boiling water test were used by Mirzababaei (2016) to determine the effect of zycotherm® on the moisture-induced damage potential of asphalt mixes. In addition to test methods, previous studies have attempted to develop moisture-conditioning processes that would represent field condition. For example, Tarefder and Ahmad (2014) evaluated the moisture-induced damage potential of asphalt mixes using two different moisture conditioning processes, namely, moisture-induced sensitivity testing (MIST) and AASHTO T 283 (AASHTO, 2014a) method. Effects of these two processes on the permeability of asphalt mixes were determined. The TSR from the AASHTO T 283 (AASHTO, 2014a) method reduced with an increase in permeability, whereas the TSR from MIST conditioning were found to be unaffected by permeability. According to LaCroix et al. (2016) the current AASHTO T 283 (AASHTO, 2014a) method affects the adhesive strength, whereas the MIST affects

the cohesive strength of a binder-aggregate system. LaCroix et al. (2016) suggested to combine both of these conditioning processes to ensure the evaluation of both adhesion and cohesion mechanisms of moisture-induced damage. A study conducted by Vargas-Nordcbeck et al. (2016) suggested to increase the number of conditioning cycles used in the AASHTO T 283 (AASHTO, 2014a) procedure to accurately simulate field performance.

Until now, no general agreement on a single test and moisture conditioning process exists among the state DOTs and asphalt industries for evaluating moisture-induced damage. Therefore, there is a need to develop efficient tools to assess compatibility between aggregates and binders that would help resist moisture-induced damage (Bhasin, 2007; Caro et al., 2008b).

A number of studies have used semi-circular bend (SCB) geometry to characterize fatigue and low temperature fracture resistance of asphalt mixes (Kim et al. 2012, Li and Marasteanu 2010, Mull et al. 2002, Ozer et al. 2016, Saeidi and Aghayan 2016, Wu et al. 2005, Mohammad et al. 2016). The SCB test is a reliable and relatively simple test method for assessment of cracking performance of asphalt mixes. Recently, two SCB test methods are gaining popularity among the transportation agencies. Louisiana Department of Transportation and Development has developed a version of the SCB test (LA-SCB), which uses the critical energy release rate or J-integral (J_c) to characterize cracking potential of mixes (Cooper Jr et al., 2016). The Illinois SCB (IL-SCB), developed by Al-Qadi et al. (2015), uses flexibility index (*FI*) and fracture energy (G_f) to characterize the fracture properties of asphalt mixes. Evaluation of

fracture properties through SCB test is expected to help understand the moisture-induced damage phenomena of an asphalt mix.

1.3.3 Studies Related to Thermodynamic Approach

Thermodynamic approach using surface free energy is widely used to define adhesion between two materials (Hefer et al., 2005). According to this concept, the physio-chemical adhesion between two materials is a function of the surface free energies of those materials. Generally, molecules in bulk of a material are surrounded by other molecules, whereas molecules at the surface has fewer attractive molecular interactions. Therefore, work needs to be done to bring molecules from the bulk to surface, i.e., to create a new surface. The surface free energy (SFE) of a material is generally defined as the work required to increase the surface of a material by a unit area under vacuum (Van Oss et al., 1988). Several methods are currently available to estimate SFE of a solid surface from contact angle measurements. These methods generally fall under the following two categories: component-based approach and equation of state approach. Fowkes (1964), Owens and Wendt (1969), Wu (Wu, 1971; Wu, 1973) and Van Oss et al. (1988) developed the SFE estimation methods using the component-based approach. The calculated values of the SFE using these component-based approaches rely on the selection of probe liquid set. Instead of using the component-based approach, Neumann and his colleagues (Neumann et al., 1974; Li and Neumann, 1990; Li and Neumann, 1992) used the equation of state approach to calculate the SFE of a material. The dependency of the SFE on probe liquid set can be eliminated using this approach. The SFE of a material was reported to vary due to the difference in mathematical relations between contact angles and SFE, used in each

estimation method (Della Volpe and Siboni, 2000; Żenkiewicz, 2006; Żenkiewicz, 2007; Rudawska and Jacniacka, 2018). Also, for component-based approaches, identification of suitable probe liquid sets is necessary to obtain accurate and consistent energy parameters. Among these estimation methods, the three component-based (acid, base and Lifshitz-van der Waals component) adhesion model by Van Oss et al. (1988), known as Good-van Oss-Choudhury (GvOC) theory, has been commonly used by the researchers to quantify the adhesion and debonding of binder-aggregate system in presence of moisture (Bhasin et al., 2006; Hefer et al., 2006; Bhasin et al., 2007a; Wasiuddin et al., 2007a; Wasiuddin et al., 2007c; Arabani et al., 2011; Buddhala et al., 2011; Alvarez et al., 2012b; Moghadas Nejad et al., 2012; Ghabchi et al., 2013; Ghabchi et al., 2014).

Bhasin et al. (2006) evaluated the moisture-induced damage potential of 16 field mixes from different states using the SFE method. The results from the SFE method was compared with the results of the mechanical testing on the field cores and laboratory produced mixes. The bond energy calculations from the SFE measurements were effective to identify compatible binder-aggregate pairs. In a related study, Bhasin et al. (2007a) investigated the effect of different types of modifications on the SFE components of the binder as well as moisture-induced damage potential of asphalt mixes. In a different study, the effect of the aggregates on the moisture susceptibility of asphalt mixes were investigated by Bhasin and Little (2007) using the SFE method. The basic component of the aggregate was reported to be the primary contributor to adhesion bond with any given binder.

The effect of antistripping additives on the SFE components of binders was investigated by Wasiuddin et al. (2007c). A chemical model was proposed to explain the changes in SFE components with the addition of antistrip additives. In a related study, Wasiuddin et al. (2007b) evaluated the effect of aging on the SFE components of binders modified with antistripping agent. In another study, Wasiuddin et al. (2008) evaluated the influence of warm mix asphalt additives on the moisture-induced damage potential of binders using thermodynamic principles.

Using the SFE method, Arabani and Hamedi (2010) evaluated the effectiveness of polyethylene polymer coating on the surface of aggregate to reduce moisture-induced damage potential of asphalt mixes. The contribution of liquid antistrip additives on the adhesive bond strength of a binder-aggregate system was quantified by Arabani and Hamedi (2014) in a different study. Good correlations were reported between the results from dynamic modulus test and the SFE method. The influence of fillers on the moisture susceptibility of asphalt mixes was evaluated by Alvarez et al. (2012a) using the SFE technique. Also, Alvarez et al. (2012b) evaluated the effectiveness of the modification of binder-aggregate interface with asphalt rubber and polymer to reduce moisture-induced damage potential using the SFE method. Ghabchi et al. (2014) investigated the effect of RAP on the adhesion bonding of binder-aggregate systems using the SFE components of RAP binder blends and aggregates. The adhesion and compatibilities between binder blends with different amounts of RAP and six different types of aggregates were evaluated using different energy parameters. The SFE method was used by Tan and Guo (2013) to determine the cohesive and adhesive strength of asphalt mastic. It was found that the van der Waals force components of asphalt binders

and fillers contributed significantly to the cohesion and adhesion bonding of asphalt mastic.

1.3.4 Effect of Chemical Compositions of Asphalt Binder and Aggregate on Moisture-induced Damage

The chemical and physical properties of both binder and aggregates have significant influence on the adhesive properties of asphalt mixes (Abo-Qudais and Al-Shweily, 2007; Shu et al., 2012; Doyle and Howard, 2013; Tong et al., 2015; Baldi-Sevilla et al., 2017). Asphalt binder exhibits complex chemical compositions. It is a mixture of hydrocarbons with polar functional groups. Few organometallic constituents such as nickel, vanadium, and iron may be present in binder (Curtis et al., 1993; Jahromi, 2009; Hofko et al., 2018). The level of complexity gets more critical with the addition of different additives (Hossain et al., 2012). Therefore, understanding the interaction between binder and additives is important to evaluate the effect of additives on the binder's performance. The relationships between rheological and chemical properties of binder with WMA and ASA were investigated by Hossain et al. (2012) using spectroscopic analysis. The addition of WMA additives caused an increase in aliphatic content of the binder which subsequently resulted in an increase in stiffness. Also, the addition of an antistripping agent was found to increase the nitrogen content in the surface composition of the binder. Wei et al. (2014) evaluated the correlation between the four fractional compositions (saturates, aromatics, resins and asphaltenes) and the SFE of binder. The SFE of binder was found to increase with the amount of resin and ratio of resins/asphaltenes. Also, the SFE exhibited good correlations with the amounts of carbon, nitrogen and sulphur present in a binder. Tarefder and Zaman

(2009) reported an improvement in moisture-induced damage performance of binders with 3% polymer (SB and SBS) by quantifying the adhesion/cohesion forces using an atomic force microscopy (AFM). Baumgardner et al. (2005) analyzed the chemical compositions of PPA-modified binders using a number of different chemical analysis tools. It was reported that the constituents of the base binder significantly influence the blending mechanism of PPA with binder. According to Fee et al. (2010), the PPA reacts with the various functional groups of the binder, breaks the asphaltene agglomerates into smaller fractions and disperses them in the maltene phase. These changes affect the rheology and physical characteristics of the binder. Also, in-service oxidative aging can significantly change the chemical properties of a binder, hence affect moisture-induced damage performance of asphalt mixes (Martin et al., 1990; Zhang et al., 2018; Liu et al., 2019). Interaction of binder constituents with atmospheric oxygen leads to the creation of several oxidized chemical species, such as carbonyl (e.g. carboxylic acid) and sulfoxide functional groups (Curtis et al., 1993; Lu et al., 2008). Curtis et al. (1993) reported that the sulfoxides and carboxylic acids functional group exhibited high affinity for the aggregate surface. However, these moieties can be highly soluble in water, which may result in an increase in moisture susceptibility of asphalt mixes. Therefore, characterization of the chemical compositions of the binder is important to understand the moisture-induced damage mechanisms of asphalt mixes.

Several chemical analysis tools including XRF, FTIR spectroscopy, differential scanning calorimetry, nuclear magnetic resonance (NMR), AFM and X-ray photo electron spectroscopy (XPS) have been used to analyze the chemical constituents of asphalt binder (Le Guern et al., 2010; Hossain et al., 2012; Hesp and Shurvell, 2013).

For example, several studies (Soleimani et al., 2009; Hesp and Shurvell, 2010; Hesp and Shurvell, 2013) have used the XRF technique to ensure quality of binders by conducting elemental analysis. Also, the XRF technique was used by Reinke and Glidden (2010) to quantify the amount of phosphorus in PPA-modified binder. The effect of the chemical functional group on the moisture-induced damage potential of the asphalt binders were evaluated by Tarefder and Zaman (2009) using atomic force microscopy (AFM). The adhesion forces between asphalt and silicon-nitride (resembles aggregate) and cohesion forces between asphalt molecules and carboxyl (-COOH), methyl (-CH3), and hydroxyl (-OH) functional groups were determined by probing the asphalt surface with chemically functionalized tips. The FTIR spectroscopy has been successfully used to determine the functional groups of binders (Huang and Grimes, 2010; Qin et al., 2014; Hofko et al., 2018; Ge et al., 2019; Arafat et al., 2020). A number of studies have used the FTIR spectroscopy to investigate the aging extent of different functional groups, such as sulfoxides and carbonyl groups. Also, FTIR spectroscopy has been used to investigate the aging mechanisms of polymer-modified binders by continuous oxidation process (Mouillet et al., 2008).

In addition to properties of binders, the moisture susceptibility of a mix can be impacted by the cleanliness, surface texture, minerology, porosity, surface charge and energy, and polarity of aggregates in a mix (Johnson and Freeman, 2002; Cui et al., 2014). Aggregate surface contains a variety of active sites which attract the polar functional groups of the binder (Curtis et al., 1992). As a result, hydrogen bonds or salt links are formed at the binder-aggregate interface (Tarrer and Wagh, 1991). A wide variation in aggregate composition, surface chemistry and morphology is possible in an

asphalt mix which can significantly affect the moisture-induced damage performance of the mix. Several studies have reported that the acid-base nature of aggregates influences the adhesive bonding at the binder-aggregate interface (Kalantar et al., 2012; Tong et al., 2015; Behnood and Gharehveran, 2019; Haider et al., 2020). Generally, aggregate rich in silica (SiO_2) exhibits acidic behavior and may increase moisture-induced damage potential of a mix. On the other hand, aggregates with high CaO (generally present as $CaCO_3$) exhibit good bonding quality (Curtis et al., 1993). Therefore, understanding the effect of the surface chemistry and chemical compositions of aggregates on the moisture susceptibility is important to identify compatible binder-aggregate combinations.

1.3.5 Effect of Different Additives on the Moisture-induced Damage

1.3.5.1 Warm Mix Asphalt (WMA) Additives

In recent years, construction of asphalt pavements using WMA technologies has increased significantly to reduce energy consumption and promote sustainable development. The asphalt production temperature can be reduced by a maximum of 40 °C lower than that of hot mix asphalt (HMA) by using WMA technologies (D'Angelo et al., 2008; West et al., 2014). Generally, WMA technologies can be divided into three categories, namely foaming technology, organic additives and chemical additives (West et al., 2014). A number of products are available commercially to help promote coating of the aggregate surface with binder at a lower temperature. Several studies have reported concerns about moisture-induced damage susceptibility of WMA mixes due to insufficient drying of aggregates at low mixing and compaction temperatures (Xiao et al., 2010b; Khodaii et al., 2012). An increase in the moisture-induced damage potential of WMA mixes was reported by several studies based on laboratory-based performance

tests (Prowell et al., 2007; Ghabchi et al., 2013). The effect of the addition of two WMA additives, namely Sasobit® and Aspha-min® was evaluated by Wasiuddin et al. (2008) using the SFE approach. The addition of Sasobit® reduced the adhesion between binders and aggregates, whereas Aspha-Min® did not exhibit any specific trend. In a similar study, Ghabchi et al. (2013) reported an increase in work of adhesion and a reduction in work of debonding of the binder-aggregate system with the addition of Sasobit®. The use of binder from different sources may be responsible for the differences observed in these two studies. Also, the use of Evotherm exhibited maximum reduction, whereas the use of Advera did not significantly increase or decrease the moisture-induced damage potential of the binder over different aggregates.

1.3.5.2 Antistripping Agent (ASA)

Liquid antistripping agents are commonly used by the paving industry to reduce moisture-induced damage potential of asphalt mixes (Taylor and Khosla, 1983). Generally, antistripping agents contain amine functional groups which are strongly basic in nature (Tunnicliff and Root, 1983). The amine group of the antistripping agent reacts with the aggregate surface to form ammonium salts and reduce the SFE of aggregate. The hydrocarbon portion of the antistripping agent acts as a bridge between the binder and aggregate surface (Wasiuddin et al., 2007b). Wasiuddin et al. (2007c) used the SFE technique to evaluate the effectiveness of two amine-based liquid antistrip additives. The antistrip additives reduced the acid SFE components and increased the basic SFE components of the asphalt binder. Aksoy et al. (2005) used Marshall stability ratio and TSR to evaluate the moisture susceptibility of two liquid heat stable anti-stripping agents. Moisture-induced damage potential of asphalt mixes reduced with the

incorporation of antistripping agents. Arabani and Hamedi (2014) reported an increase in the ratio of dynamic modulus (wet to dry) with the addition of antistripping agent. Also, Abuawad et al. (2015) conducted several laboratory tests and observed that the antistripping agent can be used effectively to reduce moisture damage potential of a mix. However, study is needed to evaluate the effectiveness of antistripping agent with polymer-modification, aging and aggregates with different mineralogical compositions.

1.3.5.3 Polyphosphoric Acid (PPA)

Asphalt binder modification has become an integral part of asphalt production to address increased traffic volume, heavier truck traffic and higher tire pressures (Isacsson and Lu, 1995; Airey, 2003). In recent years, the use of different modifiers such as polymers, crumb rubber, and PPA has increased significantly (Baumgardner, 2010). An improvement in the high-temperature rheological properties of the binder was observed with the incorporation of PPA to asphalt binder (Baumgardner, 2010; D'Angelo, 2010; Fee et al., 2010). According to Arnold et al. (2009), PPA can be used as a cross-linking agent for polymer modification. Also, Arnold et al. (2009) reported a higher sensitivity to moisture for binder with higher amount of PPA. An increase in moisture susceptibility of asphalt mixes with PPA modification was reported by other researchers as well (Orange et al., 2004; Fee et al., 2010; Al-Qadi et al., 2014). Therefore, the present study attempts to understand the interaction of PPA with binder constituents as well as moisture-induced damage potential of asphalt mixes.

1.3.5.4 Reclaimed Asphalt Pavement (RAP)

Increased environmental awareness and scarcity of high-quality aggregates resulted in an increase in the use of recycled or reclaimed materials in asphalt

pavement. Also, a significant reduction in the construction cost is possible with the use of RAP. In recent years, more than 99% of asphalt is being reused and recycled (NAPA 2011). Generally, RAP is used in producing asphalt mixes, and constructing base and shoulder for new pavement. to Several studies have reported significant improvement in rutting resistance with the use of RAP in asphalt mixes. However, a reduction in fatigue life was observed with the incorporation of RAP in the asphalt mix, when the amount of RAP exceeded certain level (Shu et al., 2008; Mohammad et al., 2016). The effect of RAP on the moisture-induced damage potential of asphalt mixes was evaluated by Ghabchi et al. (2014) using the SFE method. A reduction in the moisture-induced damage potential of the binder-aggregate system was observed with the addition of RAP binder. In a different study, Ghabchi et al. (2016) evaluated the moisture-induced damage potential of asphalt mixes using TSR test. Asphalt mixes with a RAP content up to 25% exhibited satisfactory moisture-induced damage resistance. The physio-chemical changes of the binder with the addition aged materials such as RAP needs further evaluation to properly understand its effect on the moisture susceptibility of asphalt mixes.

1.4 SCOPE, ASSUMPTIONS AND LIMITATIONS OF THE CURRENT STUDY

In this study, the surface free energy method (SFE), chemical analysis and laboratory-based performance tests were used to evaluate the effects of additives, aggregate types and aging on the moisture-induced damage potential of asphalt mixes. Attempts were made to understand the differences in the estimation of SFE of binders using different methods. Also, the effect of probe liquid sets on the calculation of SFE components of binders was evaluated. Furthermore, the chemical and thermodynamic

properties of asphalt binder and aggregates were used to evaluate the compatibility of different binder-aggregate systems. The effect of aging and additives on the moisture-induced damage performance of the binder-aggregate system was assessed by evaluating the changes in the energy parameters determined by the SFE method. In addition, the effects of aging and additives on the moisture susceptibility of asphalt mixes were evaluated using different laboratory-based performance tests. The correlations between different conventional and unconventional laboratory-based performance parameters with the SFE parameters were determined.

In this study, the SFE components of the binders were determined using contact angle measurements by the dynamic Wilhelmy plate test. The variability during contact angle measurement was reduced by keeping the measuring apparatus, conditions and measurement precision same for all binders. All the contact angle measurements were conducted at room temperature (77°F). It was assumed that the surface composition of the binder used for contact angle measurement was similar to the binder surface at a binder-aggregate interface. Also, it was assumed that the binder surface used for measurement was physically and chemically uniform. The roughness of the binder surface was not considered in the calculation of contact angle with probe liquids. The SFE values of different probe liquids used in this study were obtained from Hefer et al. (2006) and considered to remain unchanged throughout the testing. Also, the binder surface was assumed to be immiscible in the selected probe liquids.

In this study, the effects of different aggregate, namely limestone, granite and rhyolite from local sources, on the moisture-induced damage potential were identified by investigating the changes in chemical and thermodynamic properties. The moisture

sensitivity of a binder-aggregate system with aggregates from sources different than the ones used in the current study can vary depending on their compositions. Therefore, moisture-induced damage sensitivity of each binder-aggregate combination is recommended before constructing the asphalt pavement.

Due to the limited scope of the of the current study, a smaller dataset was used to develop correlations between different conventional and unconventional laboratory-based performance parameters and the SFE parameters. Future studies are needed to evaluate these relationships with a larger dataset consisting of different types of binders, aggregates, and additives.

1.5 DISSERTATION FORMAT AND CONTENT

The findings of this study are compiled in this dissertation as four journal publications (1 published and 3 under review) from Chapter 2 to Chapter 5. Chapter 1 and Chapter 6 contain the general introduction and conclusions of this study, respectively.

Chapter 1 presents the background and objectives of this study. Also, pertinent literature related to moisture-induced damage theories, current practices for moisture-induced damage evaluation, effect of additives and aging on moisture-induced damage potential of asphalt mixes is included in this chapter.

In Chapter 2, attempts were made to determine the SFE components of binders consistently as they can significantly influence the moisture-induced damage calculation of a binder-aggregate system. Suitable sets of probe liquids for the GvOC, Owens-Wendt and Wu methods were identified. Also, the differences between different surface free energy estimation methods were investigated.

In Chapter 3, chemical and thermodynamic properties of asphalt binder and aggregates were used to evaluate the compatibilities of the binder-aggregate systems. Effects of different additives and aging on the moisture-induced damage of an unmodified and a polymer-modified binder were investigated. Also, the effects of aggregate type and aging on the moisture-induced damage were determined using the SFE method and chemical analyses.

Chapter 4 presents the moisture-induced damage evaluation of asphalt mixes prepared with different additives. Also, the moisture-induced damage potentials of short-term and long-term aged asphalt mixes were evaluated using a TSR and a new SCB-based parameter. Correlations between the moisture-induced damage performance parameters from laboratory performance tests and the SFE method were also investigated.

In Chapter 5, the effectiveness of several laboratory-based performance tests for evaluating moisture-induced damage potential of asphalt mixes was investigated. Along with conventional parameters, several unconventional moisture-induced damage parameters from HWT, ITS and SCB tests were introduced in this chapter. Comparisons of the conventional and unconventional laboratory-based performance parameters with the SFE parameters were presented as well.

Chapter 6 presents the overall summary of the findings from this study. Also, a list of recommendations for future works is presented in this chapter.

CHAPTER

2

EFFECTS OF SURFACE FREE ENERGY ESTIMATION METHODS AND PROBE LIQUIDS ON THE MOISTURE-INDUCED DAMAGE POTENTIAL OF ASPHALT MIXES[1]

ABSTRACT

Determination of accurate and consistent surface free energy (SFE) of binders is an integral part of the moisture-induced damage evaluation of asphalt mixes using thermodynamic principles. Generally, the SFE of a binder is determined by measuring contact angles with different probe liquids using the dynamic Wilhelmy plate (DWP) or sessile drop (SD) test. A number of different theories are currently available to determine the SFE from contact angle measurements. These theories can be divided into two major categories, namely component-based approach and equation of state approach. Component-based approaches rely on dividing the SFE into smaller components, whereas the equation of state approach disqualifies the component-based approach and allow determination of total SFE of binders. Differences in assumptions and mathematical formulations used by these approaches are expected to influence the calculated values of the SFE. Also, for component-based approaches, the selection of probe liquids sets is expected to influence the conditioning of the equation sets, hence,

[1] This chapter has been submitted to the American Chemical Society (ACS) Omega under the title "Effects of Surface Free Energy Estimation Methods and Probe Liquids on the Moisture-Induced Damage Potential of Asphalt Mixes." The current version has been formatted for this dissertation.

affect the SFE of the binders. Therefore, in this study, differences in the SFE as well as energy parameters of binder-aggregate systems from different component-based approach (Good-van Oss-Choudhary (GvOC), Owens-Wendt and Wu method) and equation of state approach (Neumann method) were investigated. Also, the effects of the probe liquid sets on the SFE of binders were evaluated for GvOC, Owens-Wendt and Wu methods. Several different combinations of five probe liquids, namely water (W), glycerol (G), formamide (F), ethylene glycol (E) and diiodomethane (D) were used for this purpose. The probe liquid sets with consistent SFE components and energy parameters were identified. The results indicated that the consistent energy parameters can be obtained by using WGFDE, WGDE and WFED probe liquid sets by the GvOC and Owens-Wendt method, and WGFDE, WFGD and WFED probe liquid sets by the Wu method. Also, significant differences were observed in the SFE determined using component-based approach and equation of state approach. The results of this study will be helpful in the evaluation and screening of asphalt mixes for moisture-induced induced damage.

2.1 INTRODUCTION

Moisture-induced damage leads to the deterioration of the mechanical properties of asphalt mixes, and eventually, failure of flexible pavement. According to Caro et al. (2008a), moisture-induced damage is a two-step mechanism. The first step involves infiltration of the moisture into the pavement either in liquid or vapor state and reaching the binder-aggregate interface. The three primary modes of transport through which moisture can reach the binder-aggregate interface are penetration of surface water with hydrostatic pressure, infusion of water by capillary forces and permeation or diffusion

of water vapor (Masad et al., 2007; Caro et al., 2008a). The second step includes the response of the system i.e., adhesive and/or cohesive failures and reduction in the structural capacity of the pavement. Until now, five different theories have been proposed by researchers to explain the adhesion bonding in binder-aggregate system: weak boundary layer theory, electrostatic theory, chemical bonding theory, mechanical bonding theory and thermodynamic theory (Hefer et al., 2005; Caro et al., 2008a). The details associated with the mechanisms and capabilities of these theories to evaluate moisture-induced damage on a quantitative basis were explained by Hefer et al. (2005). Among these theories, the thermodynamic theory using the surface free energy (SFE) concept was reported to have the potential to quantify the adhesion of a binder-aggregate system (Bhasin et al., 2007b; Caro et al., 2008a). Several energy parameters from the surface free energy (SFE) concept, namely work of adhesion, work of debonding and energy ratios, have been used by researchers to determine moisture susceptibilities of asphalt mixes (Little and Bhasin, 2006; Bhasin et al., 2007b; Zhang and Liu, 2018)

Thermodynamic theory is one of the most widely used concepts in adhesion science (Hefer et al., 2005). According to this theory, the physio-chemical adhesion between two materials is a function of the interfacial and surface free energies of those materials. Generally, molecules in bulk of a material are surrounded by other molecules and have higher bond energy than the molecule on the surface. Therefore, work needs to be done to bring a molecule from the bulk to surface, i.e., to create new surface. The surface free energy of a material depends on the nature and the aggregate state of material, and is strongly associated to the state of equilibrium of the atoms on the

surface (Schuster et al., 2015). A number of techniques, such as static drop shape techniques, Wilhelmy plate test, capillary wave method, drop weight method and oscillating jet method have been developed and are currently being used to measure directly the surface tension or SFE of liquids (Rusanov and Prokhorov, 1996; Hartland, 2004; Lawrence, 2010). However, direct measurements of the SFE of solid surfaces are difficult due to the immobility of molecules in a solid phase. Therefore, indirect techniques are used to determine the SFE of solids. Several indirect techniques, such as force measurements between two elastic bodies, measurements of contact angle with different probe liquids, flotation of film technique, sedimentation experiment, capillary columns method and calculation of dispersion forces are being used by different researchers (Fowkes, 1964; Owens and Wendt, 1969; Johnson et al., 1971; Israelachvili and Tabor, 1972; Vargha-Butler et al., 1985; Van Oss et al., 1988; Fuerstenau et al., 1990; Grundke et al., 1996). Among these methods, the measurement of contact angles with different probe liquids is most commonly used for calculating SFE of a solid surface.

Calculation of the SFE of a solid surface from contact angles is based on the principle first proposed by Young approximately 200 years ago (Young, 1805). Young's equation (Equation (2.1)) states that the contact angle (θ) of a probe liquid on a solid surface can be determined from the mechanical equilibrium of three interfacial tensions, namely the solid-vapor surface tension or SFE of the solid (Γ_S), the liquid-vapor surface tension or SFE of the probe liquid (Γ_L) and the solid-liquid interfacial tension (Γ_{SL}). It should be noted that the subscripts 'S' and 'L' are used in this study to represent solid and liquid phase, respectively. The contact angle (θ) and the SFE of

probe liquid (Γ_L) are the only measurable quantities in Young's equation (Equation (2.1)). Additional assumptions related to the Γ_L, Γ_S and Γ_{SL} are required to solve Equation (2.1). Dupré proposed Equation (2.2) to compute the interfacial work of adhesion between a solid and a probe liquid (W_{SL}) (Dupré and Dupré, 1869). Also, Berthelot proposed Equation (2.3) at the end of the 19th century to define the W_{SL} of a solid-liquid system (Kwok and Neumann, 1999). The W_{SS} and W_{LL} in Equation (2.3) represent the free energy of cohesion for solid and liquid and can be replaced with $2\Gamma_S$ and $2\Gamma_L$, respectively. Berthelot then combined Equation (2.2) with Equation (2.3) to formulate a hypothesis, known as Berthelot hypothesis as presented in Equation (4) (Kwok and Neumann, 1999). The SFE of a solid (Γ_S) can be determined by combining Equation (2.1) with Equation (2.4), as presented in Equation (2.5). Equation (2.5) is the Young-Dupré equation with W_{SL} replaced using Equation (2.3).

$$\Gamma_S = \Gamma_{SL} + \Gamma_L cos\theta \qquad (2.1)$$

$$W_{SL} = \Gamma_S + \Gamma_L - \Gamma_{SL} \qquad (2.2)$$

$$W_{SL} = (W_{SS}W_{LL})^{0.5} \qquad (2.3)$$

$$\Gamma_{SL} = \Gamma_S + \Gamma_L - 2(\Gamma_S\Gamma_L)^{0.5} \qquad (2.4)$$

$$\Gamma_L(1 + cos\theta) = 2(\Gamma_S\Gamma_L)^{0.5} \qquad (2.5)$$

Two major approaches, namely component-based approach and equation of state approach have been used to determine the SFE of solids from contact angle measurements through Young's equation (Equation (2.1)) and Berthelot's hypothesis (Equation (2.4)). Fowkes (1964) first proposed the idea of expressing surface free energy as a sum of components. He divided the total SFE of a solid into different

components, namely dispersion (d), polar (p), hydrogen (h), induction (i), acid-base components (ab) and all remaining interactions (o) (Equation (2.6)). However, according to Fowkes (1964), the adhesive bond of a two-phase (solid-liquid) system entirely depends on the London dispersion surface energy resulting from the attractions between adjacent atom and molecules. Fowkes (1964) proposed Equation (2.7), the modified Berthelot hypothesis, to represent the interfacial bond energy of a solid-liquid system. The dispersion component of a solid can be determined easily from Equation (2.7) using a probe liquid with only dispersion component.

$$\Gamma_S = \Gamma_S^d + \Gamma_S^p + \Gamma_S^h + \Gamma_S^i + \Gamma_S^{ab} + \Gamma_S^o \qquad (2.6)$$

$$\Gamma_L(1 + cos\theta) = 2(\Gamma_S^d \Gamma_L^d)^{0.5} \qquad (2.7)$$

Owens and Wendt (1969) later used a two components approach, namely dispersion (d) and polar (p) components, to define SFE of a solid (Equation (2.8)). The dispersion component comprises of London interactions (similar to Fowkes) whereas polar components consist of the remaining components (polar, hydrogen, inductive and acid-base interactions). Also, in the Owens-Wendt model, the adhesive bond energy between two materials is represented in the form of a geometric mean of SFE components (Equation (2.9)). Wu (Wu, 1971; Wu, 1973) modified the Owens-Wendt model by using the harmonic mean of the SFE components (Equation (2.10)). In the 1980's, Van Oss et al. (1988) introduced the concept of dividing SFE into three components, namely acid (Γ^+), base (Γ^+), and Lewis van-der-Waals components (Γ^{LW}) using Equation (2.11), and postulated experimental determination of the acid-base surface free energy interactions. The SFE components of a solid can be determined from the contact angles of the probe liquids on the solid surface using Equation (2.12).

At least a set of three probe liquids is required to determine the three unknown SFE components of a solid using Equation (2.12).

$$\Gamma_S = \Gamma_S^d + \Gamma_S^p \tag{2.8}$$

$$\Gamma_L(1 + cos\theta) = 2(\Gamma_S^d \Gamma_L^d)^{0.5} + 2(\Gamma_S^p \Gamma_L^p)^{0.5} \tag{2.9}$$

$$\Gamma_L(1 + cos\theta) = 4\left[\frac{\Gamma_S^d \Gamma_L^d}{\Gamma_S^d + \Gamma_L^d} + \frac{\Gamma_S^p \Gamma_L^p}{\Gamma_S^p + \Gamma_L^p}\right] \tag{2.10}$$

$$\Gamma_S = \Gamma_S^{LW} + 2(\Gamma_S^+ \Gamma_S^-)^{0.5} \tag{2.11}$$

$$\Gamma_L(1 + cos\theta) = 2(\Gamma_S^{LW} \Gamma_L^{LW})^{0.5} + 2(\Gamma_S^+ \Gamma_L^-)^{0.5} + 2(\Gamma_S^- \Gamma_L^+)^{0.5} \tag{2.12}$$

Equations (2.8), (2.9) and (2.11) derive from the Young-Dupré equation with different expressions for the work of adhesion W_{SL}.

Alternatively, the equation of state approach disqualifies the component-based approach, stating that the interfacial free energy can be completely determined by the SFE of the probe liquid and the SFE of the solid in conjunction with Young's principle (Equation (2.13)). Neumann and his colleagues (Neumann et al., 1974; Li and Neumann, 1990; Li and Neumann, 1992) used the equation of state approach and proposed Equation (2.14) to define the relation between Γ_{SL}, Γ_S and Γ_L. In Equation (2.14) β is a constant parameter. The use of this approach eliminates the dependency of the SFE on probe liquid set. However, a number of studies reported concerns over this equation of state approach in spite of its associated benefits (Morrison, 1991; Chibowski and Perea-Carpio, 2002; Della Volpe et al., 2004). In a more recent study, Zhang (2020) proposed a modified version of the equation of state approach to determine the SFE of binders.

$$\Gamma_{SL} = F(\Gamma_L, \Gamma_S) \tag{2.13}$$

$$\Gamma_L(1 + cos\theta) = 2(\Gamma_S\Gamma_L)^{0.5}e^{-\beta(\Gamma_L-\Gamma_S)^2} \qquad (2.14)$$

Although all these approaches rely on the Young-Dupré equation and constancy of the interfacial tensions during contact angle measurement, the measured value of the SFE may vary due to the difference in mathematical relations between contact angles and SFE, used in each estimation method (Della Volpe and Siboni, 2000; Żenkiewicz, 2006; Żenkiewicz, 2007; Rudawska and Jacniacka, 2018). Among the aforementioned approaches, the three component-based adhesion model by Van Oss et al. (1988), known as Good-van Oss-Choudhury (GvOC) theory, was found to be commonly used by the researchers to quantify the adhesion and debonding of binder-aggregate system in presence of moisture (Bhasin et al., 2006; Hefer et al., 2006; Bhasin et al., 2007a; Wasiuddin et al., 2007a; Wasiuddin et al., 2007c; Arabani et al., 2011; Buddhala et al., 2011; Alvarez et al., 2012b; Moghadas Nejad et al., 2012; Ghabchi et al., 2013; Ghabchi et al., 2014). Other estimation methods, such as Owens-Wendt method, Wu method and equation of state approach were used to estimate binder's SFE at a limited scale (Zhang and Liu, 2018; Zhang, 2020). Also, to the authors' knowledge, no study has been conducted to compare the SFE components of the binder and energy parameters of binder-aggregate system obtained from different methods.

Several studies have reported that the SFE of a solid obtained from a component-based approach can be significantly influenced by the selection of probe liquid set (Holländer, 1995; Della Volpe and Siboni, 2000; Żenkiewicz, 2007). In case of binder-aggregate systems, these inaccuracies in the SFE components of the binder will influence the calculation of energy parameters, which will influence the moisture-induced damage potential of asphalt mixes. Therefore, selection of a proper probe liquid

set is important to obtaining accurate and consistent SFE components of binder and energy parameters of the binder-aggregate system. According to Bhasin (2007), probe liquids for contact angle measurement should not react with the binder and have SFE components larger than the tested binder. Also, probe liquids used in the same set should have distinctly different SFE components. Until now, five probe liquids, namely water (W), glycerol (G), formamide (F), ethylene glycol (E) and diiodomethane (D) have been found to satisfy all the criteria of probe liquids for determination of SFE of binders. Previous studies have used a number of different combinations of these five probe liquids to calculate the surface free energies as well as moisture susceptibilities of the binder-aggregate system (Bhasin et al., 2006; Hefer et al., 2006; Bhasin et al., 2007a; Wasiuddin et al., 2007a; Wasiuddin et al., 2007c; Arabani et al., 2011; Buddhala et al., 2011; Alvarez et al., 2012b; Moghadas Nejad et al., 2012; Ghabchi et al., 2013; Ghabchi et al., 2014). Most of these studies, however, did not attempt to identify proper probe liquid sets that result in consistent SFE for the tested binders. Holländer (1995) proposed a parameter called ΔQ_y, based on the difference in the ratios of acid-base components of probe liquids, to determine compatible probe liquid pairs. According to Holländer (1995), probe liquid pair with a higher ΔQ_y will result in a reliable and consistent acid-base parameters of solid surface. Hefer et al. (2006) first used a condition number approach and Γ_L versus $\Gamma_L cos\theta$ plot for selection of probe liquids for contact angle of binder using the GvOC method. A lower value of condition number was required to reduce the sensitivity to measurement error. Also, probe liquid set with a higher R^2 value from Γ_L versus $\Gamma_L cos\theta$ plot was considered a better candidate for determining the SFE components. According to Hefer et al. (2006), a combination of all

five probe liquids is expected to increase the reliability of the calculated SFE components of the binders. Singh and Mishra (2018) used similar approaches to determine proper liquid set for the GvOC method. It was found that the condition number approach is more appropriate than the Γ_L versus $\Gamma_L cos\theta$ plot for this purpose. According to Singh and Mishra (2018), WFE, WGD and WDE set can be used to determine the SFE of binders. Recently, Zhang and Liu (2018) used both the condition number and Γ_L versus $\Gamma_L cos\theta$ and found the condition number approach inadequate for determination of probe liquid set. Zhang and Liu (2018) proposed to use the Owens-Wendt model with WFGED and WFED probe liquid sets to determine consistent energy parameters for a binder-aggregate system. The inconsistencies from previous studies indicate the need for additional research on the selection of proper probe liquids sets. As most of the studies were confined to the GvOC method, research is needed to evaluate the effect of probe liquids on the SFE components obtained by other methods.

2.2 OBJECTIVES

In the present study, the effect of probe liquid sets on the calculation of SFE components is investigated for different component-based methods, namely GvOC, Owens-Wendt and Wu method. A number of different combinations of water (W), glycerol (G), formamide (F), ethylene glycol (E) and diiodomethane (D) is used for this purpose. Also, an attempt is made to identify the differences in the SFE components calculated using the GvOC, Owens-Wendt and Wu methods and the Neumann's equation of state approach. The specific objectives of this study are:

i. To evaluate the effects of probe liquid sets on the calculation of SFE components by GvOC, Owens-Wendt and Wu methods;

ii. To identify suitable probe liquid sets to obtain consistent energy parameters using GvOC, Owens-Wendt and Wu methods; and

iii. To investigate the difference between the component-based approach and the equation of state approach by comparing energy parameters of a binder-aggregate system.

2.3 MATERIALS AND METHODS

Four commonly used asphalt binders, namely S1, S2, S3 and S4 from different Oklahoma refineries were collected for the purpose of this study. The binders were selected to cover a wide range of performance grades (PG). The S1 and S2 binders were graded as PG 64-22 and were collected from two different sources. The S3 and S4 binders were graded as PG 76-28 and PG 58-28, respectively. In this study, the dynamic Wilhelmy plate (DWP) test was used to determine the dynamic contact angles of the binders. Figure 2.1 presents the sample preparation and testing procedure used in this study. Samples for DWP test were prepared by uniformly coating asphalt binders on 24 x 50 mm glass plates. For this purpose, binder was heated in an oven until it became liquid. Then the glass plate was submerged vertically approximately 10 mm into the liquid binder. The excess binder was then drained by keeping the glass plate oriented vertically for approximately 30 seconds. The glass plate was then inverted and kept vertically oriented inside an oven for approximately 3-4 minutes to ensure uniform coating. Coated glass plates were transferred to a desiccator to reduce exposure to moisture. All the samples were tested within 24-36 hours after preparation. Before testing, the glass plates were examined carefully for anomalies such as bubbles and non-homogeneous substances. Samples with any visible anomalies were discarded as a

smooth and uniform surface is required to reduce testing variability. The width and thickness of each sample were measured and recorded after testing using a caliper.

As mentioned earlier, selection of appropriate probe liquids is important to obtain consistent contact angles as well as SFE parameters of binders. All five of the aforementioned probe liquids, namely water (W), glycerol (G), formamide (F), ethylene glycol (E) and diiodomethane (D) were used in this study as they satisfied the criteria required to measure the contact angles of binders. The acid, base and Lewis van-der-Waals SFE components of these probe liquids were obtained from Hefer et al. (2006) and are presented in Table 2.1. According to Zhang and Liu (2018), the dispersion (Γ_L^d) and polar (Γ_L^p) components are similar to Lewis van-der-Waals (Γ^{LW}) and acid-base (Γ_L^{AB}) components of the liquids. The Γ_L^d and Γ_L^p components are required to determine the SFE components of binders using the Owens-Wendt and Wu method.

A Cahn DCA 220 micro balance was used to determine the contact angles of binder samples with probe liquids. The device worked by registering the difference in force as the sample was submerged into and retracted from a probe liquid container. For this purpose, the asphalt coated glass plate sample was hung using a hanger attached to the balance. The probe liquid container was placed on a platform below the sample. The platform was raised to submerge and then lowered to retract the binder sample as test progressed. The speed of the platform movement was maintained at 20 mm/min. Each sample was submerged to a depth of 4 mm for this measurement. The dynamic contact angle during the submersion and retraction phases was determined using the registered force, depth of penetration for a buoyant force correction and SFE of probe liquid using Equation (2.15). The contact angles during submersion and retraction phase are known

as advancing and receding contact angle, respectively. The advancing contact angle was used for calculating SFE parameters in this study as the receding contact angles generally exhibit higher variability (Hefer et al., 2006). Five replicates were tested for each binder-liquid combination. Calibration of the micro-balance was performed at the beginning of each day's work to ensure reliability of the test results for the contact angle θ.

$$\Gamma_L cos\theta = \frac{F+V\rho_L g}{P} \qquad (2.15)$$

where,

F = net force (balance reading),

ρ_L = density of the probe liquid,

V = volume of glass plate submerged into probe liquid = a*b*h,

P = perimeter of the plate = 2(a + b),

a = width of the plate,

b = thickness of the plate, and

h = depth of immersion,

Γ_L=SFE (surface tension) of probe liquid.

2.4 RESULTS AND DISCUSSION

2.4.1 Contact Angles of Binders

The contact angles of binders with water, glycerol, formamide, ethylene glycol and diiodomethane were determined using Equation (2.15). Table 2.2 presents the average (avg) and standard deviation (SD) of contact angle values with different probe liquids. The standard deviations for contact angles of all binders were 2.00° or less. This

relatively low standard deviation indicates a higher repeatability of the measurements. From Table 2.2, the contact angles for different binders with water were found to vary from 106.1° to 109.1°. Variations for glycerol (94.4° to 105.5°), formamide (90.6° to 101.2°), diiodomethane (84.5° to 96.3°) and ethylene glycol (78.6° to 94.1°) were found to be higher than water. The variations in the contact angles are expected to be reflected in the calculation of SFE components of the tested binders.

2.4.2 Surface Free Energy of Binders

2.4.2.1 Component-Based Approach

2.4.2.1.1 Good van Oss Choudhury (GvOC) Method:

As mentioned earlier, in the GvOC method, the SFE components of a solid is divided into three components, namely acid (Γ_A^+), base (Γ_A^-) and Lewis van der Waals (Γ_A^{LW}) components. A minimum set of three probe liquids is required to generate three equations which can be solved to determine the three unknown SFE components of a solid using Equation (2.12). In this study, the SFE components of binders were determined using 16 different sets of three to five probe liquids. Ten out of sixteen sets contain three probe liquids which formed sets of three equations. The three unknown SFE components were determined by solving these three equations. Another five sets contained four probe liquids and one set contained five probe liquids. The sets containing four and five probe liquids formed over-determinate sets of equations (i.e., the number of unknown < the number of equations). The SFE components from these probe liquid sets were determined by minimizing the summation of square error using the solver function of Microsoft Excel. Table 2.3 presents the Γ_A^+, Γ_A^- and Γ_A^{LW} SFE

components of binders S1 and S4 for different probe liquid sets. The SFE components of other binders are not presented due to space limitation.

From Table 2.3, significant variations of SFE components can be observed among different probe liquid sets. Also, a number of probe liquid sets, namely FGED, GED, GEF, FED, WGE and FGD resulted in negative square roots of SFE components for all the binders. Similar observation was reported by Zhang and Liu (2018). As the square root of the SFE components cannot be a negative value, the corresponding probe liquid sets were avoided in further calculations. Among the remaining 10 probe liquid sets, it is important to identify appropriate probe liquid sets which will result in consistent SFE components. As mentioned earlier, the condition number approach and plot of Γ_L versus $\Gamma_L cos\theta$ has been used by researchers to identify appropriate probe liquid sets (Hefer et al., 2006; Singh and Mishra, 2018; Zhang and Liu, 2018). In this study, both of these approaches were used to identify probe liquid sets with consistent SFE components.

2.4.2.1.1.1 Γ_L versus $\Gamma_L cos\theta$ Plot

The linear best fit lines of the Γ_L versus $\Gamma_L cos\theta$ plot for all probe liquid sets were determined for all four binders used in this study. Figure 2.2 presents the Γ_L versus $\Gamma_L cos\theta$ plot for all binders with all five probe liquids (WGFDE). The corresponding R^2 values of different probe liquid sets for S1 and S4 binders are presented in Table 2.3. Generally, probe liquid sets with higher R^2 values are believed to produce consistent SFE components (Singh and Mishra, 2018). From Table 2.3, it can be observed that the R^2 values for all probe liquid sets are equal or higher than 0.90 for the S1 binder. Similar results were obtained for S2, S3 and S4 binders. Therefore, no conclusions

could be drawn from the plot of Γ_L versus $\Gamma_L cos\theta$ on the selection of most desired probe liquid set.

2.4.2.1.1.2 Condition Number Approach

The condition number indicates the sensitivity of the calculated SFE components on the changes or measurement error of contact angles. The condition number of a probe liquid set is defined as the square root of the ratio of the maximum and minimum eigenvalue of $A^T A$, where A and A^T represent the coefficient matrix and it's transpose matrix, respectively. Table 2.4 presents the condition number of different probe liquid sets.

A lower value of condition number is required to reduce the sensitivity to measurement error (Hefer et al., 2006; Singh and Mishra, 2018). Probe liquid sets with condition number less than 10 are expected to be less sensitive to errors in the measurement. The probe liquid sets with negative square roots of SFE components, namely FGED, GED, GEF, FED, WGE and FGD exhibited condition numbers of greater than 10. The ill-conditioning of the equation sets may be responsible for the inaccuracies in SFE components. It was observed that the WGFDE, WFGD, WGED, WFED, WED, WGD and WFD sets satisfied the criteria for condition number of less than 10. All these sets include water and diiodomethane with different combinations of glycerol, formamide and ethylene glycol. Among these probe liquid sets, the Γ_A components of S1 binder were found to vary from 16.00 mJ/m^2 to 16.29 mJ/m^2. Other binders exhibited similar smaller variations of Γ_A components. Also, the maximum differences in Γ_A^{LW} component between the abovementioned probe liquid sets were observed to be 0.33, 0.32, 0.16, 0.42 mJ/m^2 for S1, S2, S3 and S4 binders, respectively.

These small variations (with respect to the quantity of SFE) observed for the Γ_A and Γ_A^{LW} components for different probe liquid sets can be considered within the range of measurement error. However, variations in acid and base components were observed among the abovementioned probe liquid sets. For example, a maximum variation of 76% in acid component of S1 binder was observed between the WGFDE and WED probe liquid sets. These high variations indicate the dependency of acid and base components of the binder on the probe liquid set. Also, the acid to base ratio (Γ_A^+/Γ_A^-) indicates the existence of both acid- (Γ_A^+/Γ_A^- >1) and base-dominance (Γ_A^+/Γ_A^- <1) for the same binder from different probe liquid sets. For the S1 binder, the WGFDE, WGED, WFED and WED sets resulted in Γ_A^+/Γ_A^- higher than 1, whereas the WFGD, WGD and WFD sets resulted in Γ_A^+/Γ_A^- of less than 1. The inclusion of ethylene glycol in the probe liquid set yielded higher acidic components, whereas inclusion of glycerol and formamide resulted in higher basic components. For the S1 binder, the WED resulted in Γ_A^+/Γ_A^- of 7.07, whereas the WGDE, WFDE and WGFDE sets resulted in Γ_A^+/Γ_A^- of 2.63, 1.72 and 1.46, respectively. A similar trend was observed for other binders as well. Therefore, along with water and diiodomethane, the choice of at least one or more probe liquid(s) from glycerol, formamide and ethylene glycol is expected to influence the energy ratios of a binder-aggregate system.

2.4.2.1.1.3 Energy Parameters from the GvOC Method

In this study, the effect of the variability in the SFE components was evaluated by determining the energy parameters of the tested binders with a limestone aggregate. For this purpose, the SFE components of a commonly used Oklahoma limestone aggregate was determined using a Universal Sorption Device (USD). The details of the

testing procedure can be found in a previous study conducted by the authors (Ali et al., 2019). The SFE components of the limestone aggregate are presented in Table 2.5. The work of adhesion (W_{AR}), work of debonding (W_{ARW}^{wet}) and energy ratio (ER) of the limestone aggregate with different binders were calculated by the GvOC method using Equations (2.16), (2.17) and (2.18), respectively. Equation (2.16) is obtained from $W_{ARW}^{wet} = W_{AR} + W_{WW} - W_{AW} - W_{RW}$. For the convenience of this study, subscript 'R' was used to represent aggregate.

$$W_{AR}(GvOC) = 2\left(\sqrt{(\Gamma_A^{LW}\Gamma_R^{LW})} + \sqrt{(\Gamma_A^{+}\Gamma_R^{-})} + \sqrt{(\Gamma_A^{-}\Gamma_R^{+})}\right) \tag{2.16}$$

$$W_{ARW}^{wet}(GvOC) = 2\left\{\begin{array}{c}\sqrt{(\Gamma_A^{LW}\Gamma_R^{LW})} - \sqrt{(\Gamma_W^{LW}\Gamma_R^{LW})} - \sqrt{(\Gamma_A^{LW}\Gamma_W^{LW})} + \Gamma_W^{LW} - \sqrt{\Gamma_W^{+}}\left(\sqrt{\Gamma_R^{-}} + \sqrt{\Gamma_A^{-}} - \sqrt{\Gamma_W^{-}}\right) - \\ \sqrt{\Gamma_W^{-}}\left(\sqrt{\Gamma_R^{+}} + \sqrt{\Gamma_A^{+}} - \sqrt{\Gamma_W^{+}}\right) + \sqrt{(\Gamma_A^{+}\Gamma_R^{-})} + \sqrt{(\Gamma_A^{-}\Gamma_R^{+})}\end{array}\right\} \tag{2.17}$$

$$ER\ (GvOC) = \left|\frac{\sqrt{(\Gamma_A^{LW}\Gamma_R^{LW})} + \sqrt{(\Gamma_A^{+}\Gamma_R^{-})} + \sqrt{(\Gamma_A^{-}\Gamma_R^{+})}}{\left\{\begin{array}{c}\sqrt{(\Gamma_A^{LW}\Gamma_R^{LW})} - \sqrt{(\Gamma_W^{LW}\Gamma_R^{LW})} - \sqrt{(\Gamma_A^{LW}\Gamma_W^{LW})} + \Gamma_W^{LW} - \sqrt{\Gamma_W^{+}}\left(\sqrt{\Gamma_R^{-}} + \sqrt{\Gamma_A^{-}} - \sqrt{\Gamma_W^{-}}\right) - \\ \sqrt{\Gamma_W^{-}}\left(\sqrt{\Gamma_R^{+}} + \sqrt{\Gamma_A^{+}} - \sqrt{\Gamma_W^{+}}\right) + \sqrt{(\Gamma_A^{+}\Gamma_R^{-})} + \sqrt{(\Gamma_A^{-}\Gamma_R^{+})}\end{array}\right\}}\right| \tag{2.18}$$

Table 2.6 presents the W_{AR}, W_{ARW}^{wet} and ER values of S1, S2, S3 and S4 binders with the limestone aggregate. Although, all the probe liquid sets presented in Table 2.6 yielded a condition number of less than 10, variation in W_{AR} and W_{ARW}^{wet} were observed with probe liquid sets. The sets with ethylene glycol exhibited higher W_{AR} and lower W_{ARW}^{wet} than the sets with glycerol and/or formamide. For example, the W_{AR} of S1 binder was found to be 88.59 mJ/m^2 for WFD, whereas the same for WGD was 105.98 mJ/m^2. This variation likely resulted from the higher acidic components due to the inclusion of ethylene glycol in the probe liquid set. Also, the variation in W_{AR} and W_{ARW}^{wet} was reflected in ER value. However, for all binders, probe liquid sets with WGFDE, WGED

and WFED resulted in consistent ER value with a maximum variation of ±3%. Therefore, WGFDE, WGED and WFED can be used to calculate the SFE components of asphalt binders using the GvOC method.

2.4.2.1.2 Owen-Wendt's (OW) Method

As mentioned earlier, the Owens-Wendt method (Owens and Wendt, 1969) was developed based on the Fowkes (1964) principle of dividing SFE into different components. In this method, the SFE of a material can be divided into dispersion and polar components. Therefore, at least two probe liquids are required to determine the two unknown SFE components of a solid from solid-liquid interfacial interactions using Equation (2.9). In this study, the SFE components of binders were determined using 26 different combinations of two to five probe liquids: ten combinations with two probe liquids, ten combinations with three probe liquids, five combinations with four probe liquids and one set of five probe liquids. Two equations were formed from sets with two probe liquids using Equation (2.9). The two unknown SFE components were determined by solving these two equations. However, the sets with three, four and five probe liquids formed over-determinate set of equations. Similar to the GvOC method, the solver function of Microsoft Excel was used to determine the two unknown SFE components by minimizing the summation of the square error.

The dispersion (Γ_A^d), polar (Γ_A^p) components and total SFE (Γ_A) of S1 and S4 binders from the Owens-Wendt method are presented in Table 2.7. From Table 2.7, it was observed that the dispersion component Γ_A^d is much higher than the polar component Γ_A^p and a major contributor of total SFE Γ_A of binders. This indicates that the binders are mostly non-polar in nature with significantly low polar component.

Therefore, changes in the value of Γ_A^d with probe liquid sets are expected to impact the calculation of energy parameters significantly. Therefore, in this study, obtaining a consistent result for Γ_A^d of a binder was considered as a selection criterion for probe liquid sets. For this purpose, the value of Γ_A^d that appeared most often among 26 probe liquid sets was identified. The Γ_A^d values that fall within a range of ±3% around the mode were considered as consistent, as used by Zhang and Liu (2018). In Table 2.7, the dispersion component Γ_A^d of the S1 binder exhibited a relatively high variation (from 0 mJ/m^2 to 181.19 mJ/m^2). However, a result of 15.27 mJ/m^2 was found in 10 out of 26 probe liquids sets, namely WED, WGD, WFD, GED, FED, FGD, WD, GD, FD and DE. Also, the Γ_A^d component from WGFDE, FGED, WFGD, WGED, WFED and WF were 15.00, 15.00, 15.11, 15.29, 14.96 and 15.00 mJ/m^2, respectively. These values showed a variation of ±3% among themselves can be considered as a consistent dispersion component Γ_A^d for the S1 binder. Therefore, these 16 probe liquid sets can be considered for further evaluation of the S1 binder. The other combinations, namely WFGE, WFG, WFE, GEF, WGE, WG, WE, GF, GE and FE exhibited higher variations in Γ_A^d. Therefore, these combinations are not expected to provide consistent energy parameters and are not considered in future calculations for the S1 binder. Similar to the S1 binder, WGFDE, FGED, WFGD, WGED, WFED, WED, WGD, WFD, GED, FED, FGD, WD, GD, FD and DE exhibited consistent dispersion component for S2, S3 and S4 binders. However, the WF probe liquid set did not result in consistent result for S2, S3 and S4 binders, hence, is not expected to produce consistent energy parameters.

Therefore, the above mentioned 15 probe liquid sets were considered in determining energy parameters using thermodynamic principles.

The polar components Γ_A^p of S1 and S4 binders from the abovementioned 15 probe liquid sets are summarized in Table 2.7. From Table 2.7, polar components of the binders were observed to vary significantly with probe liquid sets. For S1 binder, the FGED, GED, FED and FGD showed polar components of 16.91, 14.55, 80.02 and 33.06 mJ/m^2, which are significantly high for asphalt binders. The total SFE Γ_A from these probe liquid sets exhibited higher variations (from 29.81 to 95.29 mJ/m^2). The probe liquid sets with WGFDE, WFGD, WGED, WFED, WED, WGD, WFD, WD, WF, GD, FD and DE resulted in polar components Γ_A^p ranging from 0.82 to 3.11 mJ/m^2 while SFE Γ_A of the S1 binder for these 12 probe liquid sets varied from 16.00 to 18.38 mJ/m^2. Also, high polar component Γ_A^p and total SFE Γ_A were observed for the S2 binder with FGED, GED, FED and FGD probe liquid sets. For the S3 binder, probe liquid set FED showed a significantly higher value for Γ_A^p (18.33 mJ/m^2). Except for the FED and FGD probe liquid sets, the polar component Γ_A^p of the S4 binder varied from 0.20 to 6.29 mJ/m^2 among the 15 probe liquid sets. Therefore, although the abovementioned 15 probe liquid sets exhibited consistent Γ_A^d components, significant variations in the energy parameters of the binder-aggregate system can be observed due to the variation of polar component Γ_A^p and total SFE Γ_A.

2.4.2.1.2.1 Energy Parameters using the Owens-Wendt Method

Equations (2.19), (2.20) and (2.21) were used to calculate the W_{AR}, W_{ARW}^{wet} and *ER*, respectively, of different binder-aggregate systems using the Owens-Wendt

method. Table 2.8 presents the calculated W_{AR}, W_{ARW}^{wet} and *ER* values of S1 and S4 binders with the limestone aggregate. Variations in W_{AR} and W_{ARW}^{wet} for the same binder with different probe liquid sets were observed from Table 2.8. For example, the W_{AR} for S1 binder was found to vary from 44.38 to 167.25 mJ/m^2. Similar to W_{AR} and W_{ARW}^{wet}, the *ER* values exhibited significant variations among probe liquid sets for the same binder. The *ER* value of S1 binder varied from 0.81 to 13.14. Similar results were observed for the other binders. From Table 2.8, it was observed that a number of probe liquid sets resulted in very similar energy ratios. For example, WGFDE, WFGD, WGED, WFED, WGD, WD, WF, and FD resulted in consistent *ER* values with variation less than ±3% for the S1 binder and limestone aggregate system. However, probe liquid sets to obtain consistent *ER* value were found to vary among the tested binders. In all tested binders, WGFDE, WGED and WFED resulted in consistent *ER* values with a variation of less than ±3%. Therefore, WGFDE, WGED and WFED probe liquid sets can be used for determining consistent SFE components of binders using the Owens-Wendt method.

$$W_{AR}(Owens-Wendt) = 2\sqrt{\Gamma_A^d\Gamma_R^d} + \sqrt{\Gamma_A^P\Gamma_R^P} \qquad (2.19)$$

$$W_{ARW}^{wet}(Owens-Wendt) = 2\left(\sqrt{\Gamma_A^d\Gamma_W^d} + \sqrt{\Gamma_A^P\Gamma_W^P} + \sqrt{\Gamma_R^d\Gamma_W^d} + \sqrt{\Gamma_R^P\Gamma_W^P} - \sqrt{\Gamma_A^d\Gamma_R^d} - \sqrt{\Gamma_R^P\Gamma_W^P} - \Gamma_w\right) \qquad (2.20)$$

$$ER\ (Owens-Wendt) = \left|\frac{\sqrt{\Gamma_A^d\Gamma_R^d}+\sqrt{\Gamma_A^P\Gamma_R^P}}{\sqrt{\Gamma_A^d\Gamma_W^d}+\sqrt{\Gamma_A^P\Gamma_W^P}+\sqrt{\Gamma_R^d\Gamma_W^d}+\sqrt{\Gamma_R^P\Gamma_W^P}-\sqrt{\Gamma_A^d\Gamma_R^d}-\sqrt{\Gamma_R^P\Gamma_W^P}-\Gamma_w}\right| \qquad (2.21)$$

2.4.2.1.3 Wu Method

The Wu method (Wu, 1971; Wu, 1973) is also based on the principle that the total SFE of a solid surface can be divided into dispersion and polar component, similar

to the Owens-Wendt method. However, Wu (1971, 1973) used harmonic means of interfacial interactions instead of a geometric means. Similar to the Owens-Wendt method, 26 different sets of probe liquids were used to determine the dispersion and polar components of the tested binders. Table 2.9 presents the Γ_A^d and Γ_A^p SFE components for the S1 and S4 binders obtained from the Wu method. The SFE components obtained from the Wu method were observed to be different than those of the Owens-Wendt method. For example, SFE Γ_A from WGFDE probe liquid set was 16.03 mJ/m^2 from the Owens-Wendt method, whereas 21.63 mJ/m^2 from the Wu method. However, similar to the OW method, WGFDE, FGED, WFGD, WGED, WFED, WED, WGD, WFD, GED, FED, FGD, WD, GD, FD and DE resulted in consistent dispersion component values for all four binders. For example, Γ_A^d of the S1 binder for the abovementioned probe liquid sets was found to vary between 18.86 and 19.30 mJ/m^2, which falls within ±3% variation among themselves. Therefore, these probe liquid sets were used to calculate energy parameters of the binders with a limestone aggregate.

2.4.2.1.3.1 Energy Parameters using the Wu Method

The W_{AR}, W_{ARW}^{wet} and *ER* of the binder-aggregate systems from the Wu method were calculated using Equations (2.22), (2.23) and (2.24), respectively, and are presented in Table 2.10. Similar to the OW method, the W_{AR}, W_{ARW}^{wet} and *ER* were found to vary significantly with probe liquid sets. Also, the probe liquid sets with consistent energy parameters were found to vary with binder. Among all probe liquid sets, WGFDE, WFGD and WFED produced consistent energy ratios for all four binders with a limestone aggregate. Therefore, considering consistency, WGFDE, WFGD and

WFED were found to be a good candidate for determining the SFE components of binders using the Wu method.

$$W_{AR}(Wu) = 2\left(\frac{\Gamma_A^d\Gamma_R^d}{\Gamma_A^d+\Gamma_R^d} + \frac{\Gamma_A^d\Gamma_R^d}{\Gamma_A^d+\Gamma_R^d}\right) \quad (2.22)$$

$$W_{ARW}^{wet}(Wu) = 2\left(\frac{\Gamma_A^d\Gamma_W^d}{\Gamma_A^d+\Gamma_W^d} + \frac{\Gamma_A^P\Gamma_W^P}{\Gamma_A^P+\Gamma_W^P} + \frac{\Gamma_R^d\Gamma_W^d}{\Gamma_R^d+\Gamma_W^d} + \frac{\Gamma_R^P\Gamma_W^P}{\Gamma_R^P+\Gamma_W^P} - \frac{\Gamma_A^d\Gamma_R^d}{\Gamma_A^d+\Gamma_R^d} - \frac{\Gamma_R^P\Gamma_W^P}{\Gamma_R^P+\Gamma_W^P} - \frac{\Gamma_w}{2}\right) \quad (2.23)$$

$$ER\ (Wu) = \left|\frac{\frac{\Gamma_A^d\Gamma_R^d}{\Gamma_A^d+\Gamma_R^d}+\frac{\Gamma_A^d\Gamma_R^d}{\Gamma_A^d+\Gamma_R^d}}{\frac{\Gamma_A^d\Gamma_W^d}{\Gamma_A^d+\Gamma_W^d}+\frac{\Gamma_A^P\Gamma_W^P}{\Gamma_A^P+\Gamma_W^P}+\frac{\Gamma_R^d\Gamma_W^d}{\Gamma_R^d+\Gamma_W^d}+\frac{\Gamma_R^P\Gamma_W^P}{\Gamma_R^P+\Gamma_W^P}-\frac{\Gamma_A^d\Gamma_R^d}{\Gamma_A^d+\Gamma_R^d}-\frac{\Gamma_R^P\Gamma_W^P}{\Gamma_R^P+\Gamma_W^P}-\frac{\Gamma_w}{2}}\right| \quad (2.24)$$

2.4.2.2 Equation of State (EOS) Approach

2.4.2.2.1 Neumann Method

As noted earlier, the Neumann method of SFE determination is based on the equation of state approach which disqualifies the separation of SFE into smaller components. According to the Neumann method, the interfacial free energy is a function of surface tension of probe liquid and the solid surface free energy, as shown in Equation (2.13). Neumann and his colleagues proposed Equation (2.14) to determine SFE components of solid surfaces (Neumann et al., 1974; Li and Neumann, 1990; Li and Neumann, 1992). The constants β and Γ_S in Equation (2.14) can be determined by a multi-variable optimization using a least-square technique for a given set of Γ_L and θ, measured for different probe liquids on a solid surface. Li and Neumann (1990, 1992) conducted a series of tests on polymeric surfaces and found the weighted average of β as 0.000125 $(mJ/m^2)^{-2}$ (Li and Neumann, 1990; Li and Neumann, 1992). However, β is expected to be different for a binder as the surface is chemically and physically different than a polymeric surface. Therefore, in this study, β was considered as a variable equation parameter. The Γ_L and contact angles (θ) of water, glycerol, formamide,

ethylene glycol and diiodomethane were used to determine the Γ_A component of all binders. Figure 2.3 shows the plot of $\Gamma_L cos\theta$ versus Γ_L for S1, S2, S3 and S4 binders. The curved lines in Figure 2.3 represent the model fitting using the Neumann method. Table 2.11 presents the β and Γ_A obtained from the Neumann method. The β parameter was found to vary between 0.000029 to 0.000149 $(mJ/m^2)^{-2}$ for different binders. This variation is expected to arise from the difference in surface composition for different binders. Table 2.12 presents the differences in measured and predicted contact angles from the Neumann method. It was observed that the differences between the measured and predicted contact angles are less than 3°. A contact angle variation of 1- 3° from the Neumann model was reported by other studies (Kwok, 1998; Tavana and Neumann, 2007). This indicates good fittings of the Neumann model for all binders. The Γ_A values for S1, S2, S3 and S4 binder were 21.16, 16.92, 10.87 and 18.02 mJ/m^2, respectively, which are different from the Γ_A components obtained from the GvOC, Owens-Wendt and Wu methods. This variation among different SFE estimation method is discussed in the following section. The W_{AR}, W_{ARW}^{wet} and *ER* from the Neumann method are calculated using Equations (2.25), (2.26) and (2.27), respectively, and presented in Table 2.13. From Table 2.13, the S1 binder exhibited the highest whereas the S3 binder exhibited the lowest W_{AR} and *ER* among all the binders.

$$W_{AR}(Neumann) = \sqrt{\Gamma_A \Gamma_R} \tag{2.25}$$

$$W_{ARW}^{wet} = \sqrt{\Gamma_A \Gamma_W} + \sqrt{\Gamma_R \Gamma_W} - \sqrt{\Gamma_A \Gamma_R} - \Gamma_w \tag{2.26}$$

$$ER\ (Neumann) = \left| \frac{\sqrt{\Gamma_A \Gamma_R}}{\sqrt{\Gamma_A \Gamma_W} + \sqrt{\Gamma_R \Gamma_W} - \sqrt{\Gamma_A \Gamma_R} - \Gamma_w} \right| \tag{2.27}$$

2.4.3 Comparison of Surface Free Energy Estimation Methods

Table 2.14 presents the %difference in Γ_A SFE component of the component-based approaches (the GvOC, Owens-Wendt and Wu methods) from the Neumann method. Only probe liquid sets with consistent energy parameters from different methods were considered and are presented in Table 2.14. It was observed that the differences in total SFE Γ_A between the GvOC and Neumann methods can vary from 0.4 to 24.4%. Similar variations were observed for the Owens-Wendt method as both of these methods resulted in same total SFE for identical probe liquid sets. The Wu method was found to produce highest variation with the Neumann method. A variation of 53.5% was obtained for the S3 binder while the SFE Γ_A was calculated using the Wu method. Differences in the mathematical formulation used by different method are responsible for these variations.

Table 2.15 presents a ranking of the binder-limestone aggregate systems using *ER* values from different SFE estimation methods. A higher value of *ER* is expected to reduce moisture-induced damage potential of an asphalt mix. In Table 2.15, ranking 1 was used to represent the highest and ranking 4 to indicate the lowest *ER* value among the binder-aggregate systems. Therefore, the binder-aggregate system ranked 1 will be less susceptible, whereas the binder-aggregate system ranked 4 will be most susceptible to moisture-induced damage. It was found that WGFDE, WGED and WFED provided similar ranking using the GvOC method. Based on these probe liquid sets, S1, S4, S2 and S3 binders were ranked as 1st, 2nd, 3rd and 4th, respectively. Similar ranking was observed from the Neumann method as well. The WGFDE, WGED and WFED probe liquid set from the Owens-Wendt method provided slightly different ranking among

themselves. In the Owens-Wendt method, the WGFDE and WFED ranked the S1, S2, S3 and S4 binders as 1st, 2nd, 4th and 3rd, respectively. Also, the WGED probe liquid set ranked S1, S2, S3 and S4 binders as 2nd, 1st, 4th and 3rd, respectively. The WGFDE and WFED probe liquid sets exhibited a similar ranking of the binder-aggregate systems for the Wu method and the Owens-Wendt method. However, the Owens-Wendt method and the Wu methods ranked the binders differently than the Neumann method. Therefore, differences in the ranking of the moisture-induced damage potential of binder-aggregate system are expected from the use of different SFE estimation methods.

2.5 CONCLUSIONS

The purpose of this study was to understand the differences in the surface free energy estimation of binders using different methods, namely the GvOC, Owens-Wendt, Wu and Neumann methods. Also, the effect of probe liquid sets on the calculation of SFE components by the GvOC, Owens-Wendt and Wu method were evaluated. Furthermore, attempts were made to identify the probe liquid sets that produce consistent energy parameters for a binder-aggregate system. The specific findings from this study are summarized below.

i. Different SFE estimation methods were found to characterize binders differently. The differences in the SFE yielded from the assumptions and mathematical formulations used by different methods. The difference in the SFE was found to be reflected in the energy parameters of the binder-aggregate system. Therefore, the selection of binder-aggregate combination with respect to moisture susceptibility will be influenced by the choice of SFE estimation methods.

ii. Significant differences were observed in the SFE components of the same binder with different probe liquid sets from the GvOC methods. It was observed that, the FGED, GED, GEF, FED, WGE and FGD sets could lead to negative square root of SFE components of binders. A higher value of condition number obtained for these probe liquid sets pointed toward the ill-conditioning of the equation sets from these probe liquid sets. Also, for the GvOC method, inclusion of water and diiodomethane was found to be necessary for proper conditioning of the equation sets with at least one or more probe liquid(s). Over-determined probe liquid sets with SFE components determined by minimized the sum of the square error was more likely to yield constant results. Incorporation of ethylene glycol resulted in higher acid components of the binders, whereas formamide and glycerol resulted in higher basic components.

iii. The WGFDE, WGDE and WFDE probe liquid sets were found to provide consistent energy parameters for the GvOC method. Similar probe liquid sets are expected to produce consistent energy parameter for the OW method as well. In case of the Wu method, the WGFDE, WFGD and WFED probe liquid sets can be used to obtain consistent SFE of binders.

iv. Among different component-based approaches, only the GvOC method was found to characterize asphalt mixes similar to the Neumann method. Therefore, the GvOC method with WGFDE, WGDE and WFDE probe liquid sets is expected to provide a better evaluation of the moisture-induced potential of asphalt mixes.

Table 2.1 Surface Free Energy Components of the Probe Liquids at 20°C (Hefer et al., 2006)

Probe Liquid	Γ_L (mJ/m^2)	Γ_L^{LW} (or Γ_L^d) (mJ/m^2)	Γ_L^+ (mJ/m^2)	Γ_L^- (mJ/m^2)	Γ_L^{AB} (or Γ_L^p) (mJ/m^2)
Water (W)	72.8	21.8	25.5	25.5	51.0
Glycerol (G)	64.0	34.0	3.92	57.4	30.0
Formamide (F)	58.0	39.0	2.28	39.6	19.0
Ethylene glycol (E)	48.0	29.0	1.92	47.0	19.0
Diiodomethane (D)	50.8	50.8	0.0	0.0	0.0

Table 2.2 Contact Angles of Binders with Different Probe Liquids

Binder	Contact Angles (°)									
	Water		Glycerol		Formamide		Diiodomethane		Ethylene Glycol	
	Avg	SD	Avg	SD	Avg	SD	Avg	SD	Avg	SD
S1	107.5	0.70	94.4	0.07	90.6	0.22	84.5	0.97	78.6	0.21
S2	106.1	0.69	98.3	0.83	95.7	0.40	86.3	1.10	85.8	0.26
S3	107.2	2.00	105.5	0.78	101.2	1.94	96.3	1.14	94.1	0.31
S4	109.1	0.30	99.2	0.40	95.9	0.60	86.5	0.20	85.8	0.57

Table 2.3 Surface Free Energy Components of S1 and S4 Binders from GvOC Method

Probe liquid set	S1 Binder						S4 Binder					
	SFE Components (mJ/m^2)				Γ_A^+/Γ_A^-	R^2	SFE Components (mJ/m^2)				Γ_A^+/Γ_A^-	R^2
	Γ_A^+	Γ_A^-	Γ_A^{LW}	Γ_A			Γ_A^+	Γ_A^-	Γ_A^{LW}	Γ_A		
WGFDE	0.62	0.43	15.00	16.03	1.46	0.95	0.32	0.45	14.02	14.77	0.70	0.98
FGED	3.84	18.63*	15.00	31.91	0.21	0.98	0.64	0.84*	14.08	15.54	0.76	0.97
WFGE	3.40	0.65	6.59	9.56	5.26	0.96	3.16	0.73	5.06	8.10	4.30	0.90
WFGD	0.37	0.72	15.11	16.15	0.52	0.93	0.08	1.22	14.12	14.73	0.06	0.98
WGED	0.76	0.29	15.29	16.23	2.63	0.96	0.40	0.38	14.37	15.15	1.06	0.98
WFED	0.68	0.39	14.96	16.00	1.72	0.99	0.37	0.44	13.95	14.76	0.84	0.99
WED	1.09	0.15	15.27	16.08	7.07	1.00	0.62	0.32	14.30	15.19	1.93	0.99
WGD	0.49	0.53	15.27	16.29	0.93	0.93	0.15	0.93	14.30	15.05	0.16	0.99
WFD	0.20	0.97	15.27	16.15	0.21	0.98	0.01	1.63	14.30	14.49	0.00	1.00
WFG	1.73	0.83	9.30	11.70	2.09	0.95	1.29	1.40	7.49	10.18	0.92	0.97
WFE	7.49	0.62	2.72	7.02	12.14	0.99	5.08	1.17	2.67	7.56	4.32	1.00
GED	3.60	14.71*	15.27	29.81	0.24	0.98	1.64	6.01*	14.30	20.58	0.27	0.98
GEF	9.17	17.61*	6.55	31.97	0.52	0.99	6.16	8.04*	5.53	19.60	0.77	0.99
FED	11.97	133.78*	15.27	95.29	0.09	0.96	8.69	116.53*	14.49	78.15	0.07	0.95
WGE	37.52*	1.62*	181.19	196.80	23.13	0.95	22.25*	0.29*	119.36	124.42	77.45	0.97
FGD	2.82*	96.95	15.27	48.32	0.03	1.00	6.30*	145.52	14.30	74.87	0.04	1.00

*Indicates negative square root of SFE components

Table 2.4 Condition Number of Different Probe Liquid Sets

Probe liquid set	**WGFDE**	**FGED**	**WFGE**	**WFGD**	**WGED**	**WFED**	**WED**	**WGD**
Condition number	5.50	56.48	19.81	5.28	4.97	4.93	4.47	4.90
Probe liquid set	**WFD**	**WFG**	**WFE**	**GED**	**GEF**	**FED**	**WGE**	**FGD**
Condition number	5.17	18.66	20.75	47.70	54.10	79.87	139.16	142.67

Table 2.5 Surface Free Energy Components of Limestone aggregate

Aggregate	Γ_R^+	Γ_R^-	Γ_R^{LW} *or* Γ_R^d	Γ_R^P	Γ_R
Limestone Aggregate	33.78	416.94	56.73	237.37	294.10

Table 2.6 Energy Parameters of Binder-Aggregate Systems from GvOC Methods

Binder	**Probe Liquid Sets**	**WGFDE**	**WFGD**	**WGED**	**WFED**	**WED**	**WGD**	**WFD**
S1	W_{AR} (mJ/m^2)	98.17	93.32	100.80	99.20	105.98	96.08	88.59
	W_{ARW}^{wet} (mJ/m^2)	-142.22	-147.35	-139.62	-141.24	-134.65	-144.55	-152.04
	ER	0.69	0.63	0.72	0.70	0.79	0.66	0.58
S2	W_{AR} (mJ/m^2)	87.26	82.82	89.59	86.29	92.96	86.70	78.14
	W_{ARW}^{wet} (mJ/m^2)	-156.89	-159.49	-152.50	-155.75	-149.46	-155.51	-164.56
	ER	0.56	0.52	0.59	0.55	0.62	0.56	0.47
S3	W_{AR} (mJ/m^2)	79.07	75.72	80.29	80.76	84.64	76.33	74.68
	W_{ARW}^{wet} (mJ/m^2)	-161.70	-165.24	-160.49	-160.09	-156.31	-164.63	-166.28
	ER	0.49	0.46	0.50	0.50	0.54	0.46	0.45
S4	W_{AR} (mJ/m^2)	87.15	80.72	90.16	88.76	95.67	84.08	74.96
	W_{ARW}^{wet} (mJ/m^2)	-149.94	-157.97	-147.52	-148.61	-142.96	-154.55	-163.67
	ER	0.58	0.51	0.61	0.60	0.67	0.54	0.46

Table 2.7 Surface Free Energy Components of S1 and S4 Binders from Owens-Wendt Method

Test liquid set	S1 Binder			S4 Binder		
	SFE Components (mJ/m^2)			SFE Components (mJ/m^2)		
	Γ_A^p	Γ_A^d	Γ_A	Γ_A^p	Γ_A^d	Γ_A
WGFDE	1.03	15.00	16.03	0.76	14.02	14.77
FGED	16.91	15.00	31.91	1.46	14.08	15.54
WFGE	2.97	6.59	9.56	3.05	5.06	8.10
WFGD	1.03	15.11	16.15	0.61	14.12	14.73
WGED	0.94	15.29	16.23	0.78	14.37	15.15
WFED	1.04	14.96	16.00	0.80	13.95	14.76
WED	0.82	15.27	16.08	0.89	14.30	15.19
WGD	1.03	15.27	16.29	0.75	14.30	15.05
WFD	0.88	15.27	16.15	0.20	14.30	14.49
WFG	2.40	9.30	11.70	2.69	7.49	10.18
WFE	4.30	2.72	7.02	4.88	2.67	7.56
GED	14.55	15.27	29.81	6.29	14.30	20.58
GEF	25.42	6.55	31.97	14.08	5.53	19.60
FED	80.02	15.27	95.29	63.65	14.49	78.15
WGE	15.60	181.19	196.80	5.06	119.36	124.42
FGD	33.06	15.27	48.32	60.58	14.30	74.87
WD	1.03	15.27	16.29	0.92	14.30	15.21
WF	1.07	15.00	16.07	1.68	10.65	12.33
WG	0.43	19.81	20.24	1.14	13.05	14.19
WE	0.03	27.00	27.03	0.41	18.18	18.59
GF	3.84	10.42	14.26	3.43	8.26	11.69
GD	1.53	15.27	16.80	0.79	14.30	15.08
GE	4.18	48.85	53.03	1.67	33.97	35.64
FD	0.97	15.27	16.24	0.31	14.30	14.60
FE	44.00	0.00	44.00	30.50	0.10	30.60
DE	3.11	15.27	18.38	1.53	14.30	15.83

Table 2.8 Energy Parameters of Binder-Aggregate Systems from Owens-Wendt Method

Test liquid set	S1 Binder			S4 Binder		
	W_{AR} (mJ/m^2)	W_{ARW}^{wet} (mJ/m^2)	ER	W_{AR} (mJ/m^2)	W_{ARW}^{wet} (mJ/m^2)	ER
WGFDE	44.82	52.91	0.85	41.60	54.49	0.76
FGED	92.52	27.31	3.39	46.89	51.66	0.91
WFGD	44.95	52.86	0.85	40.33	55.18	0.73
WGED	44.38	53.19	0.83	42.16	54.24	0.78
WFED	44.81	52.91	0.85	41.95	54.29	0.77
WED	43.35	53.74	0.81	43.02	53.77	0.80
WGD	45.05	52.83	0.85	41.83	54.41	0.77
WFD	43.90	53.44	0.82	35.34	57.89	0.61
GED	88.19	29.68	2.97	67.11	40.84	1.64
FED	167.25	-12.73	13.14	151.59	-4.45	34.08
FGD	118.01	13.69	8.62	148.39	-2.76	53.75
WD	45.05	52.83	0.85	43.22	53.66	0.81
GD	48.49	50.98	0.95	42.15	54.23	0.78
FD	44.64	53.05	0.84	37.01	56.99	0.65
DE	56.61	46.63	1.21	47.54	51.34	0.93

Table 2.9 Surface Free Energy Components of S1 and S4 Binders from Wu Method

Test liquid set	S1 Binder			S4 Binder		
	SFE Components (mJ/m^2)			SFE Components (mJ/m^2)		
	Γ_A^p	Γ_A^d	Γ_A	Γ_A^p	Γ_A^d	Γ_A
WGFDE	2.70	18.93	21.63	1.86	17.80	19.66
FGED	2.66	18.96	21.62	1.41	18.16	19.57
WFGE	3.80	16.70	20.51	4.88	12.44	17.32
WFGD	2.52	18.90	21.41	1.81	17.80	19.60
WGED	2.83	19.27	22.10	2.04	18.15	20.19
WFED	2.65	18.91	21.56	1.85	17.80	19.65
WED	2.89	19.30	22.19	2.17	18.23	20.40
WGD	2.70	19.20	21.90	2.09	18.17	20.26
WFD	2.35	18.86	21.20	1.77	17.79	19.56
WFG	3.93	16.05	19.98	5.04	12.03	17.07
WFE	3.82	16.49	20.31	4.88	12.33	17.21
GED	3.00	19.18	22.18	1.71	18.33	20.04
GEF	8.13	11.48	19.60	7.61	9.59	17.20
FED	2.54	18.98	21.52	1.24	18.18	19.41
WGE	2.20	20.88	23.08	3.84	14.40	18.23
FGD	2.28	19.06	21.34	2.56	17.66	20.22
WD	2.67	19.18	21.85	2.39	18.34	20.73
WF	4.01	15.40	19.41	5.09	11.69	16.79
WG	2.54	19.62	22.16	4.01	14.00	18.01
WE	1.44	23.66	25.10	3.68	14.80	18.47
GF	8.12	11.13	19.26	7.71	9.33	17.04
GD	2.75	19.18	21.93	1.62	18.34	19.96
GE	3.48	18.23	21.71	3.10	15.61	18.71
FD	1.62	19.18	20.80	0.56	18.34	18.89
FE	47.31	0.82	48.13	17.25	4.42	21.67
DE	3.31	19.18	22.49	1.80	18.34	20.14

Table 2.10 Energy Parameters of Binder-Aggregate Systems from Wu Method

Test liquid set	S1 Binder			S4 Binder		
	W_{AR} (mJ/m^2)	W_{ARW}^{wet} (mJ/m^2)	ER	W_{AR} (mJ/m^2)	W_{ARW}^{wet} (mJ/m^2)	ER
WGFDE	16.86	17.16	0.98	15.39	17.53	0.88
FGED	16.84	17.16	0.98	15.16	17.45	0.87
WFGD	16.67	17.18	0.97	15.34	17.53	0.87
WGED	17.18	17.06	1.01	15.77	17.42	0.91
WFED	16.80	17.17	0.98	15.39	17.53	0.88
WED	17.25	17.04	1.01	15.95	17.39	0.92
WGD	17.01	17.09	1.00	15.83	17.41	0.91
WFD	16.48	17.21	0.96	15.30	17.54	0.87
GED	17.29	17.07	1.01	15.55	17.39	0.89
FED	16.73	17.16	0.98	14.99	17.45	0.86
FGD	16.52	17.16	0.96	16.00	17.52	0.91
WD	16.98	17.09	0.99	16.22	17.35	0.94
GD	17.05	17.09	1.00	15.47	17.39	0.89
FD	15.95	17.16	0.93	14.41	17.43	0.83
DE	17.60	17.04	1.03	15.64	17.38	0.90

Table 2.11 Surface Free Energy of Binders using Neumann Method

Binder	S1	S2	S3	S4
β	0.000149	0.000091	0.000029	0.000125
Γ_A (mJ/m^2)	21.16	16.92	10.87	18.02

Table 2.12 Differences in Measured and Predicted Contact Angles from Neumann Method

Probe Liquid	Change in Contact Angle, |Δθ| (°)			
	S1 Binder	S2 Binder	S3 Binder	S4 Binder
Water	1.47	0.17	0.86	0.66
Glycerol	2.81	0.90	1.57	1.53
Formamide	0.17	1.40	0.33	0.88
Ethylene glycol	0.25	0.79	0.82	1.26
Methylene Iodide	2.08	1.47	0.39	1.13

Table 2.13 Energy Ratios of Binder-Aggregate Systems from Neumann Method

Binder	S1	S2	S3	S4
W_{AR} (mJ/m^2)	78.89	70.54	56.55	72.80
W_{ARW}^{wet} (mJ/m^2)	33.88	38.08	45.11	36.94
ER	2.32	1.85	1.25	1.97

Table 2.14 %Difference in Γ_A SFE component with Respect to Neumann's Method

Binder	%Difference in Total SFE from Neumann Method								
	GvOC			OW			Wu		
	WGFDE	WGED	WFED	WGFDE	WGED	WFED	WGFDE	WFGD	WFED
S1	24.2	23.3	24.4	24.2	23.3	24.4	2.2	1.2	1.9
S2	5.6	3.1	6.2	5.6	3.1	6.2	17.6	18.0	17.9
S3	0.4	1.8	0.9	0.4	1.8	0.9	51.0	53.0	53.5
S4	18.0	15.9	18.1	18.0	15.9	18.1	9.1	8.8	9.1

Table 2.15 Susceptibility to Moisture-Induced Damage by Different SFE Method

(Least = 1, Most = 4)

Binder	GvOC			OW			Wu			Neumann
	WGFDE	WGED	WFED	WGFDE	WGED	WFED	WGFDE	WFGD	WFED	WGFDE
S1	1	1	1	1	2	1	1	1	1	1
S2	3	3	3	2	1	2	2	2	2	3
S3	4	4	4	4	4	4	4	4	4	4
S4	2	2	2	3	3	3	3	3	3	2

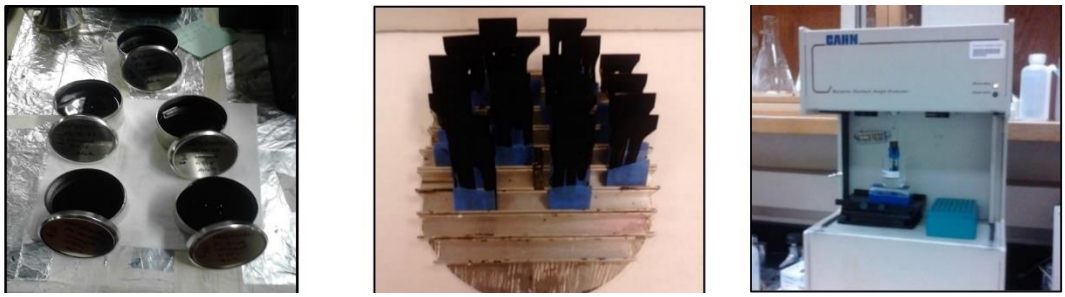

(a) (b) (c)

Figure 2.1 Contact angle measurement using DWP test: (a) asphalt binder used for testing; (b) binder coated glass plates; and (c) DWP test setup

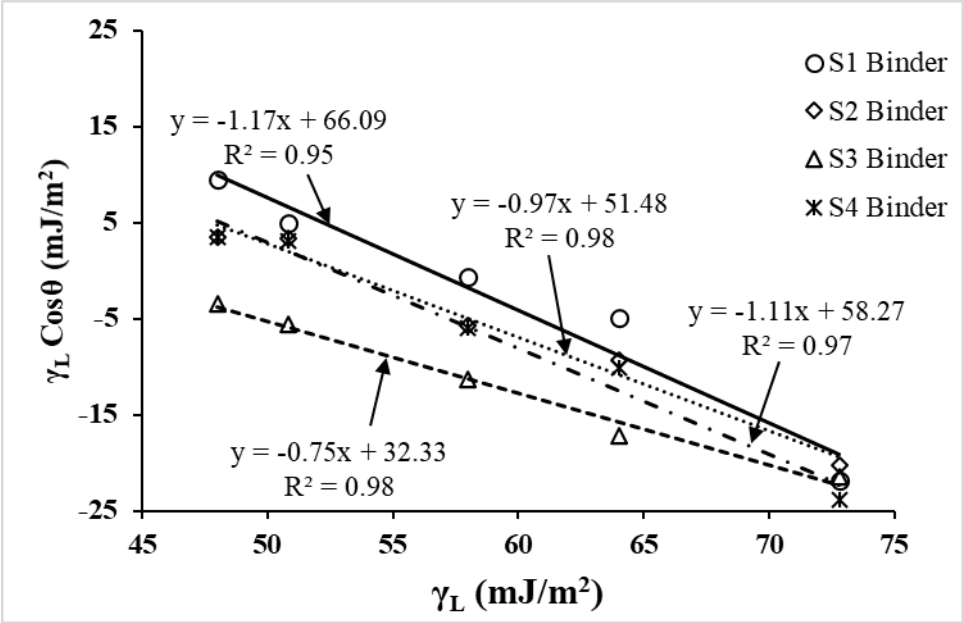

Figure 2.2 The Γ_L versus $\Gamma_L cos\theta$ plot for WGFDE probe liquid set

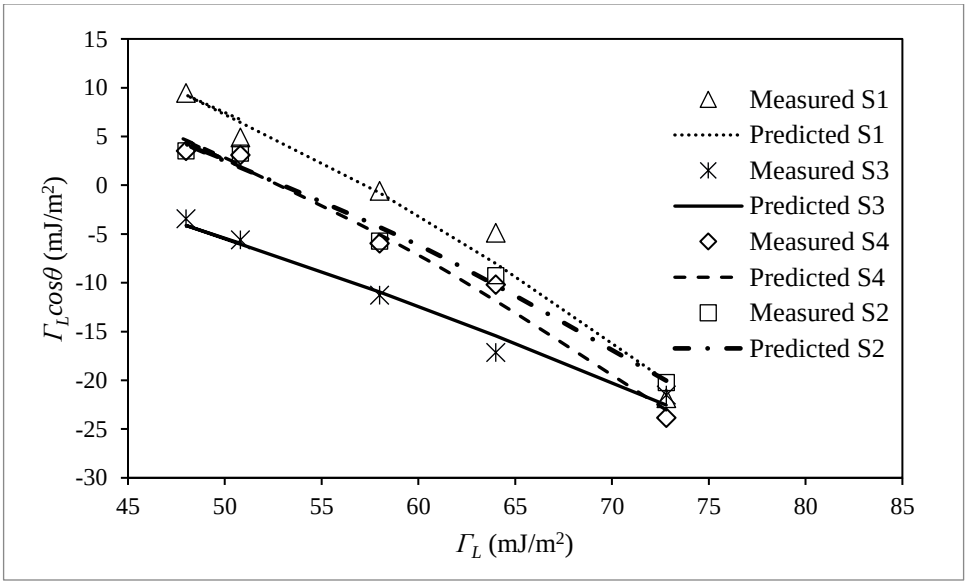

Figure 2.3 The Γ_L versus $\Gamma_L cos\theta$ plot of binders using Neumann model

CHAPTER

3

MICRO-STRUCTURAL EVALUATION OF THE EFFECTS OF AGGREGATE TYPE, AGING AND ADDITIVES ON THE MOISTURE SUSCEPTIBILITY OF BINDER-AGGREGATE SYSTEMS USING CHEMICAL AND THERMODYNAMIC APPROACHES[2]

ABSTACT

Selection of a proper binder-aggregate combination is an important step to ensure optimum resistance to moisture-induced damage in asphalt mixes. In recent years, such selection has become more crucial as the asphalt industries are using various additives and modifiers in asphalt mixes that can substantially change bonding strength of a binder-aggregate system. Also, environmental factors such as oxidative aging can affect the chemical compositions of the binder and influence moisture-induced damage resistance of a mix. In order to understand the mechanisms of moisture-induced damage, it is important to determine the chemical and thermodynamic properties of constituent materials of a mix and identify their contributions to the bond strength. The present study was undertaken to explore the effects of aggregate types, additives and

[2] This chapter has been submitted to the International Journal of Adhesions and Adhesives under the title "Micro-Structural Evaluation of the Effects of Aggregate Type, Aging and Additives on the Moisture Susceptibility of Binder-Aggregate Systems using Chemical and Thermodynamic Approaches." The current version has been formatted for this dissertation.

aging on the moisture susceptibility of asphalt mixes using chemical and thermodynamic approaches. For this purpose, a PG 64-22 and a PG 76-28 binder were blended with a warm mix asphalt (WMA) additive, an antistripping agent (ASA), a reclaimed asphalt pavement (RAP) binder and a polyphosphoric acid (PPA). The surface free energy components of these binder blends under unaged, short-term and long-term aged conditions were determined using a dynamic Wilhelmy plate (DWP) test. The chemical analyses of the binder blends were carried out using an X-ray fluorescence (XRF) analyzer and a Fourier transform infrared (FTIR) spectroscopy. The properties of five commonly available local aggregates were determined using XRF and universal sorption device (USD) test. The SFE components of the binders and aggregates were used to quantify bonding characteristics of binder-aggregate systems under dry and wet conditions. The properties of aggregates exhibited significant influence on the moisture-induced damage potential of a mix. Also, an increase in carbonyl and sulfoxide functional groups were found responsible for increased moisture susceptibility with aging. The presence of amine group in both WMA and ASA is expected to enhance, whereas presence of PPA may reduce resistance to moisture-induced damage of a binder-aggregate system.

3.1 INTRODUCTION

Intrusion of moisture and its interaction with the binder-aggregate system significantly influence the strength and durability of an asphalt pavement. Although, not a failure mode by itself, moisture plays a prominent role in increasing the severity of other distresses, such as rutting, fatigue cracking and raveling, and hence affect the performance of asphalt pavements (Al-Qadi et al., 2008; Kringos et al., 2008; Othman,

2009; Xiao et al., 2010a). A large portion of the state's pavement maintenance cost and vehicle user cost is directly related to the pavement damage related to moisture damage (Caro et al., 2008a). Typically, two types of failure can be caused by moisture intrusion in asphalt pavements: adhesive failure between binder and aggregate, and cohesive failure within the binder and mastic (Bhasin, 2007; Copeland et al., 2007; Wasiuddin et al., 2007c). Several factors can affect the moisture-induced damage of an asphalt mix. Some of these factors are directly related to the physical and chemical properties of the aggregate and binder used in the mix (Shu et al., 2012; Doyle and Howard, 2013; Tong et al., 2015). Other factors, such as traffic conditions, type and properties of additives/modifiers, drainage, air void level, permeability and film thickness were found important to realize asphalt mix's response to moisture. Also, environmental factors, such as pavement aging, temperature and freeze-thaw cycles can significantly influence the performance of an asphalt mix related to moisture-induced damage (Stuart, 1990; Gorkem and Sengoz, 2009).

Understanding properties of binder and aggregate is important for the evaluation of moisture-induced damage as their interactions significantly affect the bonding strength of an asphalt mix (Abo-Qudais and Al-Shweily, 2007; Shu et al., 2012; Doyle and Howard, 2013; Tong et al., 2015; Baldi-Sevilla et al., 2017). Typically, asphalt binder is a mixture of hydrocarbons with some polar functionalities. Also, organometallic constituents that contain metals such as nickel, vanadium, and iron may be present in binder (Curtis et al., 1993; Jahromi, 2009; Hofko et al., 2018). Aggregate constitutes approximately 95% of an asphalt mix by weight. Aggregate characteristics such as cleanliness, surface texture, minerology, porosity, surface charge and energy,

and polarity can significantly influence the moisture susceptibility of a mix (Johnson and Freeman, 2002; Cui et al., 2014). According to Curtis et al. (1992), aggregate surface contains a variety of active sites of different compositions and levels of activity. When an aggregate is coated with binder, selective adsorption of some components of binder, such as the polar functionalities of the binder takes place on the aggregate surface and hydrogen bonds or salt links are formed (Tarrer and Wagh, 1991). Association of aggregate and binder with different polarities is needed to ensure strong bonding (Curtis et al., 1993; Haider et al., 2020). In reality, aggregates for an asphalt pavement are selected based on their local availability. Therefore, a wide variation in aggregate composition, surface chemistry and morphology are possible which can affect the moisture-induced damage performance of a mix. Several studies have reported that asphalt mixes with aggregates of an acidic nature have less adhesion properties than basic aggregates (Kalantar et al., 2012; Tong et al., 2015; Behnood and Gharehveran, 2019; Haider et al., 2020). Generally, aggregate rich in silica (SiO_2) exhibits acidic behavior. Also, aggregates with high silica content exhibit hydrophilic or water loving behavior (Tarrer and Wagh, 1991). The high hydrophilicity of an aggregate may increase moisture-induced damage potential, if the adhesion bonding between binder and aggregate is not strong enough in both dry and wet states. On the other hand, calcareous aggregates, such as limestone generally show good bonding quality (Curtis et al., 1993). However, variation in performance is possible due to the variation in surface chemistry and chemical compositions. In this study, the chemical and thermodynamic properties of locally available aggregates were determined and their influence on the bonding strength of binder-aggregate system were investigated.

3.1.1 Effect of Aging

Environmental factors such as aging can alter the chemical and physical properties of a binder leading to a modification of the rheological and chemical properties of the binder (Martin et al., 1990; Zhang et al., 2018; Liu et al., 2019). Binder reacts with atmospheric oxygen during the aging process, and leads to the creation of several oxidized chemical species, such as carbonyl (C=O) (e.g. carboxylic acid (COOH) and ketone) and sulfoxide (S=O) functional groups (Curtis et al., 1993; Lu et al., 2008). These modifications can lead to changes in the performance properties of the asphalt mix. Curtis et al. (1993) reported that the sulfoxides and carboxylic acids functional group exhibited high affinity for the aggregate surface. However, as both sulfoxides and carboxylic acids form moieties on the aggregate surface which are highly soluble in water, the presence of these functional groups may increase moisture susceptibility as well. Therefore, characterization of the effects of aging on the binder composition is important to predict pavement performance, especially resistance to moisture-induced damage. Several methods are available to determine the chemical compositions of binders. However, the use of Fourier transform infrared (FTIR) spectroscopy is gaining attention for chemical analysis of asphalt binders due to its simplicity in sample preparation and testing (Mothé et al., 2008; Hofko et al., 2018; Arafat et al., 2020). A number of studies have shown that the absorbance values from FTIR can be used to indicate the aging extent of different functional groups, such as sulfoxides and carbonyl groups (Huang and Grimes, 2010; Qin et al., 2014; Hofko et al., 2018; Ge et al., 2019; Arafat et al., 2020). In this study, FTIR spectroscopic analyses were performed to evaluate the effect of aging on chemical composition of

binder. The results were used to understand the effect of these changes on the moisture susceptibility of asphalt mixes.

3.1.2 Effect of Additives and Modifiers

In recent years, increased traffic volume, heavier truck traffic, new axle designs and higher tire pressures have accelerated the need for enhanced performance of asphalt pavements (Isacsson and Lu, 1995; Airey, 2003). Also, the demand for sustainable and durable pavement have encouraged researchers to explore new additives and modifiers for asphalt mixes. One of the popular methods of improving mechanical and performance properties of asphalt mixes is the polymer modification of asphalt binder. Benefits associated with polymer modification include improved resistance to rutting, fatigue cracking, aging and better flexibility at low temperature (Bonemazzi et al., 1996; Airey, 2003; Kim et al., 2009). A number of commercially available elastomeric and plastomeric polymers are now being successfully used for modifying binders (Airey, 2003). However, the moisture-induced damage performance of these polymer-modified binders with different types of aggregate and aging conditions needs further evaluation. Recently, an increase in the use of polyphosphoric acid (PPA) for binder modification has been observed due to the associated reduction in manufacturing cost than polymer modification (Ge et al., 2017). The addition of PPA has been found to increase the high-temperature performance grade (PG) of the binder, improve stiffness of the mix and reduce early rutting potential of the pavement (Huang et al., 2008; Liu et al., 2016). Also, improvement in the fatigue cracking performance of asphalt mixes was reported with the addition of PPA (Martin et al., 2006; Nuñez et al., 2014). However, the performance of the PPA-modified binder in presence of moisture is a concern for

the highway agencies. An increased moisture-induced damage potential has been reported by several studies for asphalt mixes with PPA-modified binder (Orange et al., 2004; Fee et al., 2010; Al-Qadi et al., 2014).

In recent years, the warm mix asphalt (WMA) technologies are gaining popularity as they promotes sustainable and environmentally-friendly construction by reducing energy consumption and green-house gas emissions (Hurley and Prowell, 2006; Nazzal et al., 2011). The WMA technologies are capable of significantly reducing the mixing and compaction temperatures of asphalt mixes (Hurley and Prowell, 2005; Fakhri et al., 2013). Three categories of WMA technologies, namely organic additives, chemical additives, and asphalt foaming are currently available to the asphalt industries (West et al., 2014). Several studies have reported rutting and moisture-induced damage as major concerns for WMA (Xiao et al., 2010b; Mehrara and Khodaii, 2013; Kim et al., 2014).

The use of reclaimed asphalt pavement (RAP) in asphalt pavement has been found beneficial for the economy and environment as it saves construction costs by preserving natural resources (McDaniel et al., 2002; Mohammad et al., 2003; Al-Qadi et al., 2012). Improved rutting resistance of the asphalt pavement has been reported with the use of RAP (McDaniel et al., 2002; Mohammad et al., 2003; Al-Qadi et al., 2012; Ghabchi et al., 2014). However, the effect of RAP on the moisture-induced damage of asphalt pavement is not yet fully understood.

Also, several anti-stripping agents (ASA) are available commercially that may be used to improve the moisture-induced damage resistance of asphalt mixes (Wasiuddin et al., 2007a; Wasiuddin et al., 2007c; Xiao et al., 2010b; Abuawad et al.,

2015; Park et al., 2017). However, their effectiveness with respect to aggregate types and aging needs further investigation.

3.1.3 Surface Free Energy Technique

Till now, most of the evaluation procedures of moisture-induced damage have been focused on the performance of macro-structure (asphalt mix) not on the micro-structure such as binder-aggregate interface (Kanitpong and Bahia, 2005). Quantification of the bonding strength at the binder-aggregate interface under both dry state and in presence of moisture is expected to provide a better understanding of the moisture susceptibility of an asphalt mix. A number of studies have used the fundamental thermodynamic properties, such as surface free energy (SFE) to quantify the effect of moisture at the binder-aggregate-water interface (Bhasin et al., 2006; Bhasin, 2007; Bhasin et al., 2007a; Howson et al., 2007; Wasiuddin et al., 2007a; Wasiuddin et al., 2007c; Wasiuddin et al., 2008; Buddhala et al., 2011; Khodaii et al., 2013; Arabani and Hamedi, 2014; Moraes et al., 2017; Zhang and Luo, 2019). The SFE is the measure of the work done to form a unit area of new surface at the interface. Theories related to component-based and equation of state-based methods are available to define surface free energy of a material (Fowkes, 1964; Wu, 1971; Neumann et al., 1974; Van Oss et al., 1988; Li and Neumann, 1992). Among those, the acid-base theory proposed by Van Oss et al. (1988) is commonly used for asphaltic materials. According to the Good-van Oss-Chaudhury (GvOC) (Van Oss et al., 1988) theory, the surface free energy (Γ_S) of a material consists of two components, an apolar Lifshitz-van der Waals component (Γ_S^{LW}) of electrodynamics' origin and a polar component from Lewis acid-base interactions (Γ_S^{AB}), as presented in Equation (3.1). According to this theory (Van

Oss et al., 1988), the acid-base surface free energy (Γ_S^{AB}) component can be divided to an electron-acceptor or Lewis acid (Γ_S^+) component and an electron-donor or Lewis base (Γ_S^-) component using Equation (3.2).

$$\Gamma_S = \Gamma_S^{LW} + \Gamma_S^{AB} \qquad (3.1)$$

$$\Gamma_S^{AB} = 2(\Gamma_S^+ \Gamma_S^-)^{0.5} \qquad (3.2)$$

The work of adhesion represents the degree of intermolecular interaction in a two-phase solid-liquid system and is defined as the work required to separate the liquid from the solid surface (Luner and Ohf, 2014). In the case of an asphalt mix, the work of adhesion (W_{AR}) is related to the work done to separate binder from aggregate surface. The W_{AR} follows the definition of interfacial free energy and can be expressed using the Young-Dupré's equation (Dupré and Dupré, 1869) by Equation (3.3). It should be noted that the subscripts 'A' and 'R' in Equation (3) represent asphalt and aggregate, respectively. Also, the subscript 'W' is used to represent water throughout this dissertation.

$$W_{AR} = 2\left(\sqrt{(\Gamma_A^{LW}\Gamma_R^{LW})} + \sqrt{(\Gamma_A^+\Gamma_R^-)} + \sqrt{(\Gamma_A^-\Gamma_R^+)}\right) \qquad (3.3)$$

The Young-Dupré's equation (Dupré and Dupré, 1869) can be extended from a two-phase system to a three-phase system to incorporate the effect of moisture in a binder-aggregate system. The work of adhesion between a binder and aggregate in the presence of moisture (i.e., work of debonding (W_{ARW}^{wet})) can be expressed using Equation (3.4). The work of debonding represents the work done to displace binder by moisture from the binder-aggregate interface. The magnitude of W_{ARW}^{wet} is a characteristic of the binder-aggregate system. A higher magnitude of W_{ARW}^{wet} represents a higher amount of

free energy liberated when moisture displaces binder at the binder-aggregate interface (Bhasin et al., 2006). Hence, a higher tendency for displacement of binder by moisture may be observed which may lead to lower resistance to moisture-induced damage. The combined effect of W_{AR} and W_{ARW}^{wet} can be obtained using energy ratios, such as ER_1 and ER_2 parameters. The ER_1 and ER_2 can be calculated using Equations (3.5) and (3.6), as proposed by (Bhasin et al., 2006; Bhasin et al., 2007b). The W_{AA} in Equation (3.6) represents the cohesive bond energy of a binder. The Equation (3.7) can be used to calculate the W_{AA}. A higher value of energy ratio parameters will indicate a better resistant to moisture-induced damage.

$$W_{ARW}^{wet} = 2\begin{Bmatrix}\sqrt{(\Gamma_A^{LW}\Gamma_R^{LW})} - \sqrt{(\Gamma_W^{LW}\Gamma_R^{LW})} - \sqrt{(\Gamma_A^{LW}\Gamma_W^{LW})} + \Gamma_W^{LW} - \sqrt{\Gamma_W^+}\left(\sqrt{\Gamma_R^-} + \sqrt{\Gamma_A^-} - \sqrt{\Gamma_W^-}\right) - \\ \sqrt{\Gamma_W^-}\left(\sqrt{\Gamma_R^+} + \sqrt{\Gamma_A^+} - \sqrt{\Gamma_W^+}\right) + \sqrt{(\Gamma_A^+\Gamma_R^-)} + \sqrt{(\Gamma_A^-\Gamma_R^+)}\end{Bmatrix} \quad (3.4)$$

$$ER_1 = \left|\frac{W_{AR}}{W_{ARW}^{wet}}\right| \quad (3.5)$$

$$ER_2 = \left|\frac{W_{AR} - W_{AA}}{W_{ARW}^{wet}}\right| \quad (3.6)$$

$$W_{AA} = 2\left(\Gamma_A^{LW} + 2\sqrt{(\Gamma_A^+\Gamma_A^-)}\right) \quad (3.7)$$

3.2 OBJECTIVES

In this study, the compatibilities of the different binder-aggregate combinations with respect to moisture-induced damage were assessed through chemical analysis and thermodynamic approaches. The effects of different additives, namely WMA, ASA, PPA and RAP on the chemical composition and surface free energy components of commonly used binders were investigated. Also, the effects of short- and long-term aging on the polar functional groups and SFE components of the binder blends were evaluated. Furthermore, the elemental compositions of locally available aggregates

were determined to investigate their role in the moisture-induced damage. The specific objectives of this study are:

i. To evaluate the effects of different additives and aging (short-term and long-term) on the SFE components of an unmodified and a polymer-modified binder.
ii. To assess the effect of additives and aging on the chemical composition of binders using FTIR spectroscopy.
iii. To determine the SFE components and elemental compositions of commonly used aggregates in Oklahoma. Also, evaluate the effect of chemical composition of aggregate on the moisture-induced damage potential of a mix.
iv. Using chemical analysis and SFE technique, evaluate the moisture-induced damage potential of binders' containing different types of additives with different types of aggregates. Also, investigate the effects of aging on the moisture-induced damage potential of binder-aggregate system.

3.3 MATERIALS AND METHODOLOGIES

3.3.1 Materials

3.3.1.1 Asphalt Binder

A PG 64-22 binder and a polymer-modified (styrene-butadiene-styrene) PG 76-28 binder from Oklahoma refineries were collected for this study. Also, a chemical warm mix asphalt (WMA) additive, an antistripping agent (ASA) and a 105% polyphosphoric acid (PPA) were collected from local sources. Reclaimed asphalt pavement (RAP) binder was prepared in the laboratory by simulating long-term aging on the PG 64-22 binder using a pressure aging vessel (PAV). A number of studies have used this method for producing RAP binder in the laboratory environment (Ghabchi et

al., 2014; Zhang et al., 2019). The WMA and ASA were added to both PG 64-22 and PG 76-28 binders at a rate of 0.5% by the weight of the binder as recommended by the manufacturers. The PPA-modification was performed on only the PG 64-22 binder. Approximately 1.5% PPA, by weight of the binder, was added to the PG 64-22 binder for this purpose. Also, RAP binder blends were prepared by adding 20% (by weight of total binder) simulated RAP binder to the PG 64-22 and PG 76-28 binders. Blending of the binders and additives were performed in a high shear mixer by running at 1,000 rpm for 45 minutes. The PG 64-22 and PG 76-28 binders were blended at 155°C and 170°C, respectively. The AASHTO T 240 (AASHTO, 2017) test method was used to simulate short-term aging on the binder blends using a rolling thin film oven (RTFO). The RTFO-aging process simulates oxidative aging on the binder, which is similar to the aging in an asphalt plant. The RTFO-aged binder blends were then further aged in a PAV oven to simulate 5-10 years of field aging. The AASHTO R 28 (AASHTO, 2016) method was followed to performed the PAV-aging.

3.3.1.2 Aggregate

In this study, the surface free energy and chemical composition of aggregates from five different Oklahoma sources were evaluated. All these aggregates are commonly used for pavement construction. Three out of the five aggregates were limestone aggregates. For convenience, in this paper these aggregates are called L1, L2 and L3 aggregates. The other two aggregates were collected from a granite (G1) quarry and rhyolite (R1) quarry.

3.3.2 Methods

In this study, the surface free energy (SFE) and chemical characteristics of the binder blends were evaluated using the dynamic Wilhelmy plate (DWP), X-ray fluorescence (XRF), and Fourier transform infrared (FTIR) tests. The chemical compositions of the aggregates were determined using XRF testing. A universal Sorption device (USD) was used to determine the SFE components of aggregates. Both the chemical and SFE techniques were used to evaluate the moisture-susceptibility of the binder-aggregate combinations. The work-flow diagram for this study is presented in Figure 3.1

3.3.2.1 Dynamic Wilhelmy Plate (DWP) Test

The SFE components of the binders were determined using a contact angle measurement method known as the dynamic Wilhelmy plate (DWP) test. The contact angles of the binders with different probe liquids were determined using a dynamic contact angle (DCA) analyzer. Five different probe liquids, namely water, glycerol, formamide, ethylene glycol and diiodomethane were used for this purpose. Samples for DWP testing were prepared by coating 24 mm x 50 mm glass plates with the binders. For this purpose, binders were heated in an oven until they became liquid. The glass plates were then immersed into the binder container to get sufficient coating. The coated glass plates were then kept vertically down in the oven for few minutes to ensure an even and uniform thickness at the top of the glass plate. After being taking out of the oven, samples were kept in a desiccator to reduce contamination on the coated surface. The contact angle measurement of the coated glass plates was performed within 24-36 hours after preparation. Figure 3.2(a) shows the setup for DWP test on binder samples.

The difference in force due to the immersion of coated samples in a probe liquid was measured using a micro balance in the DCA apparatus. Equation (3.8) was then used to calculate the advancing contact angles from the force measurement during immersion of samples. To ensure consistency and repeatability, five replicates were tested with each probe liquid for each binder blend.

$$P(\Gamma_L cos\theta) = F + V\rho_L g \qquad (3.8)$$

where,

Γ_L = SFE of probe liquid,

θ = Contact angle of the binder with probe liquid,

F = force on submersion less the weight of the glass plate,

V = volume of submerged portion of glass plate = a*b*h,

P = perimeter of the plate = 2(a + b),

a, b, h = width, thickness, and depth of the plate, and

ρ_L = density of the probe liquid.

The SFE components of a binder were determined by forming a set of five equations using Equation (3.9) with five probe liquids. The SFE components (Γ_L^{LW}, Γ_L^- and Γ_L^+) of the probe liquids are known and can be found in (Zhang and Liu, 2018). A non-linear optimization program in Excel was used to solve these equations to obtain the three SFE components of the binder.

$$\Gamma_L(1 + cos\theta) = 2(\Gamma_A^{LW}\Gamma_L^{LW})^{0.5} + 2(\Gamma_A^+\Gamma_L^-)^{0.5} + 2(\Gamma_A^-\Gamma_L^+)^{0.5} \qquad (3.9)$$

3.3.2.2 Fourier Transform Infrared (FTIR) Test

The FTIR spectroscopy was used to examine the effect of the addition of different additives and aging on asphalt binders. A ThermoScientific Nicolet iS50R FT-

IR device with iSS50 ATR accessory was used for this purpose (Figure 3.2(b)). The FTIR tests were focused on collecting spectra in the region of 400 cm^{-1} to 4000 cm^{-1} at 4 cm^{-1} resolution. A semi-quantitative analysis was performed by determining the peak heights of C=O (1695 cm^{-1} and 1740 cm^{-1}) and S=O (1030 cm^{-1}) functional groups. Baseline corrections of the peaks were performed by using 3690cm^{-1}, 1900cm^{-1}, and 650cm^{-1} as zero points. The corresponding peak heights of C=O and S=O were then divided by the height of CH_2 peak at 2920 cm^{-1}, which is considered unsusceptible to aging (Yut et al., 2015), to obtain carbonyl index (I_{CO}) and sulfoxide index (I_{SO}), respectively. In addition to SFE, the changes in I_{CO} and I_{SO} were used to evaluate moisture-induced damage resistance of the binder blends.

3.3.2.3 X-ray Fluorescence (XRF) Test

The X-ray fluorescence (XRF) test was used to perform elemental analysis of the binder blends and aggregates. In XRF, the emission of characteristic "secondary" (or fluorescent) X-rays from the test sample excited by high-energy X-rays is used to identify the chemical compositions of materials being studied. (Hesp and Shurvell, 2010; Hesp and Shurvell, 2013) has explained the working principles of the XRF technique. All the tests were performed using a Rigaku NexCG X-Ray Fluorescence Device. The device is capable of providing rapid, non-destructive, multi-element analyses from very low to high concentrations of elements ranging from sodium (Na) to uranium (U). Peak heights in the spectrum were used to detect and quantify the presence of the elements. The purpose of the XRF test on binder blends was to investigate the changes in the elemental composition of the binder with the addition of different additives. Only RTFO-aged binder blends were used for XRF testing.

3.3.2.4 Universal Sorption Device (USD) Test

The SFE components of the collected aggregates were measured using a universal sorption device (USD). Aggregate particles smaller than 4.75 mm and larger than 2.36 mm were sieved from each aggregate source and prepared for the USD test. For this purpose, aggregate particles were cleaned several times with distilled water. The particles were then dried in an oven for a day at 120°C. The oven-dried samples were then allowed to cool to room temperature before testing. The USD test was conducted to determine the adsorption isotherms of different probe vapors on aggregate surfaces at a temperature of 25°C and relative pressures ranging from 0.05 to 1.00. For this purpose, three probe vapors, namely water, methyl propyl ketone (MPK) and toluene were used in the USD tests. Figure 3.2(c) shows the setup for the USD test. The spreading pressures (π_e) of these probe vapors on the aggregate surface were determined from the adsorption isotherms using Equation (3.10). The adsorption isotherms of toluene were used to determine the specific surface areas (SSA) of the aggregates needed in Equation (3.10). The projected area of toluene molecule was considered as 34 Å^2.

$$\pi_e = \frac{RT}{MA}\int_0^{Po}\frac{n}{p}dp \qquad (3.10)$$

where,

R = universal gas constant,

T = temperature,

M = molecular weight of the probe vapor,

A = specific surface area of the aggregate,

n = mass absorbed per unit mass of aggregate at a vapor pressure p,

P_0 = maximum saturation vapor pressure,

A set of three equations for each aggregate was formed using the spreading pressures of three probe vapors using Equation (3.11). The three unknown SFE components (Γ_R^{LW}, Γ_R^- and Γ_R^+) of aggregates were calculated by solving the equation set.

$$\pi_e + 2\gamma_L = 2\sqrt{(\Gamma_R^{LW}\Gamma_L^{LW})} + 2\sqrt{(\Gamma_R^+\Gamma_L^-)} + 2\sqrt{(\Gamma_R^-\Gamma_L^+)} \qquad (3.11)$$

3.4 RESULTS AND DISCUSSIONS

3.4.1 Asphalt Binder Test Results

3.4.1.1 Chemical Composition of Asphalt Binders

3.4.1.1.1 XRF Test

In this study, the chemical compositions of the binder blends were determined using the XRF and FTIR tests. Table 3.1 presents the amounts (PPM) of different elements detected in XRF tests performed on the RTFO-aged PG 64-22 and PG 76-28 binder blends. It was found that both the binders contained more than 95% hydrocarbon in their composition. Also, it was observed from the XRF spectrum that both the binders exhibited presence of Aluminium (Al), Silicon (Si), Sulfur (S), Chlorine (Cl), Calcium (Ca), Vanadium (V), Iron (Fe), Nickel (Ni), Copper (Cu), Zinc (Zn) and Tin (Sn). Similar elements were reported in other studies as well (Hesp and Shurvell, 2013). Among the detected elements, the amount of sulfur was the highest in both PG 64-22 and PG 76-28 binder blends. Also, it was found that the PG 64-22 binder contained a higher amount of sulfur (46,507 ppm) than the PG 76-28 binder (28,666 ppm). Both binders exhibited low concentrations of Al, Fe, Si, P, Cl, V, Ca, Ni, Sn, Zn, Cu, Pb and

Sr. These elements in the PG 64-22 binder can be ranked as follows: Al, V, Ni, P, Si, Cl, Fe, Sn, Zn and Cu from the highest to the lowest amount. The rankings for the detected elements in the PG 76-28 binder from the highest to the lowest composition were as follows: Al, Fe, Si, P, Cl, V, Ca, Ni, Sn, Zn, Cu, Pb and Sr. No significant changes in the compositions of both PG 64-22 and PG 76-28 binders were observed with the addition of WMA, ASA and RAP. However, an increase in the amount of phosphorus was observed for the PG 64-22+1.5% PPA binder. With the addition of PPA, the amount of phosphorus content increased from 120 ppm to 3,423 ppm. A similar increase in the phosphorus content was reported by Reinke and Glidden (2010) after PPA modification of binder.

3.4.1.1.2 FTIR Test

The FTIR test was conducted to determine the effect of additives and aging on the functional composition of binder blends. The FTIR spectra were analyzed using the OMNIC software. The FTIR spectra feature absorption bands that can be associated with specific functional groups (Hofko et al., 2018). Figure 3.3 presents the FTIR Spectra of the unaged PG 64-22 and PG 76-28 binders. From Figure 3.3, both the PG 64-22 and PG 76-28 binders exhibited very similar characteristic peaks from FTIR spectra. For both binders, the strong characteristic absorption peaks around 2920 cm^{-1} and 2850 cm^{-1} corresponded to the stretching vibration of the C-H band. The absorption peaks near 1695 cm^{-1} and 1740 cm^{-1} represented the stretching vibration of C=O bands. The C=O peak near 1695 cm^{-1} was likely resulted from a combination of an aryl carboxylic acid (COOH) band and a ketone band. Petersen (2009) reported that the ketone band formed at 1700 cm^{-1} has at the same absorption frequency as the carboxylic

acid (COOH), making the two indistinguishable. The peak at 1740 cm^{-1} represented the free (nonhydrogen bonded) absorption band of the carbonyl group of the carboxylic acids (Petersen, 2009). The conjugated peaks around 1600 cm^{-1} and 1580 cm^{-1} represented the C=C aromatic rings. The sharp peak at 1455 cm^{-1} resulted from the stretching vibration (bending vibration) in the C–H plane of $–CH_2$. The absorption peaks at 1376 cm^{-1} and 1365 cm^{-1} resulted from asymmetrical angular vibration and symmetrical angular vibration of CH_3. The presence of S=O functional group was evident from the absorption peak at 1030 cm^{-1}. The peaks at 967, 910 and 699 cm^{-1} were observed only in the PG 76-28 binder. These peaks verified the presence of styrene-butadiene-styrene (SBS) co-polymer in the PG 76-28 binder (Luo et al., 2020). The heights of the peaks at 1695, 1740 and 1030 cm^{-1} were found to increase with RTFO- and PAV-aging.

The addition of WMA additive did not exhibit any change in the absorption peaks for the PG 64-22 and PG 76-28 binders under unaged and RTFO-aged conditions (Figure 3.4). However, prominent amine functionality (peaks at 1578 and 1540 cm^{-1}) was observed after PAV-aging of both binders. Under unaged condition, the addition of ASA to the PG 64-22 binder resulted in the appearance of similar peaks at 1540 cm^{-1} and 1578 cm^{-1} bands, which were possibly N-H bending modes of an amine (Figure 3.5). However, these peaks were not observed in other samples with ASA. It is possible that the amine bands were not seen as they are often weak modes and can overlap with the C-H bending modes, aryl C=C modes, C-O stretches, and OH bending modes. Another reason could be the loss of amine group due oxidative aging.

In Figure 3.6, the emergence of an aliphatic saturated carboxylic acid C=O band around 1730 cm^{-1} likely resulted from the addition of 20% RAP. This peak was distinguishable in the RTFO- and PAV-aged PG 64-22 + 20% RAP and Unaged PG 76-28 + 20% RAP binders. For other RAP binder blends, this peak may have overlapped with the 1740 cm^{-1} peak. The PG 64-22 binder with PPA modification exhibited absorbance peaks at 1076, 962 and 500 cm^{-1}, which are related to the P=O and P-O stretches (Figure 3.7).

The effect of the aging on the functional compositions of the binders were evaluated using carbonyl and sulfoxide indices. The changes in carbonyl indices, based on the peak heights at 1695 and 1740 cm^{-1}, for the PG 64-22 and PG 76-28 binders are presented in Figures 3.8(a) and 8(b), respectively. Figures 3.9(a) and 3.9(b) present the changes in the sulfoxide indices for the PG 64-22 and PG 76-28 binders, respectively. In general, the changes in the I_{SO} were higher than the I_{CO} for both binder blends. For both I_{SO} and I_{CO}, the greatest oxidation effects were seen after the long-term PAV-aging.

For the PG 64-22 binder, the addition of RAP and PPA did not exhibit any significant changes in $I_{CO\,(1695)}$ after RTFO-aging. However, $I_{CO\,(1695)}$ similar to the PG 64-22 binder was observed after long-term aging. The addition of ASA exhibited a reduction in $I_{CO\,(1695)}$ for the unaged PG 64-22 binder. However, with aging, the $I_{CO\,(1695)}$ value was found to be similar to the PG 64-22 without any additive. From Figure 3.8(a), it was observed that the changes in $I_{CO\,(1740)}$ with aging of the PG 64-22 binder blends were not as consistent as $I_{CO\,(1695)}$. Although C=O (1695 cm^{-1}) content increased with aging, there was a decrease in the S=O content with the addition of WMA additive to

the PG 64-22 binder. This decrease may be due to the loss of the sulfoxide peak as SO_2(g) during oxidation. From Figure 3.9(a), the greatest increase in S=O indices was observed for the PG 64-22 + 1.5% PPA after long-term PAV-aging.

The polymer modified PG 76-28 binder blends showed a clear increase in the 1695 cm^{-1} C=O band with increased aging (RTFO- and PAV-aging), i.e., more consistent oxidation with aging. Also, it was found that the addition of WMA, ASA and RAP increased the $I_{CO\,(1695)}$ of the unaged PG 76-28 binder. However, after PAV-aging, the $I_{CO\,(1695)}$ values of the PG 76-28 binder with WMA and ASA were found to be similar to the $I_{CO\,(1695)}$ from the PAV-aged PG 76-28 binder. After comparing Figures 3.9(a) and 3.9(b), it can be observed that the I_{SO} values for the PG 76-28 binder blends were lower than those of the PG 64-22 binder blends. Higher sulfur content of the PG 64-22 binder than the PG 76-28 binder from XRF test (Table 3.1) is responsible for this phenomenon. Among all the PG 76-28 binder blends, the RAP blend showed significant increase in S=O indices with RTFO- and PAV- aging. The incorporation of the PAV-aged PG 64-22 binder with higher sulfur content as RAP binder resulted in the higher I_{SO} for this binder blend. As both S=O and C=O form moieties on the aggregate surface that are highly soluble in water, the presence of these functional groups may increase moisture susceptibility as well. Since I_{CO} and I_{SO} for both the PG 64-22 and PG 76-28 binder blends increased with oxidative aging, the presence of moisture is expected to reduce the resistivity of the asphalt-aggregate bond.

3.4.1.2 Surface Free Energy Components of Asphalt Binders

Table 3.2 presents the contact angles of the PG 64-22 and PG 76-28 binder blends under unaged, RTFO- and PAV-aged conditions. From Table 3.2, the contact

angles of the unaged PG 64-22 binder with all probe liquids are found to reduce due to the addition of WMA, ASA and RAP. The reactions between the binder and the amine derivatives of the WMA additive and ASA are hypothesized to be responsible for the changes in contact angles. Several studies have reported similar trends of reduction in contact angle with an increase in the WMA and ASA (Wasiuddin et al., 2007c; Buddhala et al., 2011; Ghabchi et al., 2013). Similar to the unaged condition, a reduction in contact angle for binder blends with WMA, ASA and RAP was observed under RTFO-aged condition with water, glycerol and formamide. However, under RTFO-aged condition, the contact angles for the same binder blends with diiodomethane were higher than the binder without any additive. Also, the contact angle of the PG 64-22 binder with ethylene glycol increased with the addition of WMA additive, whereas reduced with ASA and RAP. The trend was found to be different after PAV-aging. The contact angles for the PG 64-22+20% RAP with all probe liquids, except diiodomethane, were lower than the neat binder under PAV-aged condition. The addition of 1.5% PPA to the PG 64-22 binder reduced the contact angles for water, glycerol and formamide under unaged condition. The reduction in contact angles with water and glycerol were found to be higher under RTFO- and PAV-aged conditions. It should be noted that the contact angles of the PG 64-22+1.5% PPA with formamide and diiodomethane under RTFO- and PAV-aged conditions were discarded due to the high variability of the test results. Considering all three aging conditions, the maximum and minimum standard deviations of contact angles for the PG 64-22 binder blends with all probe liquids were found to be 1.90° and 0.07°, respectively.

The effects of additives and aging were found to be different for the polymer-modified PG 76-28 binder. The differences on the base binder's compositions and their reactions with different additives are responsible for these variations. From Table 3.2, it can be observed that the contact angles of the PG 76-28 binder with glycerol, formamide, diiodomethane and ethylene glycol reduced with RTFO- and PAV-aging. Under unaged condition, the additions of WMA, ASA and RAP reduced the contact angles of the PG 76-28 binder with glycerol, formamide, diiodomethane and ethylene glycol. However, addition of WMA and RAP to PG 76-28 exhibited an increase, whereas addition of 0.5% ASA resulted in a reduction in contact angle with water. Under RTFO-aged condition, the binder blends with WMA and ASA exhibited higher contact angles with water, glycerol and formamide and lower contact angles with diiodomethane and ethylene glycol than the PG 76-28 binder. A similar trend of contact angle change was observed for the PG 76-28+0.5% ASA under PAV-aging condition. Similar to the unaged condition, the addition of 20% RAP exhibited lower contact angle values than the PG 76-28 binder for all probe liquids under RTFO- and PAV-aging conditions. From Table 3.2, the maximum standard deviation of the contact angle for the PG 76-28 binder was found to be 2.04°.

Typically, a change in the contact angles of the binders with probe liquids results in a change in the SFE components of binders. The changes in the SFE components of the binder will influence the calculation of bond strength of binder-aggregate system (Bhasin et al., 2006). Table 3.3 presents the SFE components of the PG 64-22 and PG 76-28 binders with different additives. From Table 3.3, it can be observed that for both the PG 64-22 and PG 76-28 binder blends, the non-polar

Lifshitz-van der Waals (Γ_A^{LW}) component is higher than the polar (Γ_A^{LW}) components. The unaged PG 64-22 binder was found to be acidic in nature as the acid (Γ_A^+) component (0.66 mJ/m^2) is higher than the base (Γ_A^-) component (0.43 mJ/m^2). Also, the Γ_A^{LW} and Γ_A component of the PG 64-22 binder increased with RTFO- and PAV-aging. However, the acidic component of the PG 64-22 was found to decrease to 0.29 mJ/m^2 with RTFO-aging and remain same for PAV-aging. According to Bhasin (2007), the acid component of the binder combined with the base component of aggregate act as a scaling factor in the calculation of the adhesive strength of a binder aggregate system. As the acidic nature is reduced with aging, the asphalt mix with the PG 64-22 binder may exhibit a higher susceptibility to moisture-induced damage with in-service aging. The addition of WMA additive to the PG 64-22 binder increased the Γ_A^+, Γ_A^- and Γ_A SFE components. The acidic component of the PG 64-22+0.5% WMA reduced to 0.38 from 0.75 mJ/m^2 with RTFO-aging and then increased to 0.91 mJ/m^2 after PAV-aging. However, the Γ_A and Γ_A^{LW} components were observed to increase with RTFO-aging and then reduced with PAV-aging. Although the Γ^-component of the unaged PG 64-22+0.5% WMA binder was higher than the unaged PG 64-22 binder, it became similar after RTFO- and PAV-aging. From Table 3.3, the addition of WMA resulted in a higher Γ_A^+/Γ_A^- ratio than the neat binder under RTFO- and PAV-aged conditions indicating probabilities of better bonding with basic aggregates.

For unaged condition, the Γ_A^-, Γ_A^{LW} and Γ_A components of the PG 64-22 binder increased with the addition of 0.5% ASA. The PG 64-22 binder became more basic as the Γ_A^+/Γ_A^- ratio reduced from 1.54 to 0.41 with the addition of ASA. Wasiuddin et al. (2007c) reported a similar increase in the basic behavior with the addition antistripping

agent. The basic nature of the amine-based ASA is responsible for the changes in the binder SFE component. The effect of ASA may have diminished due to thermal degradation as the Γ_A^+/Γ_A^- ratio increased with RTFO- and PAV-aging. Thermal degradation of ASA with long-term aging was also reported by Wasiuddin et al. (2007a). Similar to ASA, the addition of 20% RAP increased the Γ_A^-, Γ_A^{LW} and Γ_A components under unaged condition. The Γ_A^+/Γ_A^- ratio for the PG 64-22+20% RAP was observed to increase from 0.69 to 1.36 with RTFO-aging and then reduced to 0.24 with PAV-aging. This indicates that the bonding strength of a mix with the PG 64-22+20% RAP may deteriorate with long-term aging. The aged binder from RAP is expected to be responsible for the changes in SFE components of the PG 64-22 binder.

The Γ_A^+, Γ_A^{LW} and Γ_A components of the PG 64-22 binder reduced with the addition of 1.5% PPA. However, the addition of PPA increased the Γ^- component of the PG 64-22 binder. The trend of increasing Γ_A^- component was observed under RTFO- and PAV-aging conditions as well. As a result, significant reductions in the Γ_A^+/Γ_A^- ratio were observed for the PG 64-22+1.5% PPA binder after RTFO-and PAV-aging. Therefore, addition of PPA to the binder blend may result in an increase in basic behavior of the binder. An increase in the Γ_A^- component of the binder with PPA was reported by Al-Qadi et al. (2014). Therefore, the addition of PPA may result in a weak bonding with basic aggregates. As observed from the XRF and FTIR test, the presence of phosphate in the binder is likely responsible for such changes in the binder's surface energy properties.

Unlike the PG 64-222 binder, the unaged PG 76-28 binder exhibited a higher Γ_A^- component than the Γ_A^+ component. Also, Γ_A^{LW} and Γ_A component of the unaged PG 76-

28 binder was found to be lower than the unaged PG 64-22 binder. A slight increase in the acidic nature of the PG 76-28 binder was observed with short- and long-term aging. Similar to the PG 64-22 binder, the Γ_A^{LW} and Γ_A component of the PG 76-28 binder increased with aging. The addition of 0.5% WMA resulted in a lower base component than the PG 76-28 binder for all three aging conditions. Also, almost no change in the Γ_A^+ and Γ_A^{LW} components of the PG 76-28 binder was observed with the addition of WMA for all three-aging condition. The acidic nature of the PG 76-28 binder was found to slightly increase with the addition of 0.5% ASA. Also, the Γ_A^{LW} and Γ_A component of PG 76-28 binder increased by approximately 32% and 34%, respectively, as a result of the addition of ASA. The interactions between constituents of ASA with polymer present in the PG 76-28 binder are expected to be responsible for such changes in SFE components. Similar to PG 64-22 binder, the Γ_A^- component of the PG 76-28+0.5% ASA reduced with aging. A reduction of approximately 60% and 73% of the Γ_A^- component was observed with RTFO- and PAV-aging, respectively. A significant increase in the Γ_A^+ and Γ_A^{LW} components was observed after adding 20% RAP to the PG 76-28 binder. For example, the Γ_A^+ component increased from 0.05 mJ/m^2 to 0.43 mJ/m^2 with the addition of 20% RAP. This change resulted in a significantly high Γ_A^+/Γ_A^- ratio (0.70) for binder blend with RAP. Therefore, the addition of RAP is expected to result in a stronger adhesive bond with basic aggregates than the binder without any RAP. However, the Γ_A^+/Γ_A^- ratio of the PG 76-28+20% RAP reduced to 0.19 and 0.13 after RTFO- and PAV-aging, respectively, indicating the possibility of increased moisture susceptibility with in-service aging.

3.4.2 Aggregate Test Results

3.4.2.1 Chemical Composition of Aggregates

3.4.2.1.1 XRF Test

The mineralogical composition of the aggregate has been reported to significantly influence the SFE as well as chemical reactivity of aggregates (Tarrer and Wagh, 1991). Generally, presence of aluminum, iron, magnesium, and calcium in aggregate enhance bonding with asphalt. On the other hand, such components as sodium and potassium may be detrimental for bonding. Table 3.4 presents the mineralogical compositions of the aggregates in their oxidized form from X-ray florescence (XRF) tests. Analyses showed relatively high CaO (generally present as $CaCO_3$) content (between 85.4% to 90.2%) in all three limestone aggregates. This indicates that the limestone aggregates are carbonaceous in nature. The amount of silica (SiO_2) (generally present in the form of quartz) in limestone aggregates was observed to be significantly lower (from 6.5 to 9.7%) than CaO. Also, alumina (Al_2O_3), MgO (as $MgCO_3$) and Fe_2O_3 (can be present in the form of ferro magnesian and mica) were found in limestone aggregates in relatively small amounts. Among the three limestone aggregates, the L2 aggregate exhibited the lowest amount of aluminum, iron and magnesium. The K_2O and Na_2O can be present in the aggregate as alkali-feldspar. Very small amounts of K_2O (0.2% to 0.5%) and no Na_2O were observed in Limestone aggregates. The XRF test results indicted that the G1 and R1 aggregates were mostly composed of silica (as quartz). The amounts of silica for G1 and R1 aggregates were 74.8% and 64.9%, respectively. Also, amounts of alkali-feldspar, as represented by Na_2O and K_2O, in G1 aggregates were found to be highest among all aggregates. The

presence of sodium and potassium in G1 aggregate can enhance the moisture-induced damage potential of a mix (Curtis et al., 1992; Curtis et al., 1993). The R1 rhyolite aggregate contains 6.8% Fe_2O_3 and 12.2% Al_2O_3, both are relatively high compared to other aggregates. Also, calcium and magnesium, at higher amounts than G1 aggregate, were observed in R1 aggregate which may reduce the propensity to moisture-induced damage.

3.4.2.2 Surface Free Energy Components of Aggregates

The specific surface area (SSA) and SFE components of different aggregates are presented in Table 3.5. The R1 aggregate exhibited the largest SSA among all five aggregates. Generally, rhyolite is a fine-grained volcanic rock. The finer grains resulted in the large SSA for the R1 aggregate. The G1 aggregate was of granite origin (coarse grained igneous rock) and exhibited relatively small SSA (0.83 m^2/g). Although the L1, L2 and L3 aggregates were labeled as limestone aggregates from their petrographic origin, significantly different SSA values were observed among these aggregates (from 0.34 to 1.86 m^2/g). From Table 3.5, it was observed that the Γ_R^- component is significantly higher than the Γ_R^+ and Γ_R^{LW} components for all aggregates. The granite (G1) aggregate exhibited the highest, whereas the rhyolite (R1) aggregate exhibited the lowest Γ_R^- component among all aggregates. The basic components of limestone aggregates were found to vary from 369.41 mJ/m^2 to 1153.65 mJ/m^2. A large magnitude of basic components of aggregates is expected to significantly influence the adhesion bonding of binder-aggregate system (Bhasin, 2007; Ghabchi et al., 2014). The L2 limestone aggregate showed the highest Γ_R^+ component among all aggregates. However, the Γ_R^+ component of the G1 and R1 was significantly lower than the limestone

aggregates. The non-polar Γ_R^{LW} component varied from 25.24 to 76.89 mJ/m^2 for different aggregates. A similar range of variation in the Γ_R^{LW} component of aggregates was reported in other studies (Bhasin, 2007).

3.4.3 Moisture-induced Damage Potential of Binder-Aggregate Systems

The SFE components of binder blends and aggregates were used to calculate the work of adhesion in dry state (W_{AR}) and the work of debonding in presence of moisture (W_{ARW}^{wet}). Table 3.6 presents the W_{AR} and W_{ARW}^{wet} of PG 64-22 and PG 76-28 binder blends with different aggregates. The moisture-induced damage potential was determined by calculating energy ratios (ER_1 and ER_2) of binder-aggregate systems using Equations (3.5) and (3.6), respectively. The ER_1 and ER_2 of different binder-aggregate combinations are presented in Table 3.7. The effects of aging, additives and aggregate types on the moisture-induced damage potential were evaluated using Tables 3.6 and 3.7.

3.4.3.1 Effect of Aggregate Type

From Table 3.6, it can be observed that the type of aggregate has significant influence on the W_{AR} and W_{ARW}^{wet} of binder-aggregate systems. For example, the W_{AR} values of unaged PG 64-22 binder with the L1, L2, L3, G1 and R1 aggregates were 93.5, 109.7, 113.7, 142.9, 86.6 mJ/m^2, respectively. A similar variation with aggregate type can be observed for the W_{ARW}^{wet}. As a result, the energy ratios, ER_1 and ER_2, varied with the types of aggregate. For example, the R1 (rhyolite) aggregate produced the highest energy ratios with the PG 64-22 binder and is expected to perform well to resist moisture susceptibility of a mix. The existence of a large surface area for the R1 aggregate is expected to produce greater bonding potential than other aggregates. Also,

the R1 aggregate contains aluminum, iron and magnesium which typically enhance the bonding between binder and aggregate (Curtis et al., 1993).

Limestone aggregates generally exhibit good bonding quality and resistance to moisture-induced damage. The combinations of the unaged PG 64-22 binder with the L1 and L3 aggregates were ranked as 2nd and 3rd with respect to their resistance to moisture-induced damage. The low surface areas for both the L1 and L3 aggregates (Table 3.5) indicated the presence of fewer active sites on the aggregate surface. However, according to Curtis et al. (1993), the presence of high amount of calcium in limestone aggregate can produce strong active sites. Therefore, the L1 and L3 aggregates are expected to produce mixes with good moisture-induced damage resistance. However, the L2 aggregate showed the lowest ER_1 and ER_2 values among all binder-aggregate combinations. The magnitude of the W_{ARW}^{wet} was much higher than the magnitude of the W_{AR}. This indicates that the adhesion bonds produced at the interface of the PG 64-22 and the L2 aggregate will be highly susceptible to moisture.

The G1 (granite) aggregate showed higher moisture susceptibility than the R1, L1 and L3 aggregates. The granite aggregate is mostly silicious and known for its hydrophilic character. Also, it contains high amounts of alkali-felspar, as Na_2O and K_2O, which were reported to be deleterious for binder-aggregate bonding (Curtis et al., 1993). As a result, a higher magnitude of the W_{ARW}^{wet} is expected for mixes with the G1 aggregate in the presence of moisture. A similar ranking of aggregates was observed for the PG 64-22 binders under RTFO- and PAV-aging conditions. The PG 76-28 binder exhibited a similar variation in the moisture-induced damage potential with aggregate types. However, for the PG 76-28 binder, the G1 aggregate exhibited the lowest

moisture-induced damage resistance than other aggregates. The compatibilities of different aggregates with binder blends containing additives are discussed in the following sections.

From Tables 3.6 and 3.7, it was observed that the influence of the properties of aggregate on the moisture-induced damage potential is significantly higher than the properties of binder. For example, relatively small changes in the W_{AR} and W_{ARW}^{wet} were observed among the PG 64-22 binder blends for a given aggregate. However, the differences in the $W_{AR}$and W_{ARW}^{wet} values were observed to be much higher among different aggregates for a given binder. A similar finding was observed for the ER_1 and ER_2 parameters. Several studies reported that the properties of aggregates are the most important factor contributing to the binder-aggregate bonding (Tarrer and Wagh, 1991; Curtis et al., 1992).

3.4.3.2 Effect of Aging

From Table 3.6, the W_{AR} for the PG 64-22 binder with the L1 aggregate reduced and the W_{ARW}^{wet} increased with RTFO- and PAV-aging. For example, the W_{AR} of the PG 64-22 binder and the L1 aggregate reduced from 93.5 mJ/m^2 to 87.1 and 87.6 mJ/m^2 with RTFO- and PAV-aging. A similar trend was observed for other aggregates. From Table 3.7, the ER_1 and ER_2 of PG 64-22 binder with all aggregates were observed to reduce with RTFO- and PAV-aging. For example, the ER_1 of PG 64-22 binder with L1 aggregate reduced from 0.75 to 0.67 with RTFO-aging and remained same with PAV-aging. The reduced ER_1 and ER_2 indicated an increased possibility of moisture-induced damage with aging for asphalt mix containing PG 64-22 binder.

Also, the results of the chemical analysis pointed toward an increased moisture susceptibility with aging for the PG 64-22 binder. The spectral analysis using the FTIR indicated an increase in the S=O and C=O (specifically carboxylic acid (COOH)) functional groups for the PG 64-22 binder with RTFO- and PAV-aging. Although sulfoxide and carboxylic acid have high affinity for aggregate surface, bonds produced from these interactions at the binder-aggregate interface are highly soluble to water (Curtis et al., 1993). Therefore, an increase in sulfoxide and carboxylic acid functional groups will create a thermodynamically favorable condition for debonding at the interface, hence will increase potential for moisture-induced damage.

The W_{AR} of the PG 76-28 binder with all aggregates exhibited an increase with RTFO-aging and then reduced with PAV-aging. However, the magnitude of the W_{ARW}^{wet} for the PG 76-28 binder-aggregate systems reduced with RTFO-aging and increased with PAV-aging. As a result, for all PG 76-28 binder-aggregate combinations, the ER_1 and ER_2 increased with RTFO-aging and then reduced with PAV-aging. Therefore, the increase of I_{CO} and I_{SO} may increase the moisture susceptibility of the PG 76-28 binder after long-term aging. Also, the interaction of polymer with the aggregate surface is expected to influence the interface bonds.

3.4.3.3 Effect of WMA Additive

The effect of WMA on the moisture-induced damage performance of asphalt mixes can be evaluated using Tables 3.6 and 3.7. From Table 3.6, the PG 64-22 binder with L1 aggregate exhibited a slight increase in the W_{AR} from 93.5 to 97.6 mJ/m^2 with the addition of 0.5% WMA. The increase in the W_{AR} with WMA was observed with other aggregate combinations as well. Also, the $|W_{ARW}^{wet}|$ of PG 64-22 binder with

aggregates reduced with the incorporation of WMA. The FTIR results indicated presence of amine in the binder blends with WMA additives. The presence of amine in the interface can reduce the surface energy of the aggregate surface and enhance bonding (Tarrer and Wagh, 1991). Therefore, an increase in the W_{AR} and decrease in the $|W_{ARW}^{wet}|$ was resulted from the action of amine-base. Also, the ER_1 and ER_2 values were observed to slightly increase for binder-aggregate systems with WMA additive. Therefore, the addition of WMA is expected to improve resistance to moisture-induced damage. Ghabchi et al. (2013) reported a similar reduction of moisture susceptibility potential of different binder-aggregate systems with the addition of the same WMA additive. The energy ratios of the PG 64-22+0.5% WMA with all aggregates reduced with RTFO-aging and then increased with PAV-aging. The energy ratios under PAV-aged condition are similar to that of unaged condition. Similar to the PG 64-22 binder, the R1 aggregate exhibited the highest and the L2 aggregate exhibited the lowest resistance to moisture susceptibility with the PG 64-22+0.5% WMA binder.

The energy ratios from Table 3.7 indicated that the addition of WMA to the PG 76-28 binder increased the moisture susceptibility of the binder-aggregate system. However, the ER_1 and ER_2 increased with aging indicating an improved resistance to moisture-induced damage. After long-term aging, the asphalt mix with the PG 76-28+0.5% WMA binder is expected to perform similar to the mix with the PG 76-28 binder. According to energy ratio values, the R1 aggregate exhibited the highest resistance to moisture susceptibility with the PG 76-28+0.5% WMA binder followed by the L1, L3, L2 and G1 aggregates.

3.4.3.4 Effect of Antistripping Agent

Similar to the WMA, the addition of ASA to the PG 64-22 binder resulted in an increase in the W_{AR} and energy ratios with all five aggregates. For example, an approximately 7% increase in the ER_1 parameter was observed for the PG 64-22+0.5% ASA with the L1 aggregate. Therefore, use of the PG 64-22+0.5% ASA is expected to produce a mix with improved moisture-induced damage resistant than the neat PG 64-22 binder. The presence of amine-base is responsible for this increase in the resistance to moisture-induced damage. However, a reduction in the ER_1 value was observed with the thermal degradation of the ASA with RTFO- and PAV-aging. A similar reduction in moisture-induced damage resistance with aging for binders blended with ASA was reported by Wasiuddin et al. (2007c). From Tables 3.6 and 3.7, it was observed that, the use of L2 aggregate with the PG 64-22+0.5% ASA may increase the potential for moisture-induced damage.

Similar to the PG 64-22 binder, the addition of ASA to the PG 76-28 binder contributed to the improvement of moisture-induced damage resistance. The trend is similar for all aggregates. The ER_1 and ER_2 reduced with RTFO-aging indicating a higher susceptibility to moisture-induced damage with aging. No further change in the energy ratios were observed with PAV-aging.

3.4.3.5 Effect of Reclaimed Asphalt Pavement (RAP)

The addition of 20% RAP to the PG 64-22 binder exhibited similar W_{AR} and energy ratios as the PG 64-22 binder without any additive. However, based on energy ratios, the moisture-induced damage potential of a mix containing the PG 64-22+20% RAP is expected to increase with aging. The steady increase of the I_{CO} and I_{SO} with

aging pointed to the generation of water-soluble bonds at the interface when the PG 64-22+20% RAP binder come into contact with an aggregate. Therefore, an increase in the moisture-induced damage potential is expected. According to the ER_1 and ER_2, the moisture-induced damage resistance of the binder-aggregate combinations with the R1, L1, L3, G1 and L2 were ranked as 1st, 2nd, 3rd, 4th and 5th, respectively.

The W_{AR} increased and the $|W_{ARW}^{wet}|$ reduced with the addition of 20% RAP to the PG 76-28 binder. As a result, the ER_1 and ER_2 of all binder-aggregate combinations with the PG 76-28+20% RAP exhibited higher values than the PG 76-28 binder. Also, the moisture-induced damage potential is expected to slightly increase with short- and long-term aging. Also, it was observed that, combining the PG 76-28+20% RAP with the L2 aggregate will result in a high moisture susceptible mix.

3.4.3.6 Effect of Polyphosphoric Acid (PPA)

For the PG 64-22 binder, the effect of the addition of 1.5% PPA on the W_{AR} and $|W_{ARW}^{wet}|$ was observed to be influenced by the type of aggregate used in the binder-aggregate system. For example, the W_{AR} for the L2 aggregate with the PG 64-22 binder was 109.7 mJ/m^2, which increased to 112.3 mJ/m^2 for PG 64-22+1.5% PPA. However, the use of the R1, G1 and L3 aggregates reduced the W_{AR} with the PG 64-22+1.5% PPA binder. Furthermore, the PPA modification increased the $|W_{ARW}^{wet}|$ for the L1, L3, G1 and R1 aggregates. The use of the L1, L3, G1 and R1 aggregates with PG 64-22+1.5% PPA binder resulted in a reduction in the ER_1 and ER_2 values indicating an increase in moisture susceptibility. The amounts of reduction in energy ratios were found to be the largest for the R1 aggregate. Other studies have reported similar reduction in moisture-induced damage resistance with PPA modification (Reinke and Glidden, 2010; Al-Qadi

et al., 2014). The increase of the I_{CO} and I_{SO} with aging pointed to a higher moisture susceptibility for PPA-modified binder. However, the L2 aggregate exhibited an increase in the ER_1 and ER_2. The interaction of the high Γ_R^+ component of the L2 aggregate with the high Γ_A^- component of the PPA-modified binder is responsible for this increase.

For PPA-modified PG 64-22 binder, the binder-aggregate systems containing the G1 and R1 aggregates exhibited a steady reduction in the ER_1 and ER_2 values with RTFO- and PAV-aging. However, all three limestone aggregates (L1, L2 and L3) exhibited an increase in energy ratios with RTFO-aging followed by a reduction with PAV-aging. The relatively high Γ_A^- component of the RTFO-aged PPA-modified binder combined with the high Γ_R^+ component of limestone aggregates resulted in higher W_{AR} than the unaged condition, and, hence, an increase in energy ratios. However, the Γ_A^+ component of the PPA-modified binder reduced significantly after PAV-aging, which led to an increase in moisture-induced damage potential with limestone aggregates. Therefore, it can be concluded that, with time and aging, the addition of PPA will reduce the resistance of an asphalt mix to moisture-induced damage.

3.5 CONCLUSIONS

In this study, chemical and thermodynamic properties of asphalt binder and aggregates were used to evaluate the compatibility of binder-aggregate system. The FTIR test results were used to characterize the functional groups of the binder blends. The XRF test results were used to determine the elemental compositions of both binders and aggregates. The SFE components of the binder blends and aggregates were determined using dynamic Wilhelmy plate and universal sorption device test. Effects of

aggregate types, aging and additives on the moisture-induced damage potential were identified by investigating the changes in chemical and thermodynamic properties. Important findings from the present study are as follows:

i. The properties of aggregates have significantly higher influence on the moisture-induced damage potential of a mix than the properties of binder.
ii. Based on the chemical analysis and surface free energy method, the rhyolite (R1) and limestone (L1 and L3) aggregates are expected to exhibit good resistance to moisture-induced damage when used in a mix. The test results indicated poor moisture-induced damage resistance for L2 limestone and G1 granite aggregate.
iii. The analyses of FTIR spectra provided valuable information on the functional groups present in the binders. Also, the FTIR test was able to detect the additives and modifiers used in binders.
iv. A general increasing trend of the carbonyl and sulfoxide functionalities for binders with short and long-term aging was observed from the FTIR analyses. The increase in these functional groups may produce water soluble bonds at the interface making it susceptible to moisture.
v. The addition of WMA and ASA are expected to reduce moisture susceptibility of asphalt mix. The presence of amine group in both WMA and ASA is expected to enhance bonding between binder and aggregate.
vi. Use of 20% RAP is expected improve the resistance to moisture-induced damage. However, the performance the binder blend with RAP may deteriorate

with aging. In general (except L2 aggregate), PPA modification increased the potential for moisture-induced damage of a binder-aggregate system.

vii. The quantification of adhesive strength through the SFE method and interfacial bonding through chemical analyses will help better understand the performance of a binder-aggregate system in the presence of moisture.

The current study explored the mechanisms of moisture-induced damage of different binder-aggregate combinations under different aging conditions. The study was limited to the limestone, granite and rhyolite aggregates commonly used in the production of asphalt mixes in Oklahoma. The moisture-induced damage performance of asphalt mixes produced with aggregates from other sources can be different depending on their mineralogical and surface compositions. Therefore, future studies should address moisture-induced damage evaluation of other aggregates and selection of binder-aggregate combinations. Also, future studies are needed to compare the findings of the present study with laboratory produced mixes. Also, comparison with field performance will enhance the reliability of the test results.

Table 3.1 Elemental compositions of PG 64-22 and PG 76-28 binder blends from XRF tests

Binder Type	Elements Detected (ppm)														Hydro-carbon (%)
	S	Al	Ca	Si	Cl	P	Fe	V	Zn	Ni	Cu	Sn	Pb	Sr	
PG 64-22	46507.0	331.0	13.0	78.2	60.1	120.0	39.0	183.0	3.4	78.2	3.0	13.8	0.0	0.0	95.3
PG 64-22 + 0.5% WMA	47192.0	375.0	12.7	89.7	65.7	122.0	38.9	185.0	3.4	78.3	3.5	12.2	0.0	0.0	95.2
PG 64-22 + 0.5% ASA	46722.0	350.0	9.8	80.8	64.7	122.0	42.4	182.0	3.7	78.0	3.2	14.2	0.0	0.0	95.2
PG 64-22 + 20% RAP	44699.0	345.0	8.3	73.3	56.3	120.0	38.8	179.0	3.0	76.0	3.4	14.2	0.0	0.0	95.4
PG 64-22 + 1.5% P1	45979.0	335.0	10.3	75.7	55.1	3423.0	38.2	180.0	3.2	76.7	3.0	22.0	0.0	0.0	96.9
PG 76-28	28666.0	241.0	26.1	116.0	46.3	80.1	183.0	45.2	8.4	25.2	3.3	14.5	2.5	1.2	97.1
PG 76-28 + 0.5% WMA	28936.0	273.0	33.8	117.0	51.3	83.2	181.0	47.2	9.0	26.0	3.2	12.9	2.6	1.3	97.0
PG 76-28 + 0.5% ASA	29109.0	248.0	28.3	123.0	50.2	78.9	181.0	43.5	8.1	25.4	3.5	14.5	2.3	1.3	97.0
PG 76-28 + 20% RAP	27730.0	259.0	20.9	105.0	47.7	83.5	151.0	71.1	7.4	35.4	3.9	15.9	1.7	1.0	96.9

Table 3.2 Contact angles of PG 64-22 and PG 76-28 binder blends with probe liquids

Binder Type	Aging	Contact Angle (°)									
		Water		Glycerol		Formamide		Diiodomethane		Ethylene Glycol	
		Avg	SD	Avg	SD	Avg	SD	Avg	SD	Avg	SD
PG 64-22	unaged	107.4	0.70	94.4	0.07	90.6	0.22	85.0	0.94	78.6	0.21
	RTFO	107.9	0.10	94.3	0.11	90.5	0.13	78.7	0.57	78.4	0.62
	PAV	107.1	0.59	95.2	0.19	91.2	0.21	80.8	0.34	78.8	0.41
PG 64-22 + 0.5% WMA	unaged	104.7	0.67	93.4	0.16	88.1	0.85	84.1	1.36	75.1	0.37
	RTFO	107.7	0.16	94.1	0.36	89.8	0.38	80.3	1.39	78.8	0.08
	PAV	107.5	0.74	94.9	0.20	91.0	0.27	88.4	0.81	78.6	0.39
PG 64-22 + 0.5% ASA	unaged	102.2	1.55	92.4	0.68	87.8	0.44	84.5	0.46	76.1	0.28
	RTFO	107.0	0.09	93.9	0.14	89.7	0.32	80.0	0.99	78.2	0.58
	PAV	107.3	0.62	94.7	0.26	91.0	0.34	81.4	0.43	76.8	1.90
PG 64-22 + 20% RAP	unaged	105.5	0.58	93.1	0.22	89.3	0.17	82.7	2.05	78.4	0.40
	RTFO	107.1	0.26	93.1	0.18	89.2	0.21	81.4	0.70	78.5	0.24
	PAV	107.0	0.55	95.1	0.12	91.7	0.80	76.7	0.23	78.4	0.56
PG 64-22 + 1.5% PPA	unaged	106.5	0.55	94.1	0.63	90.5	0.35	86.6	0.70	82.0	0.54
	RTFO	101.0	0.03	91.9	0.62	-	-	-	-	77.9	0.31
	PAV	100.7	0.93	93.2	0.91	-	-	-	-	76.8	0.30
PG 76-28	unaged	107.2	2.03	105.5	0.78	101.2	1.94	96.3	0.99	94.1	0.31
	RTFO	106.4	0.29	101.2	0.23	97.5	0.43	93.7	1.96	89.3	0.86
	PAV	107.5	0.32	100.4	0.10	100.7	0.26	89.1	0.18	87.3	1.48
PG 76-28 + 0.5% WMA	unaged	108.8	0.88	103.0	1.13	98.4	1.18	85.6	1.63	84.3	0.50
	RTFO	107.1	0.44	101.5	1.11	98.2	0.62	89.1	1.05	86.6	0.10
	PAV	107.4	0.50	100.1	0.58	98.9	1.36	87.1	1.37	85.6	0.88
PG 76-28 + 0.5% ASA	unaged	102.7	0.44	96.8	0.37	96.3	1.09	88.2	1.45	86.4	1.04
	RTFO	107.8	0.68	99.2	1.73	98.5	0.37	86.2	0.45	85.9	0.43
	PAV	109.5	0.38	101.2	0.85	97.5	0.44	86.9	0.31	85.9	1.45
PG 76-28 + 20% RAP	unaged	108.4	0.42	97.8	1.27	93.1	0.45	86.6	1.54	81.5	0.25
	RTFO	105.4	0.31	98.9	0.31	96.0	0.49	91.3	0.27	85.5	0.44
	PAV	106.4	0.73	98.7	0.48	97.5	1.01	90.0	0.59	83.0	0.62

Table 3.3 SFE components of PG 64-22 and PG 76-28 binder blends at different aging conditions

Binder Type	Aging	SFE components (mJ/m2)					
		Γ+	Γ-	ΓLW	ΓAB	ΓTotal	Γ+/Γ-
PG 64-22	unaged	0.66	0.43	14.76	1.07	15.83	1.54
	RTFO	0.29	0.28	17.78	0.57	18.35	1.06
	PAV	0.30	0.52	16.76	0.79	17.55	0.58
PG 64-22 + 0.5% WMA	unaged	0.75	0.76	14.76	1.51	16.27	0.98
	RTFO	0.38	0.31	17.78	0.69	18.47	1.24
	PAV	0.91	0.50	13.20	1.34	14.54	1.82
PG 64-22 + 0.5% ASA	unaged	0.65	1.61	15.06	2.05	17.11	0.41
	RTFO	0.36	0.41	17.20	0.78	17.98	0.87
	PAV	0.44	0.38	16.43	0.82	17.25	1.17
PG 64-22 + 20% RAP	unaged	0.51	0.74	15.90	1.23	17.13	0.69
	RTFO	0.50	0.37	16.53	0.86	17.39	1.36
	PAV	0.12	0.51	18.76	0.50	19.26	0.24
PG 64-22 + 1.5% PPA	unaged	0.61	0.79	14.25	1.39	15.64	0.77
	RTFO	0.56	2.50	14.35	2.38	16.73	0.23
	PAV	0.31	3.00	14.96	1.93	16.90	0.10
PG 76-28	unaged	0.05	3.67	9.96	0.87	10.83	0.01
	RTFO	0.21	2.66	10.99	1.51	12.50	0.08
	PAV	0.09	2.03	12.64	0.87	13.51	0.05
PG 76-28 + 0.5% WMA	unaged	0.05	1.22	9.96	0.49	10.45	0.04
	RTFO	0.10	2.02	10.99	0.92	11.91	0.05
	PAV	0.09	1.73	12.64	0.80	13.44	0.05
PG 76-28 + 0.5% ASA	unaged	0.12	3.67	13.15	1.31	14.47	0.03
	RTFO	0.10	1.48	13.97	0.75	14.72	0.06
	PAV	0.12	0.99	13.82	0.69	14.50	0.12
PG 76-28 + 20% RAP	unaged	0.43	0.61	14.04	1.02	15.07	0.70
	RTFO	0.30	2.34	11.92	1.68	13.59	0.13
	PAV	0.33	1.75	12.32	1.51	13.83	0.19

Table 3.4 Mineralogical composition of aggregates from XRF test

Composition (%)	Aggregate Type				
	L1 (Limestone)	**L2 (Limestone)**	**L3 (Limestone)**	**G1 (Granite)**	**R1 (Rhyolite)**
CaO	85.4	90.2	85.8	0.8	1.5
Na_2O	0.0	0.0	0.0	3.9	3.1
MgO	2.9	1.4	2.0	0.1	1.4
Al_2O_3	1.2	1.0	1.5	11.4	12.2
SiO_2	6.6	6.5	9.7	74.8	68.9
K_2O	0.5	0.2	0.2	5.9	4.0
Fe_2O_3	2.0	0.3	0.4	2.4	6.8
Others	1.4	0.3	0.3	0.7	2.3

Table 3.5 Surface free energy components of different aggregates from USD test

		Aggregate Type				
		L1 (Limestone)	**L2 (Limestone)**	**L3 (Limestone)**	**G1 (Granite)**	**R1 (Rhyolite)**
SSA (m^2/g)		0.34	0.7	1.86	0.83	8.56
SFE Components (mJ/m^2)	Γ_R^{LW}	52.06	25.24	51.29	76.89	52.87
	Γ_R^+	26.17	143.83	18.91	0.16	0.39
	Γ_R^-	369.41	1153.65	1056.25	2120.17	336.94
	Γ_R^{AB}	196.66	814.69	282.65	37.38	23.04
	Γ_R	248.72	839.93	333.94	114.27	75.91

Table 3.6 The W_{AR} and W^{wet}_{ARW} of PG 64-22 and PG 76-28 binder blends with different aggregates

Binder Type	Aging	Work of Adhesion (mJ/m^2)					Work of Debonding (mJ/m^2)				
		Aggregate Type					Aggregate Type				
		L1	L2	L3	G1	R1	L1	L2	L3	G1	R1
PG 64-22	Unaged	93.5	109.7	113.7	142.9	86.6	-124.8	-306.5	-230.5	-313.2	-78.2
	RTFO	87.1	91.9	100.2	124.3	81.9	-130.6	-323.8	-243.4	-331.3	-82.3
	PAV	87.6	95.8	100.7	123.1	80.7	-131.0	-320.7	-243.8	-333.4	-84.4
PG 64-22 + 0.5% WMA	Unaged	97.6	118.3	118.8	147.7	88.7	-123.4	-300.6	-228.0	-311.1	-78.7
	RTFO	90.3	97.7	105.4	131.3	84.7	-128.5	-319.0	-239.3	-325.3	-80.5
	PAV	96.2	118.1	120.0	151.9	88.7	-122.0	-298.1	-224.0	-304.1	-76.0
PG 64-22 + 0.5% ASA	Unaged	100.0	124.3	119.1	143.5	87.7	-124.7	-298.4	-231.5	-319.1	-83.5
	RTFO	89.6	98.0	104.1	128.7	83.2	-129.3	-318.8	-240.6	-328.0	-82.1
	PAV	90.4	100.8	106.7	133.0	84.2	-128.0	-315.5	-237.5	-323.3	-80.6
PG 64-22 + 20% RAP	Unaged	93.8	109.3	111.1	136.5	85.3	-126.9	-309.3	-235.5	-322.0	-81.8
	RTFO	92.1	103.5	109.6	137.0	85.9	-126.7	-313.2	-235.1	-319.6	-79.4
	PAV	83.3	84.4	91.0	108.7	76.7	-135.5	-332.2	-253.6	-347.9	-88.5
PG 64-22 + 1.5% PPA	Unaged	93.6	112.3	112.6	138.8	84.7	-126.1	-305.3	-233.0	-318.7	-81.5
	RTFO	99.7	127.0	116.8	136.9	84.7	-126.8	-297.4	-235.5	-327.4	-88.3
	PAV	95.0	118.3	106.8	120.7	78.9	-131.8	-306.4	-245.9	-344.0	-94.3
PG 76-28	Unaged	73.9	93.1	76.6	77.8	56.6	-144.8	-323.5	-267.9	-378.8	-108.5
	RTFO	82.3	103.9	91.8	102.1	67.3	-137.3	-313.7	-253.8	-355.4	-98.9
	PAV	77.6	90.6	83.1	91.5	64.7	-140.6	-325.6	-261.0	-364.5	-100.0
PG 76-28 + 0.5% WMA	Unaged	65.4	73.4	69.3	76.8	55.5	-145.0	-335.0	-267.0	-371.5	-101.4
	RTFO	74.8	89.3	80.8	89.0	61.8	-141.3	-324.7	-261.2	-365.0	-100.8
	PAV	76.5	88.0	82.2	91.5	64.6	-140.6	-327.0	-260.8	-363.4	-99.0
PG 76-28 + 0.5% ASA	Unaged	85.1	105.7	90.9	96.8	67.7	-139.1	-316.5	-259.2	-365.3	-103.0
	RTFO	78.3	87.8	84.2	95.0	67.2	-139.6	-328.0	-259.5	-360.8	-97.1
	PAV	77.1	84.7	84.3	97.7	68.0	-138.7	-329.1	-257.4	-355.9	-94.3
PG 76-28 + 20% RAP	Unaged	87.3	100.9	103.1	126.7	79.5	-129.8	-314.1	-239.9	-328.2	-84.0
	RTFO	86.5	108.6	98.3	112.2	72.2	-134.3	-310.1	-248.3	-346.4	-95.0
	PAV	86.1	105.7	98.9	115.2	73.6	-133.3	-311.6	-246.5	-342.1	-92.3

Table 3.7 Energy ratios (ER_1 and ER_2) of PG 64-22 and PG 76-28 binder blends with different aggregates

Binder Type	Aging	ER_1					ER_2				
		Aggregate Type					Aggregate Type				
		L1	L2	L3	G1	R1	L1	L2	L3	G1	R1
PG 64-22	unaged	0.75	0.36	0.49	0.46	1.11	0.50	0.25	0.36	0.36	0.70
	RTFO	0.67	0.28	0.41	0.38	0.99	0.39	0.17	0.26	0.26	0.55
	PAV	0.67	0.30	0.41	0.37	0.96	0.40	0.19	0.27	0.26	0.54
PG 64-22 + 0.5% WMA	unaged	0.79	0.39	0.52	0.47	1.13	0.53	0.29	0.38	0.37	0.71
	RTFO	0.70	0.31	0.44	0.40	1.05	0.42	0.19	0.29	0.29	0.59
	PAV	0.79	0.40	0.54	0.50	1.17	0.55	0.30	0.41	0.40	0.78
PG 64-22 + 0.5% ASA	unaged	0.80	0.42	0.51	0.45	1.05	0.53	0.30	0.37	0.34	0.64
	RTFO	0.69	0.31	0.43	0.39	1.01	0.41	0.19	0.28	0.28	0.58
	PAV	0.71	0.32	0.45	0.41	1.04	0.44	0.21	0.30	0.30	0.62
PG 64-22 + 20% RAP	unaged	0.74	0.35	0.47	0.42	1.04	0.47	0.24	0.33	0.32	0.62
	RTFO	0.73	0.33	0.47	0.43	1.08	0.45	0.22	0.32	0.32	0.64
	PAV	0.61	0.25	0.36	0.31	0.87	0.33	0.14	0.21	0.20	0.43
PG 64-22 + 1.5% PPA	unaged	0.74	0.37	0.48	0.44	1.04	0.49	0.27	0.35	0.34	0.66
	RTFO	0.79	0.43	0.50	0.42	0.96	0.52	0.31	0.35	0.32	0.58
	PAV	0.72	0.39	0.43	0.35	0.84	0.46	0.28	0.30	0.25	0.48
PG 76-28	unaged	0.51	0.29	0.29	0.21	0.52	0.36	0.22	0.21	0.15	0.32
	RTFO	0.60	0.33	0.36	0.29	0.68	0.42	0.25	0.26	0.22	0.43
	PAV	0.55	0.28	0.32	0.25	0.65	0.36	0.20	0.21	0.18	0.38
PG 76-28 + 0.5% WMA	unaged	0.45	0.22	0.26	0.21	0.55	0.31	0.16	0.18	0.15	0.34
	RTFO	0.53	0.28	0.31	0.24	0.61	0.36	0.20	0.22	0.18	0.38
	PAV	0.54	0.27	0.32	0.25	0.65	0.35	0.19	0.21	0.18	0.38
PG 76-28 + 0.5% ASA	unaged	0.61	0.33	0.35	0.26	0.66	0.40	0.24	0.24	0.19	0.38
	RTFO	0.56	0.27	0.32	0.26	0.69	0.35	0.18	0.21	0.18	0.39
	PAV	0.56	0.26	0.33	0.27	0.72	0.35	0.17	0.21	0.19	0.41
PG 76-28 + 20% RAP	unaged	0.67	0.32	0.43	0.39	0.95	0.44	0.23	0.30	0.29	0.59
	RTFO	0.64	0.35	0.40	0.32	0.76	0.44	0.26	0.29	0.25	0.47
	PAV	0.65	0.34	0.40	0.34	0.80	0.44	0.25	0.29	0.26	0.50

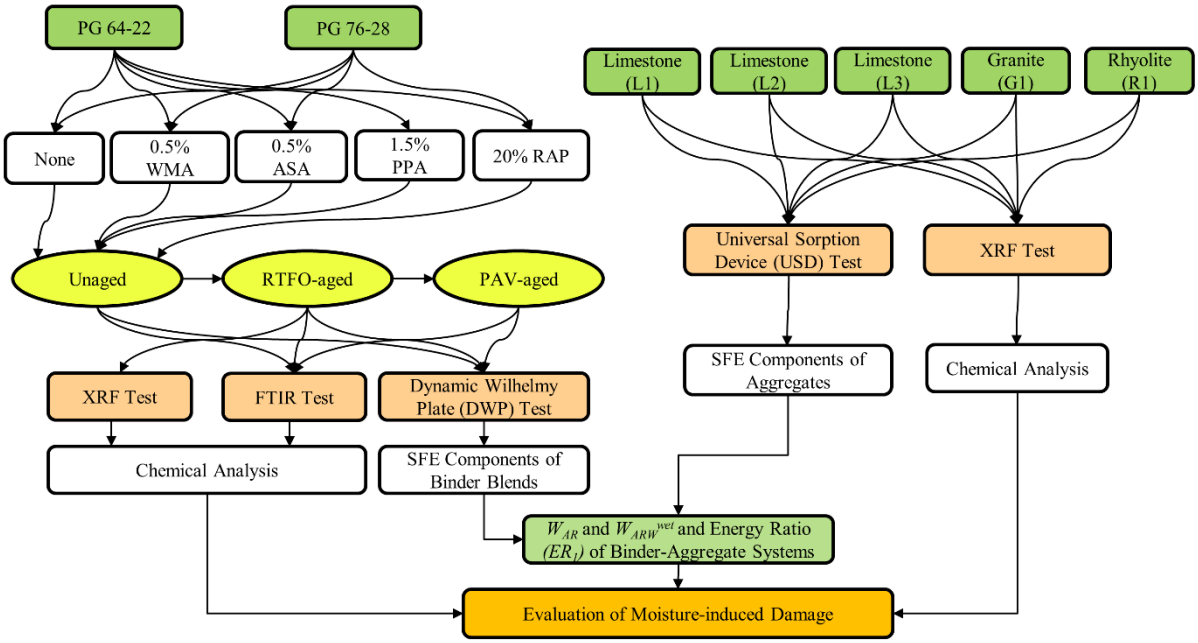

Figure 3.1 Work-flow diagram for the study

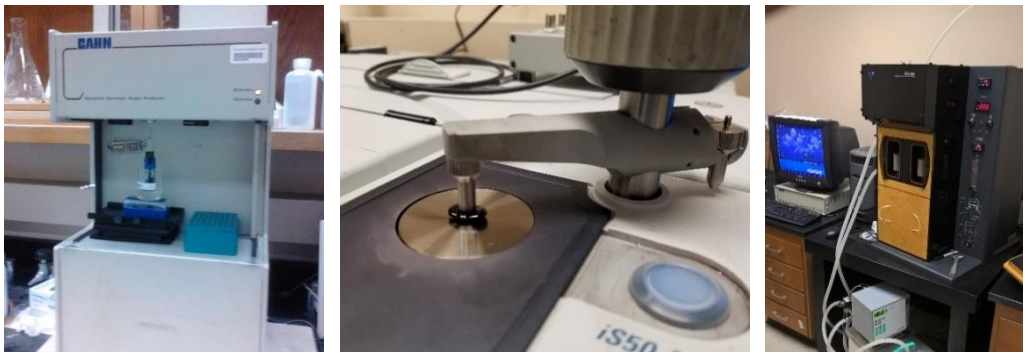

(a) (b) (c)

Figure 3.2 Setup for (a) DWP test on binder coated glass plates, (b) FTIR test on binder, and (c) USD test on aggregate.

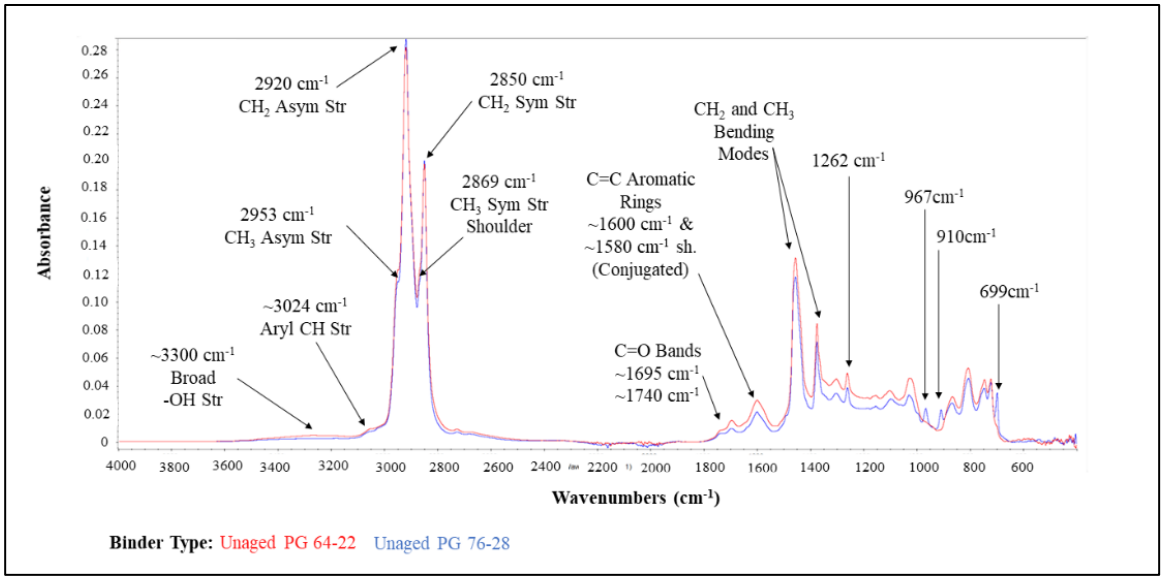

Figure 3.3 FTIR Spectra of unaged PG 64-22 and PG 76-28 binders

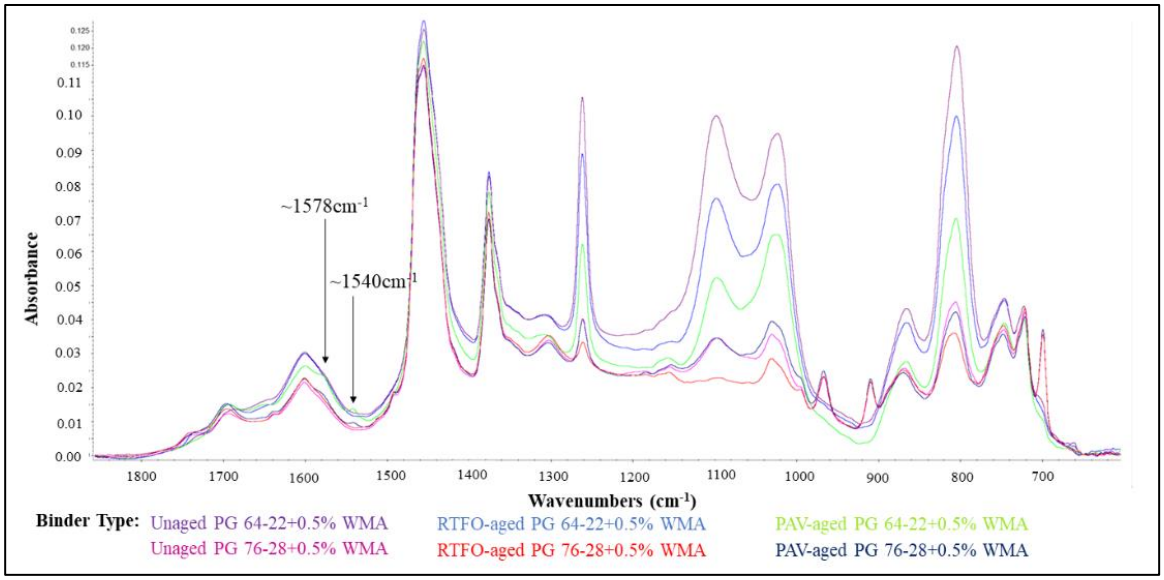

Figure 3.4 FTIR Spectra for PG 64-22 and PG 76-28 binders with WMA additives at different aging conditions

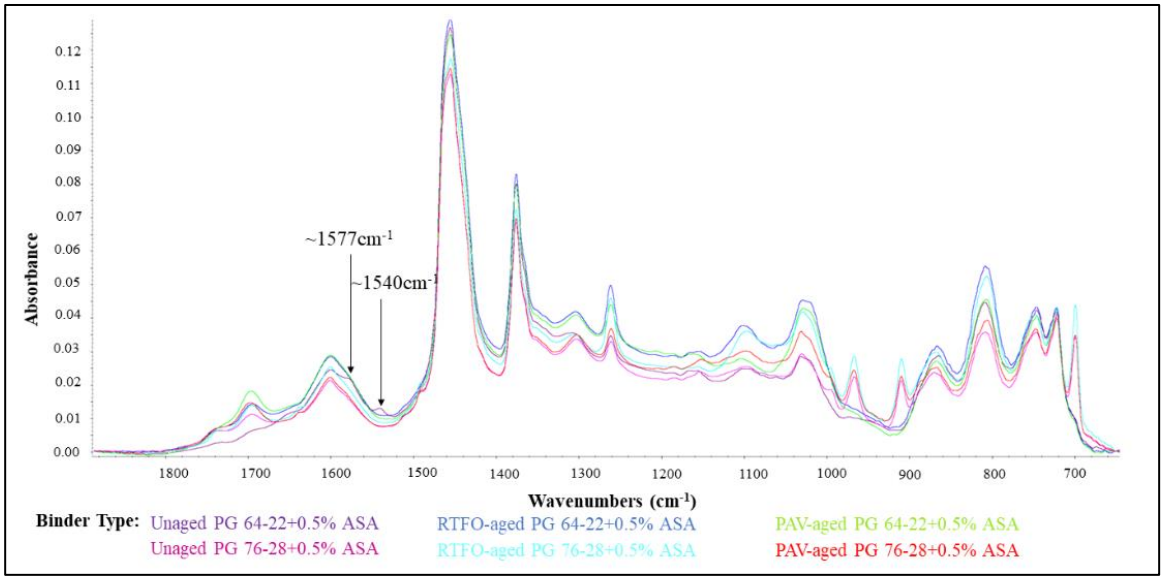

Figure 3.5 FTIR Spectra for PG 64-22 and PG 76-28 binders with ASA additives at different aging conditions

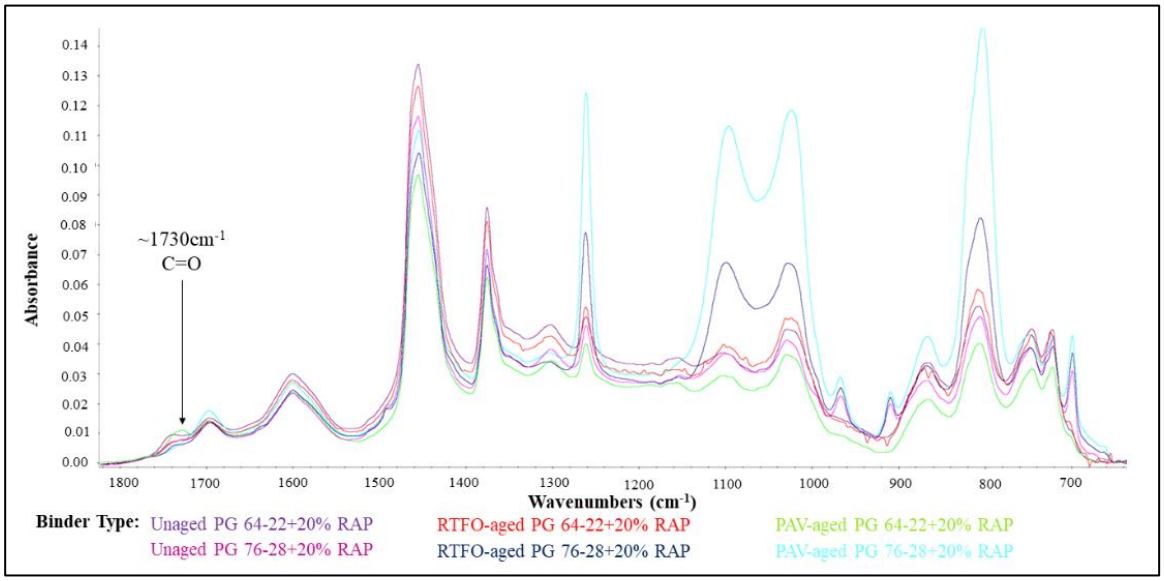

Figure 3.6 FTIR Spectra for PG 64-22 and PG 76-28 binders with 20% RAP binder at different aging conditions

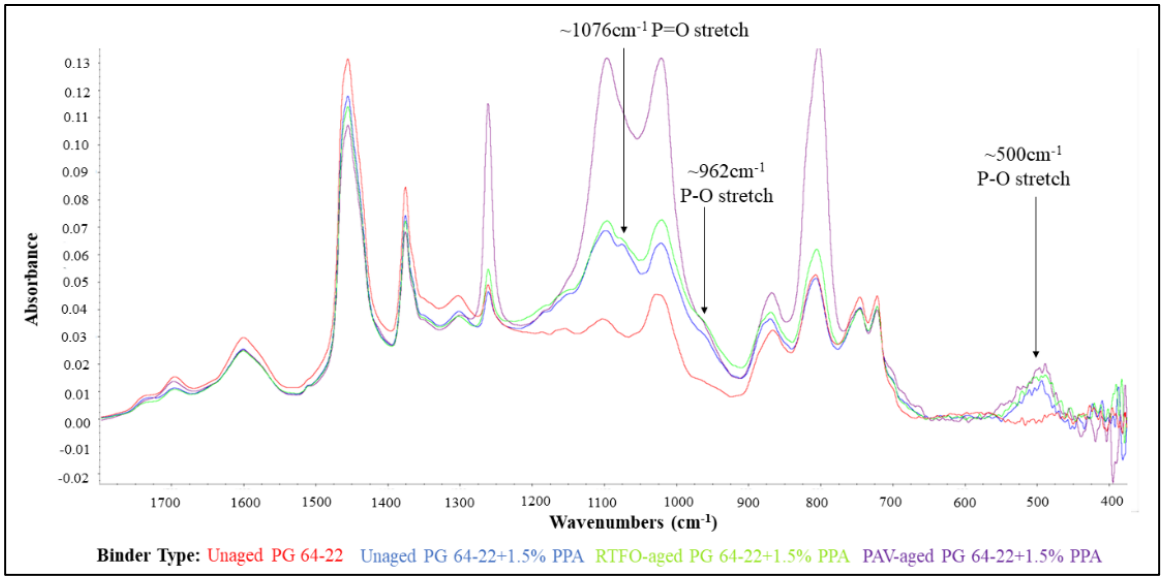

Figure 3.7 FTIR Spectra for PG 64-22 binder with 1.5% PPA at different aging conditions

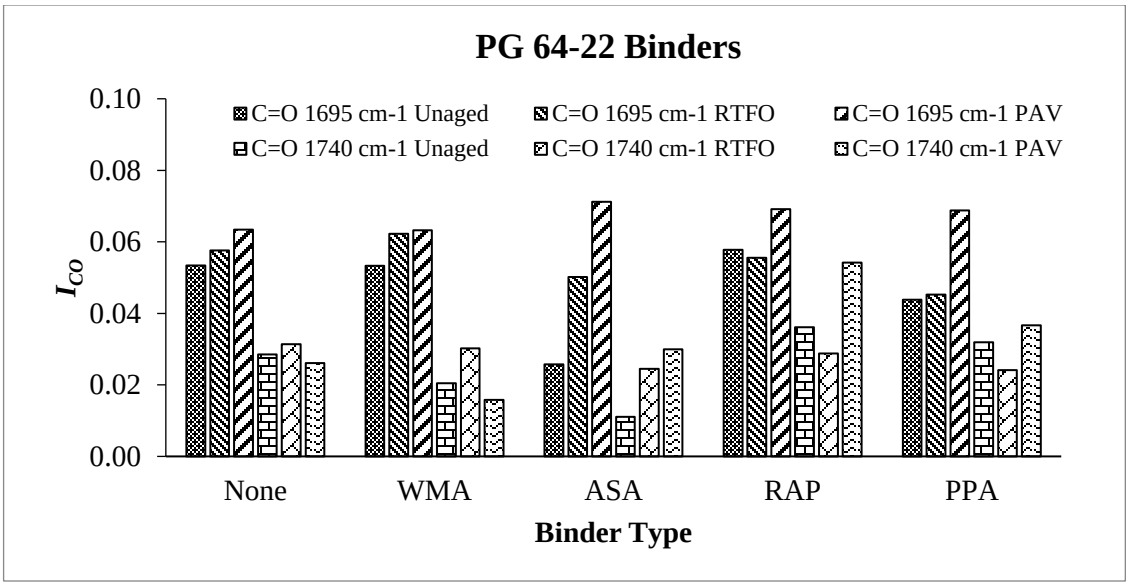

(a)

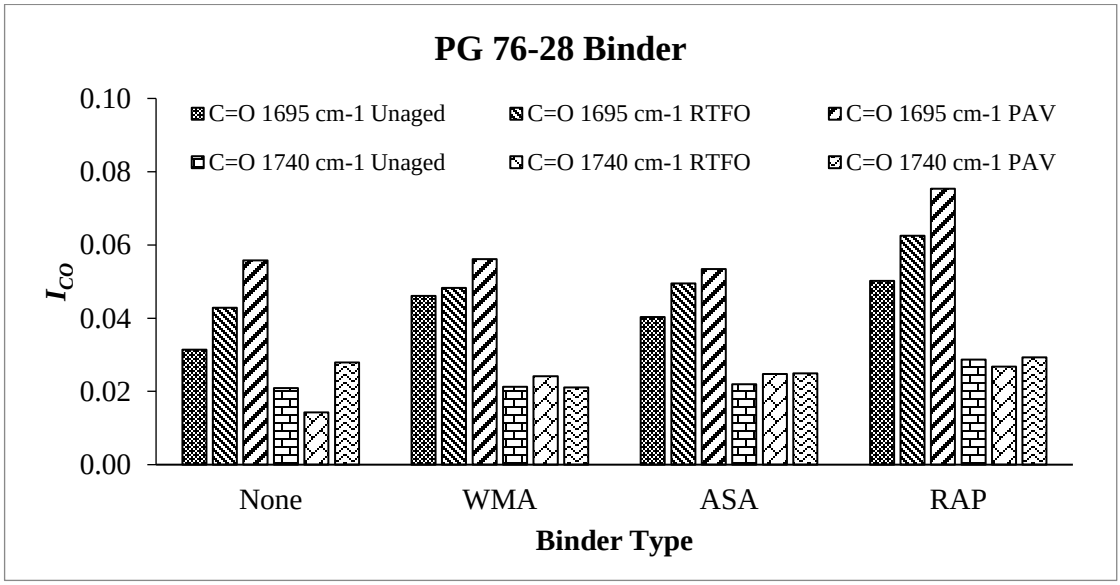

(b)

Figure 3.8 I_{CO} based on peak heights at 1695 and 1740 cm^{-1} for (a) PG 64-22 and (b) PG 76-28 binders

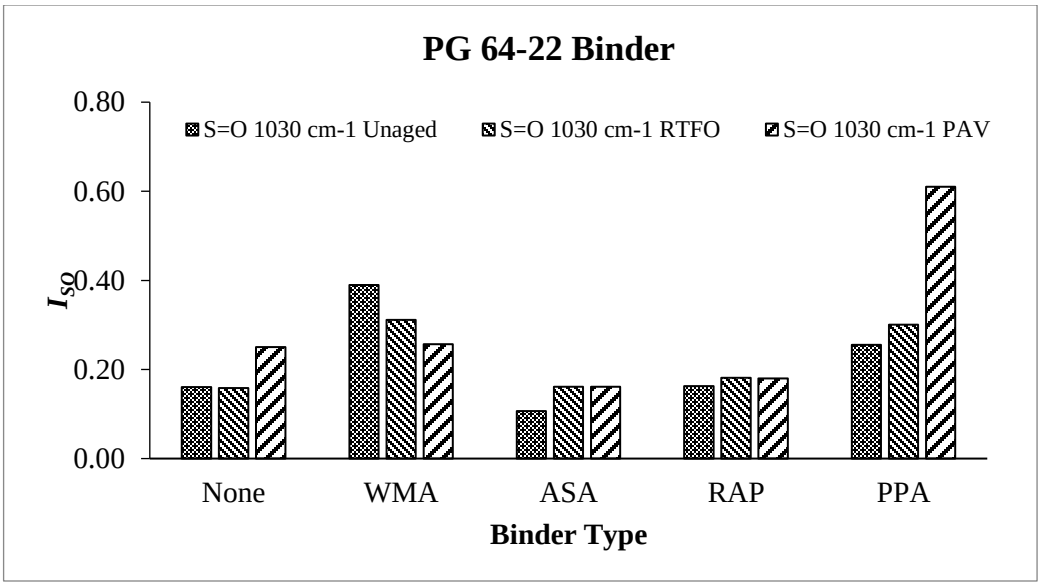

(a)

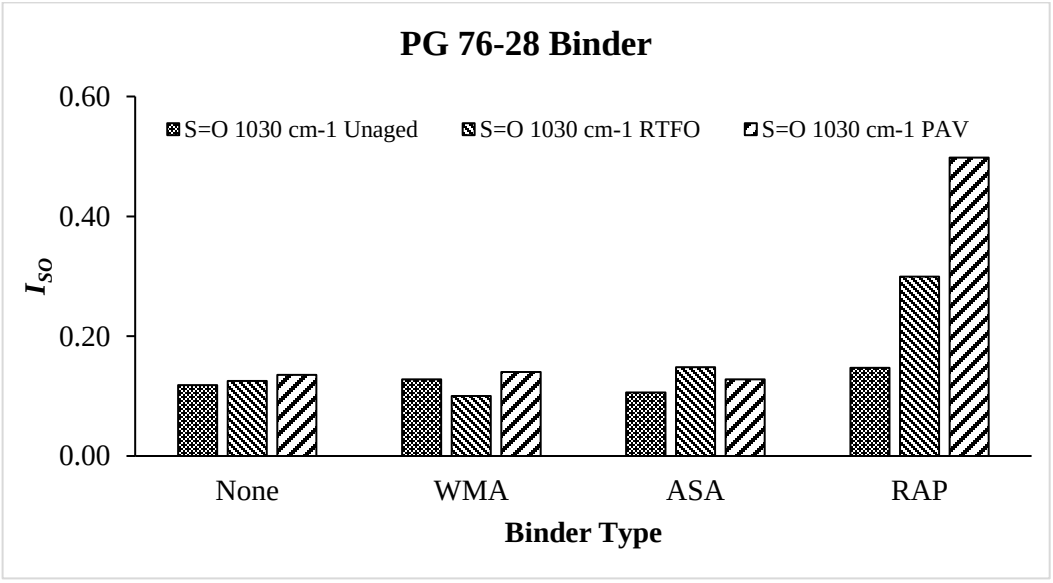

(b)

Figure 3.9 I_{SO} based on peak height at 1030 cm^{-1} for (a) PG 64-22 and (b) PG 76-28 binders

CHAPTER

4

EFFECT OF ADDITIVES AND AGING ON MOISTURE-INDUCED DAMAGE POTENTIAL OF ASPHALT MIXES USING SURFACE FREE ENERGY AND LABORATORY-BASED PERFORMANCE TESTS[3]

ABSTRACT

Lack of mechanistic foundation and poor correlations with field performance of conventional laboratory-based tests accelerated the search for a mechanistic-based approach for screening of asphalt mixes for moisture-induced damages. According to recent studies, surface free energy (SFE) method can be used to quantify mechanistically bond strength and debonding of binder-aggregate system in presence of water. This study was undertaken to evaluate the effects of different additives, such as warm mix asphalt (WMA) additive (amine-derived), amine-based anti-stripping agent (ASA), polyphosphoric acid (PPA) and reclaimed asphalt pavement (RAP) on the moisture-induced damage performance of asphalt mixes through the use of laboratory-based performance tests and SFE method. For this purpose, different energy parameters, namely spreading coefficient ($S_{A/S}$), work of adhesion ($W_{A/S}$), work of debonding (W_{ASW}^{wet}) and energy ratios were calculated from the SFE components of the binder

[3] This chapter was published in the International Journal of Pavement Engineering under the title "Effect of Additives and Aging on Moisture-induced Damage Potential of Asphalt Mixes Using Surface Free Energy and Laboratory-Based Performance Tests." The current version has been formatted for this dissertation.

blends and aggregate. Asphalt mixes consisting of different additives were produced in the laboratory for evaluation of moisture-induced-damage using indirect tensile strength (ITS) and Illinois semi-circular bend (IL-SCB) tests. A new parameter, known as fracture energy ratio (G_f *ratio*) and obtained from the IL-SCB, test was used to correlate fracture energy with moisture-induced damage potential of asphalt mixes. Also, the effect of the short-term and long-term aging on the moisture-induced performance of asphalt mixes were evaluated. Furthermore, correlations between different moisture-induced damage parameters from laboratory-based performance tests and the SFE method were investigated. From this study, the proposed G_f *ratio* was found to be an effective parameter for screening of asphalt mixes in the laboratory for moisture-induced damage.

4.1 INTRODUCTION

Deterioration of mechanical properties of asphalt mixes due to the presence or intrusion of moisture in a liquid or vapor state is generally defined as moisture-induced damage (Caro et al., 2008a). Although moisture-induced damage is not a failure mode by itself, it can accelerate other modes of failures as well as lead to severe damage of the pavement (Abuawad et al., 2015). From a mechanistic point of view, the moisture-induced damage can be assessed by evaluating the bond strength between binder and aggregate, in presence of moisture. A better resistance to moisture-induced damage can be ensured by improving the adhesion bond in the binder-aggregate system (Harvey and Lu, 2005; Masad et al., 2006).

The evaluation of moisture-induced damage remains a challenge for the transportation agencies because of the complex nature of the problem (Abuawad et al.,

2015). Several test methods have been developed and improved over the last few decades to characterize moisture-induced damage potential of asphalt mixes (Caro et al., 2008a; Caro et al., 2008b). Modified Lottman test, indirect tensile strength ratio (TSR), resilient modulus ratio, Marshall stability ratio, and Hamburg wheel tracking (HWT) test have been used by several agencies for evaluating the moisture-induced damage potential of asphalt mixes (Bagampadde et al., 2006; Gorkem and Sengoz, 2009; Ghabchi et al., 2015; Mirzababaei, 2016). However, many of these test methods are empirical and have several drawbacks, such as inability to simulate field condition, dependency on moisture conditioning process, and poor correlations with field performance (Caro et al., 2008b; Abuawad et al., 2015). Currently there is no general agreement on a single test and moisture conditioning method for evaluating moisture-induced damage. Therefore, mechanistic emphasis is needed for assessing the compatibility between aggregates and binders to resist moisture-induced damage (Bhasin, 2007; Caro et al., 2008b).

As the use of different additives and modifiers such as warm mix asphalt (WMA) additives, poly-phosphoric acid (PPA), anti-stripping agents (ASA) and reclaimed asphalt pavement (RAP) in asphalt mixes continues to increase, the mechanistic evaluation of the moisture-induced damage potential becomes even more important. Also, the changes in the physical-chemical properties of binder from oxidative aging may promote the occurrence of microcracks. These microcracks can facilitate moisture intrusion in asphalt pavement, accelerating the moisture-induced damage process (Aguiar-Moya et al., 2015). The cohesive and adhesive bonding within the binder-aggregate system are directly related to the surface free energy (SFE) of the

both materials (Bhasin, 2007). A number of recent studies have used the thermodynamic or adhesion theory by applying the SFE approach to mechanistically quantify the adhesion between aggregate and binder (Bhasin and Little, 2006; Bhasin et al., 2006; Hefer et al., 2006; Bhasin, 2007; Bhasin et al., 2007a; Bhasin et al., 2007b; Wasiuddin et al., 2007c; Wasiuddin et al., 2008; Buddhala et al., 2011; Ghabchi et al., 2013). Also, the SFE approach has been used successfully to evaluate the changes in the moisture-induced damage potential of asphalt mixes containing different additives (Wasiuddin et al., 2007c; Moghadas Nejad et al., 2012; Arabani and Hamedi, 2014).

Wasiuddin et al. (2007c) evaluated the effect of antistrip additives on asphalt binders using the SFE technique. A chemical model was proposed to explain the change in SFE components with the addition of antistrip additives. In a different study, thermal degradation of the antistripping agent as a result of aging of binder was evaluated by Wasiuddin et al. (2007b) using the same technique. The beneficial effect of antistripping additives on the SFE components of binders was found to be significantly reduced by short-term and long-term aging. Also, the influence of different warm mix asphalt additives on the moisture-induced damage potential of binders was studied and reported by Wasiuddin et al. (2008). The effect of different types of binder modifications on the surface free energy components of the binder was evaluated by Bhasin et al. (2007a). The changes in surface free energy due to the addition of polymers and anti-stripping agent and oxidative aging were determined and different energy parameters were calculated to correlate with the performance of the asphalt mixes. In another study, Bhasin and Little (2007) compared the surface free energy characteristics of five aggregates of different chemical compositions. The aggregates

exhibited widely different base SFE components which were found to be the primary contributors to the differences in the compatibility ratio with any given binder. Arabani and Hamedi (2010) evaluated the effects of polyethylene polymer coating on aggregates using the SFE characteristics of aggregates. It was observed that the polyethylene polymer coating treatment brought the total SFE of aggregates to the same level although they exhibited significant differences before treatment. In another study, Arabani and Hamedi (2014) used surface free energy (SFE) concept to evaluate the effect of liquid antistrip additives. A good correlation was observed between the moisture-induced damage results from dynamic modulus test and SFE technique. Alvarez et al. (2012a) evaluated the effect of three different fillers on binder-aggregate interfaces of asphalt mixes based on surface free energy approach. It was observed that the inclusion of filler in the mix can lead to changes in the fracture and moisture-induced damage resistance of the mastic-aggregate systems. In a different study, asphalt rubber-aggregate and polymer modified binders-aggregate interfaces were evaluated using the same procedure (Alvarez et al., 2012b). The cohesion and adhesion of asphalt mastic were also studied by Tan and Guo (2013). Sessile drop and column wicking method were used to measure the SFE components of asphalt and fillers, respectively. The van der Waals force of surface free energy was found to play an important role in the cohesion and adhesion of asphalt mastic. Ghabchi et al. (2014) evaluated the effect of the addition of different amounts of RAP to the asphalt binders on their surface energies. The compatibilities of different amounts of RAP blended binders with six different types of aggregates were evaluated using wettability, work of adhesion, work of debonding and energy ratio parameters.

With the advent of balanced mix design (Cooper III et al., 2014; Ozer et al., 2016b), many Departments of Transportation (DOTs) are considering adopting a fatigue evaluation procedure using semi-circular bend (SCB) geometry (Kim et al., 2012; Al-Qadi et al., 2015; Mohammad et al., 2016; Ozer et al., 2016a; Ozer et al., 2016b). As the fatigue damage and healing in asphalt mixes are directly related to the cohesive and adhesive bonding of the binder-aggregate system, the incorporation of fracture mechanics through SCB test is expected to better explain the mechanisms responsible for the moisture-induced damage phenomenon. The Illinois semi-circular bend (IL-SCB) test evaluates the fracture properties of asphalt mixes using the flexibility index (*FI*) following the AASHTO TP 124 (AASHTO, 2018) method. The *FI* is derived from the fracture energy (G_f) and post peak slope of the load-deformation curve (Al-Qadi et al., 2015). A comparison of the fracture energy of the moisture-conditioned and dry specimens, i.e. G_f *ratio* from the IL-SCB test is expected to provide important insight on the moisture-induced damage potential of asphalt mixes.

4.2 OBJECTIVES

In this study, the moisture-induced damage potential of binder-aggregate systems was evaluated using the SFE method. In addition, moisture-induced damage potential of asphalt mixes was investigated using indirect tensile strength (ITS) and a new test method based on the IL-SCB test. The specific objectives of this study were as follows:

i. Evaluate the effects of different additives and aging on the moisture-induced damage potential of binder-aggregate systems using the SFE approach.

ii. Investigate the effect of different additives and aging on the moisture-induced damage potential of asphalt mixes using conventional, i.e. ITS test and a new method based on the IL-SCB test.

iii. Evaluate the suitability of *TSR* and G_f *ratio* to predict moisture-induced damage by correlating with energy parameters from SFE method.

4.3 THERMODYNAMIC APPROACH OF EVALUATING MOISTURE-INDUCED DAMAGE

Thermodynamic theory (also known as adsorption theory) is one of the most widely used concepts in adhesion science (Hefer et al., 2005). According to this theory, the physio-chemical adhesion between two materials is a thermodynamic phenomenon and a function of surface free energies of those materials. According to the Good-Van Oss-Chaudhury theory, the SFE of a material can be divided into three independent components, namely a non-polar or Lifshitz-van der Waals component, a monopolar acidic component, and a monopolar basic component (Van Oss et al., 1988). These components can be obtained by measuring the work of adhesion of that material with other liquids or vapors (Van Oss et al., 1988). The total SFE of a material can be expressed by combining all these components using Equation (4.1).

$$\Gamma^{Total} = \Gamma^{LW} + 2\sqrt{(\Gamma^{+}\Gamma^{-})} \qquad (4.1)$$

where,

Γ^{+}= Lewis acid component,

Γ^{-}= Lewis base component,

Γ^{LW} = Lifshitz-van der Waals component,

Γ^{Total} = total SFE component.

For convenience of this study, subscripts *A, L, S, and W* are used to represent asphalt binder, probe liquids, aggregate (stone) and water, respectively.

The tendency of a binder and an aggregate to bind together or form a binder-aggregate system in dry condition can be represented by the work of adhesion (W_{AS}). The W_{AS} of a binder-aggregate system can be calculated from Equation (4.2) using the SFE components of the binder and aggregate.

$$W_{AS} = 2\sqrt{(\Gamma_A^{LW}\Gamma_S^{LW})} + 2\sqrt{(\Gamma_A^{+}\Gamma_S^{-})} + 2\sqrt{(\Gamma_A^{-}\Gamma_S^{+})} \qquad (4.2)$$

In presence of water, the amount of work required for debonding of the binder from the aggregate surface is defined as work of debonding (W_{ASW}^{wet}) and can be determined using Equation (3).

$$W_{ASW}^{wet} = \Gamma_{AW} + \Gamma_{SW} - \Gamma_{AS} \qquad (4.3)$$

where,

Γ_{AW} = interfacial energy between binder and water,

Γ_{SW} = interfacial energy between aggregate and water,

Γ_{AS} = interfacial energy between binder and aggregate.

The interfacial energy is the energy equal to the surface energy at an interface. The interfacial energy between materials *i* and *j* can be calculated using Equation (4.4).

$$\Gamma_{ij} = \Gamma_i^{Total} + \Gamma_j^{Total} - 2\sqrt{(\Gamma_i^{LW}\Gamma_j^{LW})} - 2\sqrt{(\Gamma_i^{+}\Gamma_j^{-})} - 2\sqrt{(\Gamma_i^{-}\Gamma_j^{+})} \qquad (4.4)$$

The tendency of the binder to spread and coat the surface of the aggregate can be determined using the wettability or spreading coefficient ($S_{A/S}$). A higher value of $S_{A/S}$ is required to ensure a better coating of the binder to the aggregate surface (Buddhala et al., 2011). The $S_{A/S}$ can be calculated using Equation (4.5).

$$S_{A/S} = \Gamma_S^{Total} - \Gamma_{AS} - \Gamma_A^{Total} \quad (4.5)$$

where,

Γ_S^{Total} = total SFE of aggregate,

Γ_{AS} = interfacial energy between asphalt binder and aggregate,

Γ_A^{Total} = total SFE of asphalt binder.

Bhasin et al. (2007b) combined the effect of W_{AS} and W_{ASW}^{wet} and proposed a single valued parameter to evaluate moisture damage. The energy ratio parameter can be calculated using Equation (4.6).

$$ER_1 = \left|\frac{W_{AS}}{W_{ASW}^{wet}}\right| \quad (4.6)$$

To consider the effect of wettability, a modified version of Equation (4.6) was also proposed by Bhasin et al. (2007b). The parameter is known as ER_2 and can be calculated using Equation (4.7).

$$ER_2 = \left|\frac{W_{AS} - W_{AA}}{W_{ASW}^{wet}}\right| \quad (4.7)$$

where, W_{AA} is the cohesive bond energy of the asphalt binder and can be calculated using Equation (4.8).

$$W_{AA} = 2\left(\Gamma_A^{LW} + 2\sqrt{(\Gamma_A^+ \Gamma_A^-)}\right) \quad (4.8)$$

As recommended by Bhasin et al. (2007b), all the parameters, such as W_{AS} and W_{ASW}^{wet}, $S_{A/S}$ and energy ratios were used in this study to evaluate moisture-induced damage potential of asphalt mixes.

4.4 MATERIALS AND METHODS

4.4.1 Materials

The work-flow diagram used for this study is presented in Figure 4.1. For the purpose of this study, a commonly used dense-graded mix design with a nominal maximum aggregate size (NMAS) of 12.5 mm was selected and pertinent materials were collected from an Oklahoma, USA plant. Five different mixes with two different aging conditions (short-term and long-term aging) were prepared in the laboratory following the collected mix design protocol. Mix-1-None was the control mix without any additives, whereas Mix-2-WMA, Mix-3-ASA, Mix-4-PPA and Mix-5-RAP contained WMA additive, ASA, PPA and RAP, respectively. The amount of WMA additive (0.5% of total binder) and ASA (0.5% of total binder) used in Mix-2-WMA and Mix-3-ASA, respectively, was selected based on the manufacturers' recommendations. For Mix-4-PPA, the amount of PPA (1.5% of total binder) was selected based on the experience from a previous project conducted by the authors (Rani, 2019a). Mix-1-None through Mix-4-PPA were prepared with approximately 25 percent 5/8" stone chips, 15 percent ½" stone chips, 30 percent 3/8 screens, 15 percent 3/16" screens and 15 percent sand, and 5.2 percent PG 64-22 binder. The gradation curve for the mixes is presented in Figure 4.2. The sand used for this study was natural sand collected from Canadian river near Oklahoma City. Except sand, all the aggregates were rhyolite aggregate and were collected from an Oklahoma quarry. Therefore, mixes contain 85% rhyolite aggregate and 15% natural sand. Although the initial design does not contain RAP, changes were made in the mix design to incorporate 20% RAP and maintain a similar gradation. A slightly higher binder content (5.5%) was required for

Mix-5-RAP compared to other mixes to satisfy the mix design requirement set by Oklahoma DOT (ODOT, 2009). The PG 64-22 was an unmodified binder and collected from an Oklahoma refinery. The RAP required to produce asphalt mixes was collected from an Oklahoma asphalt plant. Also, a chemical WMA additive, one type of PPA and an amine-based ASA were collected from material suppliers of Oklahoma. Additives were mixed with the binder at their mixing temperatures before adding to the aggregates. Of the selected mixes, four (Mix-1-None, Mix-3-ASA, Mix-4-PPA and Mix-5-RAP) were mixed and compacted at 163° and 149°C, respectively. A lower mixing (135°C) and compaction (128°C) temperatures were used for Mix-2-WMA as it contained WMA additive-modified binder. For the purpose of this study, the AASHTO R 30 (AASHTO, 2015a) procedure was followed to prepare samples using both short-term and long-term aging. For simulating short-term aging, all the loose mixes were placed in an oven for four (4) hours at 135°C before compaction. After short-term aging, cylindrical samples of different dimensions needed to conduct ITS and IL-SCB tests were compacted using a Superpave gyratory compactor (SGC). The AASHTO T 312 (AASHTO, 2015b) method was followed for compaction. For this purpose, batch weights of the mixes were adjusted to obtain specimens with 7% air voids after compaction. Specimens were compacted in height-controlled mode in SGC to obtain 7% air voids at desired height. Long-term aging on the samples were simulated by placing the compacted samples in the oven for 120 hours at 85°C following AASHTO R 30 (AASHTO, 2015a). Laboratory tests were conducted on samples that satisfied the air voids requirement of 7±0.5%.

The surface free energy components of the collected PG 64-22 binder with 0.5%

WMA additive, 0.5% ASA, 1.5% PPA and 20% RAP (by weight of the total binder) were determined using dynamic Wilhelmy plate (DWP) test. For this study, simulated RAP binder was used instead of extracted binder to avoid any chemical contamination from the use of solvent during the extraction and recovery process. The simulated RAP binder was prepared following the procedure described in the literature (Ghabchi et al., 2014). For this purpose, a PG 64-22 binder was short-term aged using a rolling thin film oven (RTFO) following the AASHTO T 240 (AASHTO, 2017) method and then long-term aged using a pressure aging vessel (PAV) following the AASHTO R 28 (AASHTO, 2016) method. Asphalt binder was blended with the additives using a high shear mixer at 1,000 rpm for 45 minutes at 155°C. The mixing time and speed was kept same for all the binder blends (including control binder) to avoid the effect of aging during mixing. The short-term aging and long-term aging of the binder blends were simulated following the AASHTO T 240 (AASHTO, 2017) and AASHTO R 28 (AASHTO, 2016) method, respectively.

The SFE components of the rhyolite aggregate used in the mixes was measured using a universal sorption device (USD). For aggregate sample preparation, the size fraction with particles larger than 2.36 mm (retaining on a No. 8 sieve) and smaller than 4.75 mm (passing a No. 4 sieve) was selected. The selected fraction of aggregates was washed several times with distilled water to obtain dust-free clean surfaces. Then they were oven-dried at 120°C for 24 hours and allowed to cool down to room temperature in a desiccator sealed with silica gel, before testing. It should be noted that, in the current study, SFE components of sand was not determined and not included in the energy parameter calculation using thermodynamic equations. As the amount of sand is

small (15% of the aggregate) compared to the rhyolite aggregate (85% of the aggregate), it was assumed to have insignificant effect on the energy parameter calculation. However, the effect of the SFE components of sand will be addressed in a future study.

4.4.2 Test Methods

4.4.2.1 Indirect Tensile Strength Test

The ITS test was conducted in accordance with the AASHTO T 283 (AASHTO, 2014a) test method. The reduction in tensile strength as a result of the freeze-thaw conditioning was measured as an indicator of the moisture-induced damage. For this purpose, asphalt mix specimens of 150 mm diameter and 95 mm height were prepared in the laboratory. The compacted specimens of each mix were divided into three subsets, short-term aged dry conditioned, short-term aged moisture conditioned and long-term aged moisture conditioned. The short-term aged dry conditioned specimens were prepared by keeping the sample at 25°C, whereas short-term moisture conditioned specimens were subjected to moisture conditioning by AASHTO T 283 (AASHTO, 2014a). The third subset was long-term aged by keeping in the oven for 120 hours at 85°C following AASHTO R 30 (AASHTO, 2015a). After conducting long-term aging, the specimens from the third subset were moisture conditioned following AASHTO T 283 (AASHTO, 2014a) method. According to AASHTO T 283 (AASHTO, 2014a) method, samples were conditioned by saturating with water (70-80% saturation) under a 13 to 67 kPa absolute vacuum pressure. After vacuum saturation, samples were tightly sealed with a plastic film and placed in leak-proof plastic bag containing 10 mL of water. The samples were then subjected to a freeze cycle at -18°C for a minimum of 16

hours followed by a thaw cycle at 60°C for 24 hours. All specimens were brought to 25°C before conducting the ITS test. The short-term aged *TSR* (*TSR*$_{ST}$) and long-term aged *TSR* (*TSR*$_{LT}$) for the mixes were calculated using Equations (4.9) and (4.10).

$$TSR_{ST} = \frac{ITS\ of\ short-term\ aged\ moisture-conditioned\ Specimens}{ITS\ of\ short-term\ aged\ Dry-conditioned\ Specimens} \quad (4.9)$$

$$TSR_{LT} = \frac{ITS\ of\ long-term\ aged\ moisture-conditioned\ Specimens}{ITS\ of\ short-term\ aged\ Dry-conditioned\ Specimens} \quad (4.10)$$

The short-term aged *TSR* (*TSR*$_{ST}$) value was determined by dividing the average tensile strength of short-term aged moisture conditioned by short-term aged dry conditioned specimens. The reduction in tensile strength due to long-term aging and AASHTO T 283 (AASHTO, 2014a) moisture conditioning was determined using long-term aged *TSR* (*TSR*$_{LT}$). The *TSR*$_{LT}$ is the ratio of the average tensile strength of long-term aged moisture conditioned to that of short-term aged dry conditioned specimens.

4.4.2.2 Illinois Semi-Circular Bend Test

The fracture potential of asphalt mixes was evaluated using the fracture energy (G_f) determined by IL-SCB test following the AASHTO TP 124 (AASHTO, 2018) method. For this purpose, cylindrical SGC samples of 150 mm diameter and 120 mm thickness were compacted in the laboratory. The sample was then cut into two cylindrical specimens with a diameter of 150 mm and a thickness of 50 mm. Specimens having a diameter of 150 mm, a height of 75 mm, and a thickness of 50 mm were obtained by cutting the cylindrical specimens into semi-circular halves. The moisture conditioning using only one freeze-thaw cycle was reported to be inadequate in simulating field conditions (Vargas-Nordcbeck et al., 2016). Therefore, another relatively new moisture conditioning process using Moisture Induced Sensitivity Test

(MIST) device, following ASTM D 7870 (ASTM, 2013), was used in this study as a part of the development of new test method using IL-SCB test. The MIST conditioning simulates the distress experienced by a wet pavement from a passing vehicle tire. Similar to ITS test, the samples were divided into three subsets, short-term aged dry conditioned, short-term aged MIST conditioned and long-term aged MIST conditioned. Following ASTM D 7870 (ASTM, 2013), compacted sample were placed inside the chamber of the MIST device. The chamber was then filled with sufficient water and the lid was secured. The chamber temperature was then raised to 60°C. The sample was conditioned at this temperature for 20 hours to simulate chemical and adhesion effects. After the adhesion phase, samples were subjected to 3,500 pressure cycles at 275 kPa to generate the effect of pore pressure inside the sample (ASTM, 2013). After the completion of cycling process, the water drained through the drain valve. These steps were automatically controlled and performed by the MIST device. The sample was then carefully removed from the chamber and brought back to room temperature. After conditioning, specimen for IL-SCB test was prepared by cutting into desired shape with a notch of 15 mm depth and 1.5 mm width. The test was conducted at room temperature (25°C) with a loading rate of 50 mm/min following the AASHTO TP 124 test method (AASHTO, 2018). The fracture work (W_f) was calculated by determining the area under the load vs. deformation curve from the IL-SCB test. The fracture energy, G_f, was then calculated by dividing the fracture work with ligament area (A_{lig}) using Equation (4.11). The ligament area was calculated by multiplying the ligament length (sample height minus notch depth) with sample thickness. The fracture energy ratios of short-term ($(G_f\ ratio)_{ST}$) and log-term aged ($(G_f\ ratio)_{LT}$) specimens were determined using Equations

(4.12) and (4.13), respectively.

$$G_f = \frac{W_f}{A_{lig}} \qquad (4.11)$$

$$(G_f\ ratio)_{ST} = \frac{G_f\ of\ short-term\ aged\ MIST-conditioned\ Specimens}{G_f\ of\ short-term\ aged\ Dry-conditioned\ Specimens} \qquad (4.12)$$

$$(G_f\ ratio)_{LT} = \frac{G_f\ of\ long-term\ aged\ MIST-conditioned\ Specimens}{G_f\ of\ short-term\ aged\ Dry-conditioned\ Specimens} \qquad (4.13)$$

4.4.2.3 Dynamic Wilhelmy Plate Test

The SFE components of a binder can be calculated by solving Equation (4.14) using contact angle values measured with different probe liquids of known SFE components. A number of probe liquids such as water (W), glycerol (G), formamide (F), diiodomethane (D) and ethylene glycol (E) has been used by researchers to determine the SFE components of the binder. Contact angles of the binder with at least three probe liquids are required to establish an equation set in order to simultaneously solve the three SFE components of the binder. However, the WGFDE probe liquid set was found to obtain consistent energy parameters. Therefore, in this study, the contact angles of the binder blends with the abovementioned five probe liquids were determined by DWP test using a dynamic contact angle (DCA) analyzer. However, contact angles of the RTFO-aged and PAV-aged binder blends containing 1.5% PPA were found to be inconsistent with formamide and diiodomethane, therefore, excluded from the calculation. In order to solve the overdetermined equation set (i.e. number of equations > number of unknowns), the Solver function incorporated into Microsoft Excel was used to compute the SFE components of the binder blends by minimizing the sum of the square errors. The binder samples for DWP testing were prepared using a 24 mm x 50 mm glass plate coated with the asphalt binder blends. The details of the testing

procedure are described in the literature (Ghabchi et al., 2014). Five replicates were tested for each probe liquid to ensure consistency and repeatability of the test results.

$$\Gamma_L^{Total}(1 + cos\theta) = 2(\Gamma_A^{LW}\Gamma_L^{LW} + \Gamma_A^{+}\Gamma_L^{-} + \Gamma_A^{-}\Gamma_L^{+}) \qquad (4.14)$$

4.4.2.4 Universal Sorption Device (USD) Test

The SFE components of the rhyolite aggregate were measured using a universal sorption device (USD). In this study, the adsorption isotherms of three probe vapors, namely water, methyl propyl ketone (MPK), and toluene were determined by conducting the adsorption tests on aggregate at 25°C and different relative pressure ranging from 0.05 to 1.00. About 20 grams of the prepared aggregate sample was introduced in the sample chamber of the USD device to obtain adsorption isotherms. The equilibrium spreading pressure (π_e) of each vapor was then calculated based on the mass absorbed at maximum saturated vapor pressure using Equation (4.15). Equation (4.16) presents the relation between work of adhesion, spreading pressure and the SFE components of the aggregate using Good-van-Oss-Chaudhury (GVOC) theory. The three unknown SFE components of the aggregate in Equation (16) were determined by arranging a set of three equations using spreading pressures of three different probe vapors.

$$\pi_e = \frac{RT}{MA}\int_0^{Po}\frac{n}{p}dp \qquad (4.15)$$

$$\pi_e + 2\gamma_{LV} = 2\sqrt{(\Gamma_S^{LW}\Gamma_L^{LW})} + 2\sqrt{(\Gamma_S^{+}\Gamma_L^{-})} + 2\sqrt{(\Gamma_S^{-}\Gamma_L^{+})} \qquad (4.16)$$

where,

R = universal gas constant,

T = temperature,

n = mass absorbed per unit mass of aggregate at a vapor pressure p,

M = molecular weight of the probe vapor,

P_0 = maximum saturation vapor pressure,

A = specific surface area of the aggregate.

4.5 RESULTS AND DISCUSSIONS

4.5.1 Surface Free Energy Components of Binder Blends

4.5.1.1 Effect of Additives

The average (avg) and standard deviation (SD) of contact angles of RTFO-aged and PAV-aged PG 64-22 binder with 0.5% WMA, 0.5% ASA, 1.5% PPA and 20% RAP are presented in Table 4.1. From Table 4.1, the effect of the addition of different additives on contact angle of binder blends with different probe liquids were found to be different. The reactions of the PG 64-22 binder with different additives are likely responsible for these variations. The contact angles of the binder blends with different probe liquids were used to calculate the SFE components of the tested binders using Equation (4.14). The SFE components of the RTFO-aged and PAV-aged PG 64-22 binders with different additives are presented in Table 4.2. Typically, a change in the SFE components of a binder is expected to result in a change in the moisture-induced damage potential of the corresponding binder-aggregate system. It was observed that the acid component of the asphalt acts as a scale factor in calculation of dry adhesive bond strength (Bhasin et al., 2006).

From Table 4.2, it was observed that the acid (Γ^+) and base (Γ^-) components of RTFO-aged PG 64-22 binder increased with the addition of the WMA additive. However, non-polar Lifshitz-van der Waals (Γ^{LW}) component of PG 64-22 binder was

found not to change with the addition of WMA additive. From Table 4.2, it was also observed that the Γ^+ and the Γ^- components of PG 64-22 binder increased as a result of the addition of ASA. Also, the Γ^+/Γ^- ratio was found to reduce from 1.06 to 0.87 indicating more basic behavior with the addition of 0.5% ASA. The reaction of the amine-based ASA, which is basic in nature, with binder constituents are expected to be responsible for the changes in the binder surface energy properties. Similar increase in the basic behavior with the addition antistripping agent was reported by other study (Wasiuddin et al., 2007c). Also, it was observed that the Γ^+ and Γ^- components of PG 64-22 binder increased and Γ^{LW} components reduced due to the addition of simulated RAP. The Γ^+/Γ^- ratio was found to increase from 1.06 to 1.36 indicating more acidic behavior with the addition of 20% RAP, which is consistent with the previous studies (Ghabchi et al., 2014). As a result of the addition of PPA, the Γ^+/Γ^- value for the PG 64-22 binder was found to reduce from 1.06 to 0.24 indicating a substantial increase in basic behavior with the addition of PPA to binder blend. Increase in the basic SFE component of the binder with an increase in PPA amount was also reported in the available literature (Al-Qadi et al., 2014). Therefore, the addition of PPA may result in a weak bonding with aggregates that generally have a higher basic component than acid component. Similar to contact angles, the reactions of the PG 64-22 binder constituents with PPA are likely to be responsible for such changes in the binder's surface energy properties.

4.5.1.2 Effect of Aging

From Table 4.2, it was observed that the Γ^{LW} and Γ^{Total} components of PG 64-22 binder decreased with PAV-aging. However, the Γ^+ and Γ^- components of the PG 64-22

binder was found to increase with long-term aging. Also, the Γ^+/Γ^- ratio of PG 64-22 binder was found to reduce significantly (from 1.06 to 0.58) as a result of PAV-aging. A similar trend in reduction of Γ^+/Γ^- ratio was observed for PG 64-22 with 20% RAP. These results indicate that the binder became more basic in nature with long-term aging, which may result in weak bonding with basic aggregates. However, the Γ^+/Γ^- ratio was found to increase from 1.24 to 1.82 for WMA modified binder and from 0.87 to 1.17 for ASA-modified binders. This phenomena may be resulted from the degradation of ASA with aging (Wasiuddin et al., 2007a). Therefore, the reduction in basic properties of amine-based ASA with long-term aging is expected to be responsible for this observation. The Γ^+ component was found to reduce and the Γ^- component was found to increase for 1.5% PPA-modified binder with long-term aging making the binder more susceptible to moisture-induced damage.

4.5.2 Surface Free Energy Components of Aggregates

The SFE components of the tested aggregate are presented in Table 4.2. The magnitude of Γ^+ (0.39 mJ/m^2) and Γ^{LW} (52.87 mJ/m^2) components of the SFE was found to be much lower than the Γ^- component of the aggregate. For basic aggregates (Γ^- component greater than Γ^+ component), Bhasin (2007) reported that the adhesion between the binder and aggregate is significantly influenced by the large magnitude of the Γ^- component of the aggregates.

4.5.3 Energy Parameters from SFE Method

4.5.3.1 Effect of Additives

The $S_{A/S}$, W_{AS} and W_{ASW}^{wet} were determined by combining the SFE components of the RTFO-aged binder blends with the SFE components of rhyolite aggregate and are

presented in Figures 4.3(a), 4.3(b) and 4.3(c), respectively. A higher magnitude of $S_{A/S}$ of a binder-aggregate system means a greater tendency of the liquid asphalt binder to wet and coat the surface of that aggregate (Buddhala et al., 2011). From Figure 4.3(a), the $S_{A/S}$ of PG 64-22 binder was found to increase with the addition of 0.5% WMA. Other studies also reported an increase in the $S_{A/S}$ with the addition of amine-derived WMA additive (Ghabchi et al., 2013; Ghabchi, 2014). The reaction of the amine derivatives from the WMA additives with the binder constituents are expected to be responsible for this increase in $S_{A/S}$. Also, the coating ability of the PG 64-22 binder was found to increase with the addition of ASA and RAP, which is consistent with other studies (Wasiuddin et al., 2007c; Ghabchi et al., 2014).

A higher W_{AS} value indicates a stronger bond between asphalt binder and aggregate under dry condition. From Figure 4.3(b), it was observed that the W_{AS} for PG 64-22 binder increased due to the addition of all the additives. The work of adhesion for PG 64-22 binder was found to be 81.88 mJ/m^2, whereas the W_{AS} increased to 84.71, 83.22, 85.88 and 85.05 mJ/m^2 with the addition of WMA, ASA, RAP and PPA, respectively.

Generally, the W_{ASW}^{wet} for a specific binder-aggregate system in the presence of water is negative, which indicates that the process is thermodynamically favorable for debonding of asphalt binder and aggregate. A lower magnitude of $|W_{ASW}^{wet}|$ is desirable as it reduces the tendency of the binder-aggregate system to debond. The magnitude of the $|W_{ASW}^{wet}|$ was found to decrease upon the addition of WMA, ASA and RAP. However, the $|W_{ASW}^{wet}|$for the PG 64-22 binder with rhyolite aggregate was found to increase from 82.31 mJ/m^2 to 87.9 mJ/m^2 with the addition of PPA (Figure 4.3(c)).

Based on the results of the $|W_{ASW}^{wet}|$, it can be concluded that the addition of PPA may increase the moisture-induced damage potential of an asphalt mix containing basic aggregate such as rhyolite.

The ER_1 and ER_2 parameters were used to evaluate the moisture-induced damage potential of different combinations of PG 64-22 with the rhyolite aggregate and are presented in Figure 4.5(a). It was found that both ER_1 and ER_2 increased with the addition of WMA, ASA and RAP indicating better resistance to moisture-induced damage potential of asphalt mixes. These findings are consistent with other studies (Wasiuddin et al., 2007c; Ghabchi et al., 2013; Ghabchi et al., 2014). On the contrary, lower magnitudes of ER_1 and ER_2 were observed for PPA modified binder indicating a greater tendency of debonding between asphalt binder and aggregate. A reduction in the moisture damage resistance of a PPA-modified binders with basic aggregate was also reported in other studies (Reinke and Glidden, 2010; Al-Qadi et al., 2014).

4.5.3.2 Effect of Aging

Figures 4.4(a), 4.4(b) and 4.4(c) presents the $S_{A/S}$, W_{AS} and W_{ASW}^{wet} of the PAV-aged PG 64-22 binders with rhyolite aggregate, respectively. Comparing Figures 4.3(a) and 4.4(a), the $S_{A/S}$ value of the PG 64-22 binder was found to remain almost the same with long-term aging. However, the W_{AS} reduced and W_{ASW}^{wet} increased for PAV-aged PG 64-22 binder. From Figures 4.5(a) and 5(b), the ER_1 was also found to reduce from 0.99 to 0.96 indicating a higher moisture-induced damage potential for PAV-aged binder. A similar trend was observed for PG 64-22 with 20% RAP binder. However, with long-term aging, no significant variation in moisture-induced damage potential was observed with the addition of ASA. Also, the PG 64-22 with 0.5% WMA exhibited an increase in

resistance to moisture-induced damage with long-term aging as the ER_1 value increased from 1.05 for RTFO-aged binder to 1.16 for PAV-aged binder. A significant increase in W_{ASW}^{wet} and reduction in ER_1 was observed for PPA modified binder after PAV-aging. The ER_2 energy ratio parameter was found to follow similar trend as ER_1 for all the additives at PAV-aged condition.

4.5.4 Indirect Tensile Strength Test

Figure 4.6(a) presents the *ITS* values of the dry, short-term aged moisture conditioned and long-term aged moisture conditioned specimens. For each mix, three specimens were tested at each condition. The average of the three specimens are presented in Figure 4.6(a). The error bar indicates one standard deviation from the average value. From Figure 4.6(a) it is evident that the *ITS* values for dry and wet conditioned Mix-4-PPA and Mix-5-RAP specimens are significantly higher than the other three mixes. Therefore, addition of PPA and RAP are expected to increase the strength of the mixes, which is consistent with other studies (Abuawad et al., 2015; Ghabchi et al., 2016). The addition of WMA additive and ASA did not exhibit noticeable changes in dry strength compared to the control mix. However, short-term aged moisture conditioning was found to reduce the *ITS* values for all mixes compared to the dry conditioned mixes. Also, except Mix-1-None, all the mixes exhibited further reduction in the *ITS* values with long-term aging followed by moisture conditioning. Therefore, TSR_{LT} was found to be lower than TSR_{ST} for all mixes, except Mix-1-None (Figure 4.6(b)). From Figure 4.6(b), the control mix (Mix-1-None) was found to exhibit a TSR_{ST} value of 0.73 which increased to 0.90 for TSR_{LT}. The long-term aging of the specimens might have contributed to the increase in strength for Mix-1-None. From

Figure 4.6(b), it was observed that the addition of WMA (Mix-2-WMA) and ASA (Mix-3-ASA) increased the TSR_{ST} value to 0.93 and 0.99, respectively, indicating a reduction in moisture-induced damage potential of the mix. The *ITS* values of both Mix-2-WMA and Mix-3-ASA were observed to reduce with long-term aged moisture conditioning process and thus resulted in a TSR_{LT} value of 0.88 for both mixes. Mix-4-PPA was found to show a significant reduction in both TSR_{ST} and TSR_{LT} values from the control mix indicating an increase in moisture-induced damage potential of asphalt mixes due to the incorporation of PPA. A reduction in *TSR* value with the addition of PPA was also reported by other researchers (Orange et al., 2004; Abuawad et al., 2015). From Figure 4.6(b), it was also observed that the addition of RAP produced *TSR* values of 0.73 and 0.59 for short-term and long-term aged moisture conditioned mixes indicating an increase in moisture-induced damage potential of mixes.

4.5.5 Illinois Semi-Circular Bend Test

Figure 4.7(a) presents the average fracture energy (G_f) values of the short-term aged dry, short-term aged MIST and long-term aged MIST conditioned specimens for all mixes from IL-SCB tests. Three specimens were tested for each mix at each condition. In Figure 4.7(a), the variation of one standard deviation from the average value is illustrated using the error bar. From Figure 4.7(a), the G_f value of Mix-4-PPA was found to be the lowest among all mixes indicating a higher fracture susceptibility with the addition of PPA. The increase in brittleness of the mix with the addition of PPA is expected to be responsible for this phenomenon. One the other hand, the addition of ASA softens the mix resulting a lower susceptibility to fracture (Abuawad et al., 2015). The Mix-5-RAP shows the highest G_f value among all the mixes. The

increased binder content of the Mix-5-RAP could be the reason behind this phenomenon. However, significant changes in the fracture energy were observed among the mixes after MIST conditioning on short-term aged and long-term aged specimens. For short-term aged conditioning, the Mix-1-None was found to exhibit a G_f *ratio* of 0.90 whereas, the Mix-2-WMA, Mix-3-ASA, Mix-4-PPA and Mix-5-RAP exhibited G_f *ratios* of 0.94, 0.87, 0.58 and 0.73, respectively. Therefore, the addition of WMA is expected to produce mixes which is less susceptible to moisture-induced damage, whereas, addition of PPA and RAP are expected to increase the moisture-induced damage potential of the mix significantly. The long-term aging followed by MIST conditioning was found to further reduce the G_f values as well as the G_f *ratios* for all the mixes. Mixes with PPA (Mix-4-PPA) and RAP (Mix-5-RAP) were found to exhibit higher increase in moisture-induced damage potentials than other mixes. Addition of WMA and ASA were found to exhibit higher G_f *ratios* than the control mix (Mix-1-None) indicating improved moisture-induced damage resistance for asphalt mixes.

4.5.6 Comparison of Moisture-induced Damage Parameters

Figures 4.8(a) and 4.8(b) present the comparisons of *TSR* and G_f *ratio* with ER_1, respectively. From Figure 4.8(a), the TSR_{ST} was found to exhibit no meaningful correlation with *ER1* from RTFO-aged binder-aggregate system. However, TSR_{LT} was found to exhibit a better correlation with a R^2 value of 0.70. On the other hand, the R^2 values for $(G_f\ ratio)_{ST}$ and $(G_f\ ratio)_{LT}$ with ER_1 from RTFO-aged and PAV-aged binder-aggregate system were found to be better than TSR_{ST} and TSR_{LT}. Strongest correlation was observed between the $(G_f\ ratio)_{LT}$ and ER_1 from PAV-aged binder-aggregate system as compared to other correlations considered in this study. The energy

parameter ER_1 is the ratio of work of adhesion and work of debonding between binder and aggregate which are quantified mechanistically using thermodynamic properties of both materials. On the other hand, the behavior of dry and moisture conditioned specimens during peak load is representative by the *TSR* value. Therefore, no strong correlation was expected between the ER_1 and *TSR*. However, the fracture energy represents the work required to initiate and propagate fracture, i.e. complete damage (adhesion and cohesion failure) characteristics of the mixes. Therefore, the correlation between G_f *ratio* and ER_1 was found to be stronger than *TSR*. Therefore, IL-SCB test with MIST conditioning can be used as an alternative tool for mechanistic evaluation of the moisture-induced damage of asphalt mixes. The correlations of *TSR* and G_f *ratio* with ER_2 were found similar to those of ER_1.

4.6 CONCLUSIONS

In this study, SFE method was used to mechanistically quantify the changes in the moisture-induced damage potential of binder-aggregate systems with the addition of different additives. Also, the effect of aging on the moisture-induced damage performance of the binder-aggregate system was assessed by evaluating the changes in the energy parameters from SFE method. In addition, the moisture-induced damage potentials of short-term and long-term aged asphalt mixes were evaluated using a conventional (*TSR*) and a new (G_f *ratio*) parameter. Correlations between the moisture-induced damage performance parameters from laboratory performance tests and the SFE technique were also investigated. Based on the test results obtained from different laboratory tests conducted on asphalt mixes, aggregates and binders, the following conclusions were made:

i. An improved resistance to moisture-induced damage of asphalt mixes was observed with the addition of WMA and ASA from SFE method. Similar improvements were also observed from the *TSR* and G_f *ratio* parameters. The mix containing PPA was found to exhibit the lowest ER_1, *TSR* and G_f *ratio* values among all mixes indicating the highest susceptibility to moisture-induced damage.

ii. Asphalt mixes, in general, were found to become more prone to moisture-induced damage with long-term aging. Significant changes in the SFE components, *ITS* and G_f values were observed due to the thermal degradation of the constituents of binder and additives.

iii. The G_f *ratio* obtained from IL-SCB test was found to exhibit a strong correlation with energy parameters from SFE method. Therefore, G_f *ratio* can be used in mechanistic evaluation of the moisture-induced damage potential of asphalt mixes.

Although the G_f *ratio* exhibited the potential to be used as an effective parameter for evaluating moisture-induced damage in the laboratory, additional studies are needed to correlate the G_f *ratio* with the field performance of asphalt mixes. Also, the current study was limited to one type of aggregate (rhyolite). Therefore, future studies including other types of aggregates such as limestone, granite and dolomite need to be conducted to obtain a better understanding of additives and aging for different binder-aggregate combinations.

Table 4.1 Contact Angles of the Binder Blends with Different Solvents

Binder Type	Aging Condition	Additive	Contact Angle (°)									
			Water		Glycerol		Formamide		Diiodomethane		Ethylene Glycol	
			Avg	SD	Avg	SD	Avg	SD	Avg	SD	Avg	SD
PG 64-22	RTFO-aging	None	107.91	0.10	94.27	0.11	90.46	0.13	78.73	0.57	78.38	0.62
		0.5% WMA	107.75	0.16	94.12	0.36	89.83	0.38	80.32	1.39	78.85	0.08
		0.5% ASA	106.98	0.09	93.95	0.14	89.74	0.32	79.97	0.99	78.17	0.58
		20% RAP	107.08	0.26	93.13	0.18	89.18	0.21	81.36	0.70	78.47	0.24
		1.5% PPA	100.98	1.89	91.95	0.62	-	-	-	-	77.93	0.31
	PAV-aging	None	107.13	0.59	95.17	0.19	91.17	0.21	80.78	0.34	78.75	0.41
		0.5% WMA	107.48	0.74	94.95	0.20	91.00	0.27	88.42	0.81	78.64	0.39
		0.5% ASA	107.30	0.62	94.69	0.26	90.97	0.34	81.35	0.43	76.82	1.90
		20% RAP	107.02	0.55	95.14	0.12	91.72	0.80	76.68	0.23	78.41	0.56
		1.5% PPA	100.73	0.93	93.20	0.91	-	-	-	-	76.82	0.30

Table 4.2 SFE Components of the Binder Blends and Aggregate

SFE Components of Binder Blends								
Binder Type	Aging Condition	Additive	SFE (mJ/m^2)					
			Γ^+	Γ^-	Γ^{LW}	Γ^{AB}	Γ^{Total}	Γ^+/Γ^-
PG 64-22	RTFO-aging	None	0.29	0.28	17.78	0.57	18.35	1.06
		0.5% WMA	0.38	0.31	17.78	0.69	18.47	1.24
		0.5% ASA	0.36	0.41	17.20	0.78	17.98	0.87
		20% RAP	0.50	0.37	16.53	0.86	17.39	1.36
		1.5% PPA	0.60	2.52	14.11	2.46	16.57	0.24
	PAV-aging	None	0.30	0.52	16.76	0.79	17.55	0.58
		0.5% WMA	0.91	0.50	13.20	1.34	14.54	1.82
		0.5% ASA	0.44	0.38	16.43	0.82	17.25	1.17
		20% RAP	0.12	0.51	18.76	0.50	19.26	0.24
		1.5% PPA	0.18	2.86	16.44	1.44	17.88	0.06
SFE Components of Aggregate								
Aggregate Type			SFE (mJ/m^2)					
			Γ^+	Γ^-	Γ^{LW}	Γ^{AB}	Γ^{Total}	Γ^+/Γ^-
Rhyolite			0.39	336.94	52.87	23.04	75.91	0.001

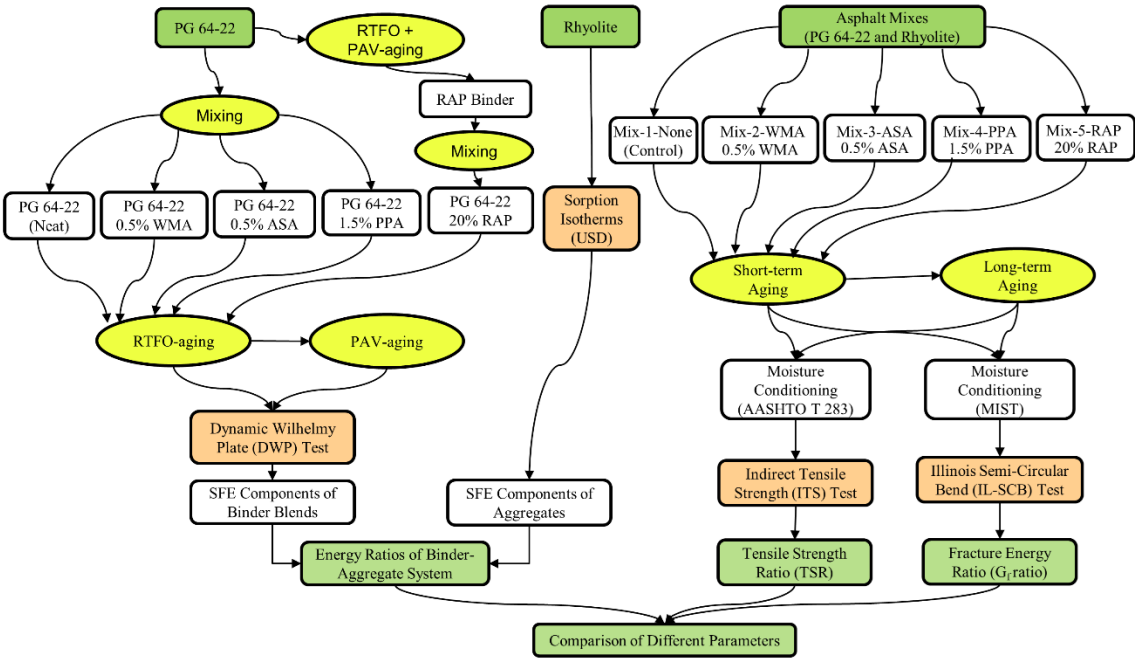

Figure 4.1 Work-flow diagram for the present study

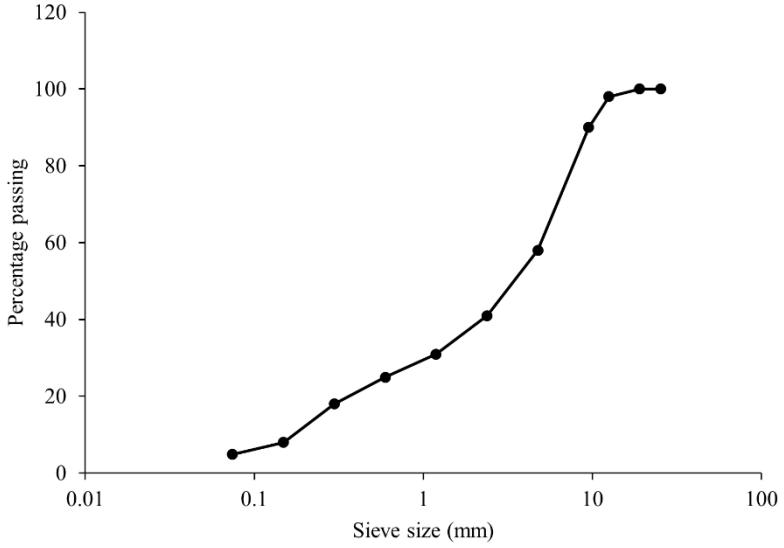

Figure 4.2 Gradation curve for the mixes

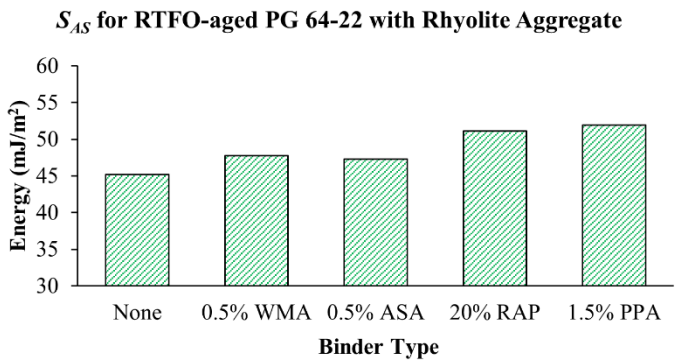

(a)

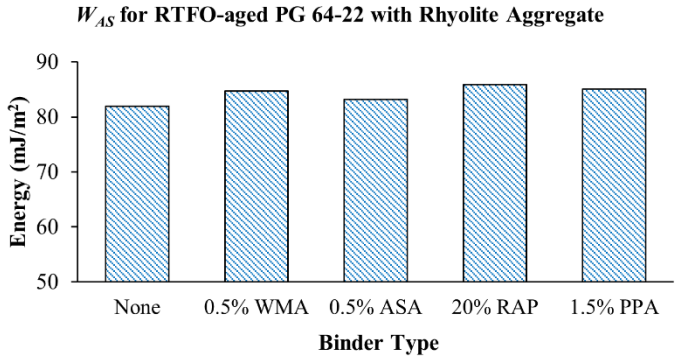

(b)

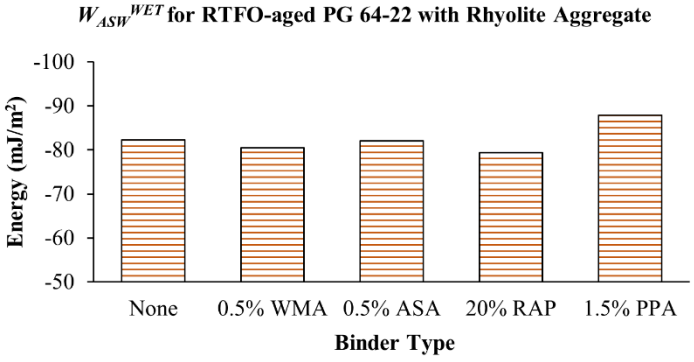

(c)

Figure 4.3 The (a) $S_{A/S}$, (b) $W_{A/S}$ and (c) W^{wet}_{ASW} of RTFO-aged PG 64-22 binder containing different additives with rhyolite aggregate

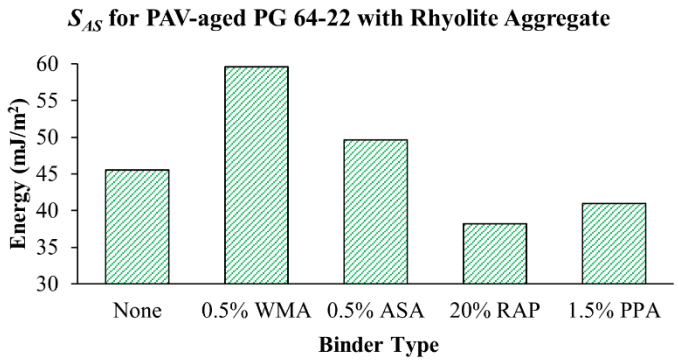

(a)

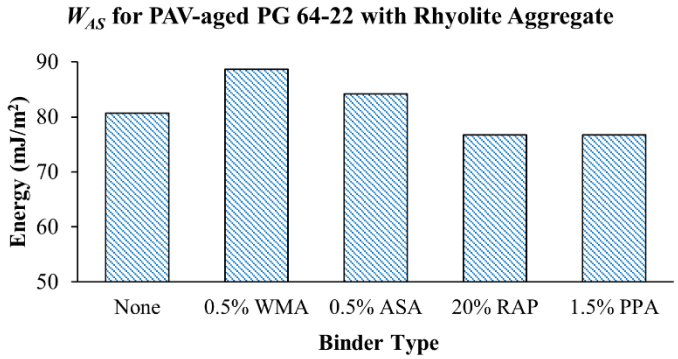

(b)

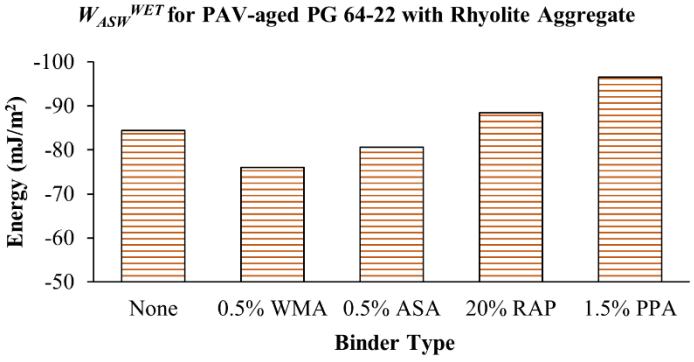

(c)

Figure 4.4 The (a) $S_{A/S}$, (b) $W_{A/S}$ and (c) W^{wet}_{ASW} of PAV-aged PG 64-22 binder containing different additives with rhyolite aggregate

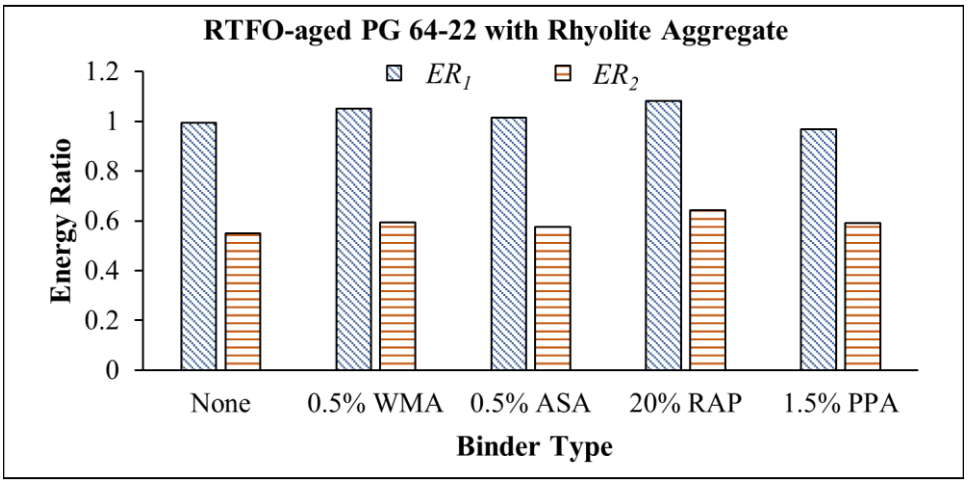

(a)

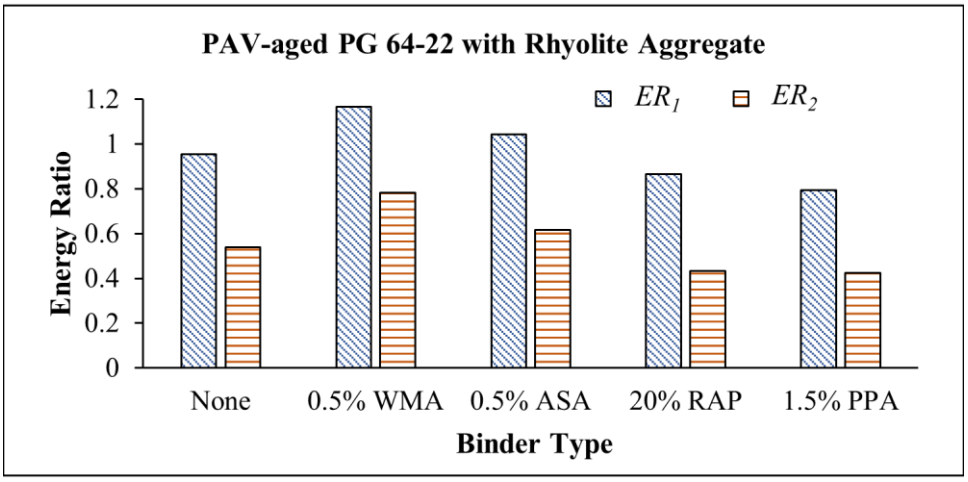

(b)

Figure 4.5 The ER_1 and ER_2 of (a) RTFO-aged and (b) PAV-aged PG 64-22 containing different additives with rhyolite aggregate

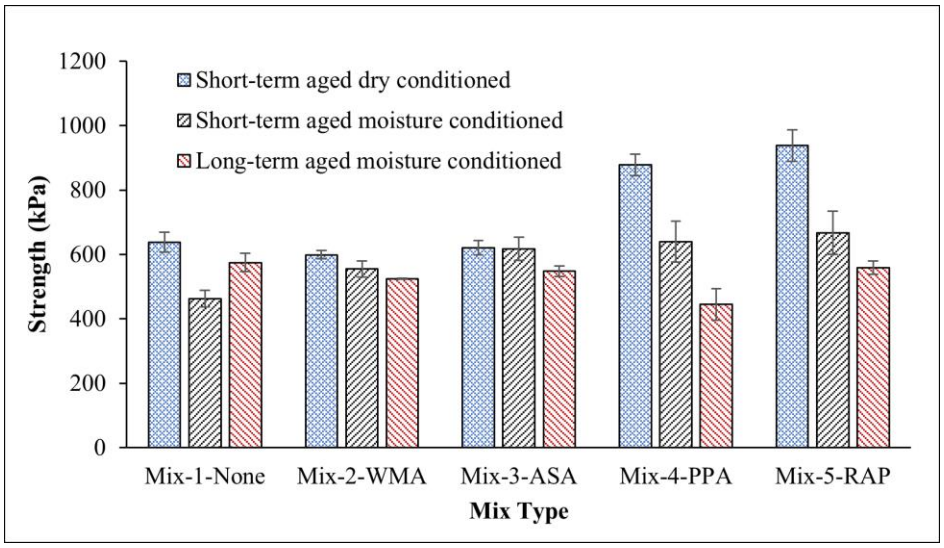

(a)

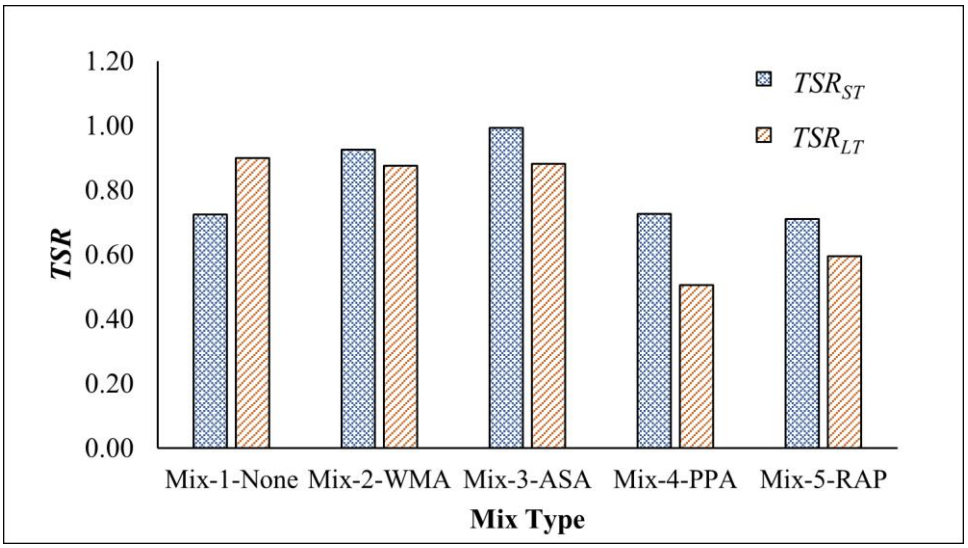

(b)

Figure 4.6 (a) Indirect tensile strength (*ITS*) and (b) tensile strength ratio (*TSR*) of the tested asphalt mixes

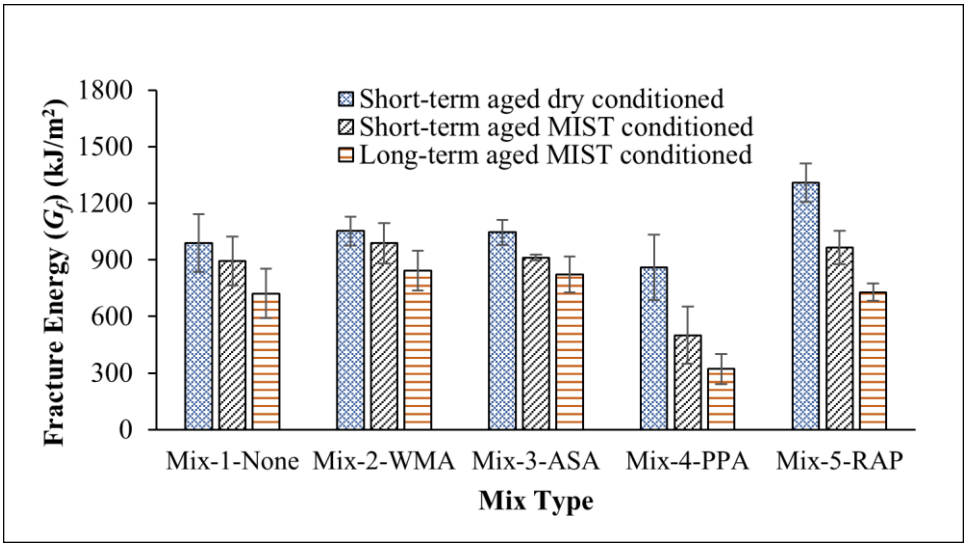

(a)

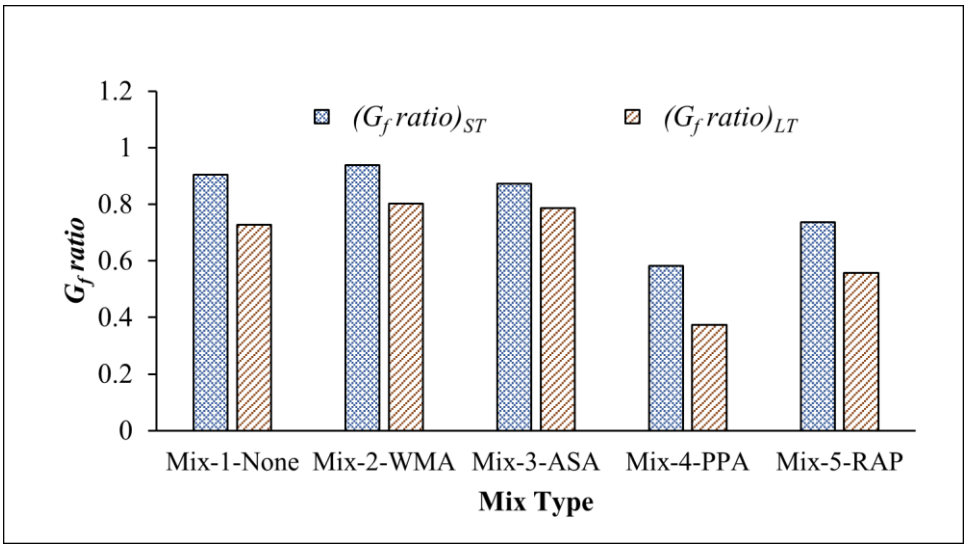

(b)

Figure 4.7 (a) Fracture energy (G_f) and (b) fracture energy ratio (G_f *ratio*) of tested asphalt mixes

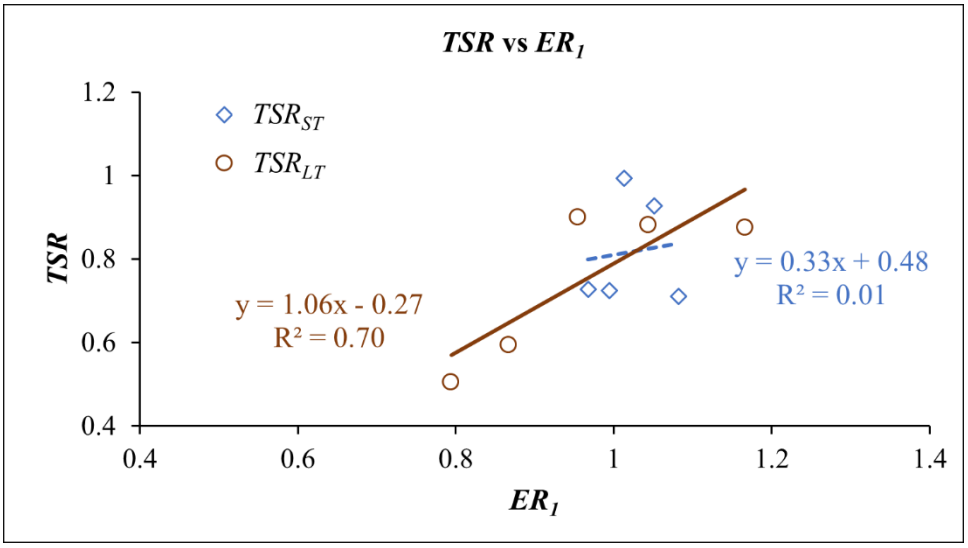

(a)

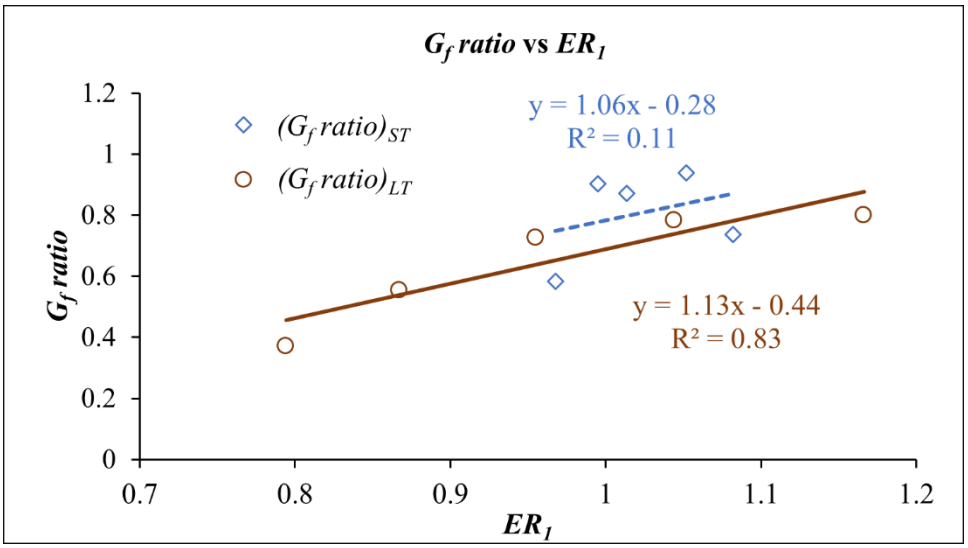

(b)

Figure 4.8 Comparison of moisture-induced damage parameters: (a) *TSR* vs. ER_1 and (b) G_f *ratio* vs. ER_1

CHAPTER

5

LABORATORY CHARACTERIZATION OF MOISTURE-INDUCED DAMAGE POTENTIAL OF ASPHALT MIXES USING CONVENTIONAL AND UNCONVENTIONAL PERFORMANCE-BASED TESTS[4]

ABSTRACT

Moisture-induced damage is one of the major distresses responsible for premature deterioration of asphalt pavements. The stripping inflection point (*SIP*) from the Hamburg wheel tracking (HWT) test and tensile strength ratio (*TSR*) from the indirect tensile strength (ITS) test are the two most commonly used parameters by state Department of Transportation (DOT) to evaluate moisture-induced damage. However, variability in test results and poor correlations with field performance have raised concerns on the reliability of these parameters. Therefore, there is a need to identify relatively simple, reliable, and mechanistic methods for evaluating moisture-induced damage potential of asphalt mixes. In this study, new approaches for evaluating the HWT test and ITS test data were introduced and compared with the conventional data analysis procedures. Also, moisture-induced damage was evaluated using a new parameter, namely J-integral ratio (J_c *ratio*)

[4] This chapter has been submitted to the International Journal of Pavement Research and Technology under the title "Laboratory Characterization of Moisture-Induced Damage Potential of Asphalt Mixes using Conventional and Unconventional Performance-Based Tests." The current version has been formatted for this dissertation.

from Louisiana semi-circular bend (LA-SCB) test. For this purpose, surface course mixes containing warm mix asphalt additive, antistripping agent, polyphosphoric acid and reclaimed asphalt pavement (RAP) were prepared and tested in the laboratory. Bond strength of the binder-aggregate system was mechanistically quantified using surface free energy (SFE) method. Also, propensity of debonding of binder from aggregate surface in presence of moisture was determined using a similar approach. Relationships between different laboratory-based parameters and the SFE parameters were determined. Different parameters ranked mixes differently based on their failure mechanisms. Based on the results from this study and the DOT practices, the stripping number (LC_{SN}) from HWT, toughness index ratio (*TI ratio*) from ITS and J_c *ratio* from LA-SCB test exhibited potential for evaluating moisture-induced damage during the mix design phase.

5.1 INTRODUCTION

Moisture-induced damage can be defined as the loss of strength and durability of asphalt mixes due to loss of bond between aggregate and binder in presence of moisture (Harvey and Lu, 2005; Masad et al., 2006; Bhasin et al., 2007b). The effect of moisture on the performance of asphalt pavement was first recognized in the early 1930s. One of the earlier efforts to quantify moisture-induced damage was reported in the late 1960s through visual inspection (Caro et al., 2008a; Abuawad et al., 2015). The phenomenon starts with the transport of moisture into the pavement which subsequently leads to pavement deterioration due to the loss of either cohesive or adhesive bonds or both (Wasiuddin et al., 2007c; Caro et al., 2008b). Serious distresses in asphalt pavements,

such as potholes, particle degradation and disintegration, bleeding, rutting, shoving, and cracking can result from the moisture-induced damage (Wasiuddin et al., 2007c; Caro et al., 2008b). Significant resources are spent annually by state and federal transportation agencies to maintain and reconstruct pavements subjected to moisture-induced damage (Caro et al., 2008a; Abuawad et al., 2015).

Evaluation of moisture-induced damage is a complex problem (Wasiuddin et al., 2007c). Over the past few decades, a number of empirical test methods have been developed to evaluate this phenomenon (Caro et al., 2008a; Caro et al., 2008b). However, many of these methods exhibit poor correlations with field performance (Caro et al., 2008b; Abuawad et al., 2015). Previously, moisture-induced damage tests were classified based on the state of mix (loose or compact), mode of loading, moisture conditioning process and performance measure. Caro et al. (2008b) introduced a new classification based on the generic nature of the test methods. The classification involved the following: subjective quantification, quantification using performance index, and a parametric ratio involving dry- and moisture-conditioned specimens. Among these three methods, the use of parametric ratio between dry- and moisture-conditioned specimens from a particular test is commonly used to characterize moisture-induced damage by state DOTs. Moisture conditioning in the laboratory is an integral part of this type of testing. The purpose of laboratory moisture conditioning is to simulate the environment and moisture affecting the performance of an asphalt mix in the field.

A number of tests and moisture conditioning procedures have been investigated by researchers and the asphalt industry (Gorkem and Sengoz, 2009; Liu et al., 2014;

Tarefder and Ahmad, 2014; LaCroix et al., 2016). For example, Gorkem and Sengoz (2009) used the Nicholson stripping test and the modified Lottman test to evaluate the effect of the addition of hydrated lime and elastomeric and plastomeric polymers on the moisture-induced damage potential of loose and compacted asphalt mixes. Analysis of microscopically captured images using a software was found to improve the estimation of degree of stripping. Liu et al. (2014) evaluated the moisture-induced damage of aggregates and binders using five empirical test methods, namely the static immersion test, rolling bottle test (RBT), boiling water test (BWT), total water immersion test, and the ultrasonic test. Among these different test methods, the BWT and the RBT were observed to be the most sensitive while the static immersion test and the ultra-sonic test were found to be the least sensitive. The moisture-induced damage potential of asphalt mixes due to two different wet conditioning methods, namely, moisture-induced sensitivity testing (MIST) and AASHTO T 283 (AASHTO, 2014a) method was evaluated and the relationship with permeability was determined by Tarefder and Ahmad (2014). The indirect tensile strength (ITS) tests conducted on samples conditioned according to the AASHTO T 283 (AASHTO, 2014a) method were found to result in reduced tensile strength ratio (*TSR*) values with an increase in permeability. However, the TSR values of samples conditioned in a MIST equipment were found to be unaffected by permeability. Mirzababaei (2016) used different conventional test methods, namely AASHTO T 283 (AASHTO, 2014a), resilient modulus ratio (*RMR*), Marshall stability ratio (*MSR*), fracture energy ratio (*FER*) and boiling water to determine the effect of Zycotherm® on the moisture-induced damage potential of asphalt mixes. LaCroix et al. (2016) used both AASHTO T 283 (AASHTO, 2014a) and

MIST to condition their samples and tested them for moisture-induced damage. It was found that the current AASHTO T 283 (AASHTO, 2014a) method affects the adhesive strength of the binder and the aggregate whereas the MIST only affects the cohesive strength. Vargas-Nordcbeck et al. (2016) used the modified Lottman ITS test procedure with different conditioning levels and found that an increase in the number of conditioning cycles was required to accurately simulate field performance.

Among all test methods, the stripping inflection point (*SIP*) from the Hamburg wheel tracking (HWT) test and *TSR* from the ITS test are the most commonly used parameters to evaluate the moisture-induced damage (Caro et al., 2008b; Abuawad et al., 2015). Conventionally, the *SIP* and rut depth at a certain number of wheel passes are widely used as the two main HWT parameters to evaluate the moisture susceptibility and rutting resistance of asphalt mixes, respectively. However, it has been reported that the current HWT parameters are not always able to accurately evaluate asphalt mixes for moisture-induced damage (Yin et al., 2014). Therefore, an improved methodology is needed to accurately characterize the stripping phase using the HWT data. In this study, a new method, known as Texas A & M University (TAMU) method, proposed by Yin et al. (2014), was used for analyzing the HWT data. The *TSR* value from ITS test is used as an indicator of moisture-induced damage. This evaluation is based on the peak load and it does not provide any information about the post peak behavior of the asphalt specimen. Generally, the peak strength relates to the initiation of crack whereas the post peak behavior corresponds to the propagation of cracks in an asphalt mix specimen. Toughness index (*TI*) from the ITS test can be used to evaluate the post-peak behavior of asphalt mixes (Shu et al., 2008; Huang et al., 2010). Therefore, in this study, in

addition to *TSR*, toughness indexes of the conditioned and unconditioned specimens were used to evaluate moisture-induced damage potential.

The measurements of fracture, healing, and viscoelastic properties are necessary to conduct a comprehensive characterization of moisture-induced damage of asphalt mixes (Bhasin et al., 2006). Several previous studies have used semi-circular bend (SCB) test to characterize fatigue and low-temperature fracture resistance of asphalt mixes (Mull et al., 2002; Wu et al., 2005; Li and Marasteanu, 2010; Kim et al., 2012; Mohammad et al., 2016; Ozer et al., 2016b; Saeidi and Aghayan, 2016). It has been found that the SCB test is a reliable and relatively simple test method for assessment of cracking potential of asphalt mixes. Recently, two cracking test methods using semi-circular specimens are gaining popularity. Louisiana Department of Transportation and Development (DOTD) has been using a version of the SCB test (LA-SCB), which uses the critical energy release rate or J-integral (J_c) to characterize cracking potential of mixes (Cooper Jr et al., 2016). Another version of SCB test, the Illinois SCB (IL-SCB), uses flexibility index (*FI*) to characterize the fracture properties of asphalt mixes (Al-Qadi et al., 2015). Several DOTs are in the process of adopting one of these SCB test methods to characterize fatigue performance during the mix design. Evaluation of fracture properties of conditioned and unconditioned mixes through SCB test will help understand the mechanisms of moisture-induced damage. Therefore, in this study, the ratio of J-integral (J_c *ratio*) of conditioned and unconditioned specimens from LA-SCB test was used to characterize the moisture-induced damage potential of asphalt mixes based on the fracture mechanics' concept.

Recently, surface free energy (SFE) method has been used by several researchers to characterize the adhesion and debonding potential of binder-aggregate systems in presence of moisture (Hefer et al., 2006; Bhasin, 2007; Bhasin et al., 2007a; Bhasin et al., 2007b; Wasiuddin et al., 2007c; Buddhala et al., 2011; Ghabchi et al., 2013; Kakar et al., 2016; Zhang and Luo, 2019). Bhasin (2007) investigated the correlation between the SFE parameters and the moisture-induced damage potential of asphalt mixes based on their field performance. It was found that the SFE parameters can be effectively used to differentiate mixes based on their sensitivity to moisture-induced damage. The SFE method was used to determine the effects of polymer modification and oxidative aging on the fracture properties and moisture-induced damage sensitivity of asphalt mixes (Bhasin et al., 2007a). Also, several other studies have used the SFE method to evaluate the effects of different additives, such as anti-stripping agent (ASA) (Hefer et al., 2006; Wasiuddin et al., 2007b; Wasiuddin et al., 2007c; Arabani et al., 2011; Buddhala et al., 2011), warm-mix asphalt (WMA) (Wasiuddin et al., 2008; Ghabchi et al., 2013; Rani et al., 2020) and polyphosphoric acid (PPA) (Rani, 2019b) on the moisture-induced damage potential of asphalt mixes. The effect of different aggregates on the bond energy characteristics of binder-aggregate systems was evaluated by Bhasin and Little (2007). Furthermore, several studies have investigated the changes in the moisture-induced damage potential of asphalt mixes due to styrene-butadiene rubber (Wasiuddin et al., 2010), polyethene (Arabani and Hamedi, 2010) and lime (Hesami et al., 2013) coatings on aggregate surface using the SFE method. The effect of the addition of different amounts of RAP on the stripping potential of asphalt mixes was evaluated by Ghabchi et al. (2014) using the SFE

parameters. Although SFE method has its advantages as a mechanistic-based approach, state DOTs may not be in favor of incorporating this method in their specification because of the skills and time require to generate the necessary data. Therefore, suitable and easy-to-use laboratory performance-based parameters are needed to screen asphalt mixes for moisture-induced damage. In this study, moisture-induced damage potential of asphalt mixes was characterized using both SFE method and other laboratory-based tests, namely HWT, ITS and LA-SCB. Relationships between different laboratory-based parameters and SFE parameters were explored.

5.2 OBJECTIVES

In the present study, effects of a WMA additive, ASA, PPA and RAP on the moisture-induced damage potentials of asphalt mixes were examined using SFE method and laboratory performance tests, namely HWT, ITS and SCB. Also, the results were compared to understand the differences in moisture-induced damage mechanisms addressed by these parameters. The specific objectives of this study were:

i. To assess effects of WMA, ASA, PPA and RAP on the moisture-induced damage potential of asphalt mixes through the SFE method and laboratory performance tests.

ii. To evaluate and compare the conventional and unconventional methods for analysis of HWT, ITS and LA-SCB test results for characterizing moisture-induced damage potential of asphalt mixes. Investigating the differences in mechanisms used to address moisture-induced damage by these laboratory-based parameters.

iii. To determine relationships between different laboratory-based moisture-induced damage parameters and the SFE parameters.

5.3 MATERIALS AND METHODS

5.3.1 Materials

5.3.1.1 Asphalt Mixes

Figure 5.1 presents the workflow diagram used in this study. As shown in Figure 5.1, five different mixes with a nominal maximum aggregate size (NMAS) of 12.5 mm were prepared in the laboratory following a mix design collected from a local asphalt plant. A PG 64-22 binder from a local source was used as the base binder for all mixes. Mix-1-None did not contain any additive. However, Mix-2-WMA, Mix-3-ASA and Mix-4-PPA contained 0.5% WMA additive, 0.5% ASA and 1.5% PPA (by weight of total binder), respectively. The dosages for these additives were selected in consultation with the Oklahoma DOT. An asphalt binder content of 5.2% was used to prepare Mix-1-None, Mix-2-WMA, Mix-3-ASA and Mix-4-PPA specimens (see Table 5.1 for specifics). These mixes contained 5/8” stone chips (25%), 1/2” stone chips (15%), 3/8” screens (30%), 3/16” screens (15%) and sand (15%). All aggregates, except sand, were rhyolite aggregates and were collected from local sources. Mix-5-RAP was prepared with 20% RAP. For Mix-5-RAP, the amounts of different aggregates were adjusted to maintain the same gradation after the addition of RAP. However, a binder content of 5.5% (neat binder- 4.5%, binder from RAP- 1.0%) was used to prepare Mix-5-RAP to meet the DOT requirements. Additives were added to the binder at their mixing temperatures before mixing with the aggregates. The same mixing (163°C) and compaction (149°C) temperatures were used for all mixes, except Mix-2-WMA.

Different mixing (135°C) and compaction (128°C) temperatures were used for Mix-2-WMA to account for the effect of WMA additive. All mixes were short-term aged for four hours in an oven at 135°C as per the AASHTO R 30 method (AASHTO, 2015a), before compaction.

5.3.2 Sample Preparation

A Superpave® gyratory compactor (SGC) was used to compact samples for HWT, ITS and SCB testing following the AASHTO T 312 method (AASHTO, 2015b). Samples with 7% ± 0.5% air voids were used for performance testing. The test matrix for the asphalt mixes is presented in Table 5.1.

5.3.3 Moisture Conditioning of Compacted Samples

5.3.3.1 AASHTO T 283 Method

The AASHTO T 283 test method was used for simulating moisture conditioning of laboratory compacted specimens before conducting the ITS test (AASHTO, 2014a). According to this procedure, ITS samples were conditioned by saturating with water (70-80% saturation) followed by a freezing cycle (-18°C for 16 hours) and a thawing cycle (60°C water bath for 24 hours).

5.3.3.2 Moisture Induced Sensitivity Test (MIST) Conditioning (ASTM D7870, (2013))

As noted by Vargas-Nordcbeck et al. (2016), a single freeze-thaw cycle used in the AASHTO T 283 method (AASHTO, 2014a) may not be sufficient for simulating field condition in the laboratory. According to LaCroix et al. (2016), the AASHTO T 283 moisture conditioning process (AASHTO, 2014a) only affects the adhesive strength of the asphalt mix. However, the ASTM D7870 method (AASHTO, 2013) uses a

moisture induced sensitivity test (MIST) for conditioning asphalt mix specimens. This method simulates both adhesion and cohesion properties of the mix due to passing of vehicles on a wet pavement (Mallick et al., 2000; LaCroix et al., 2016). Therefore, in this study, moisture conditioning of compacted asphalt samples was performed using the MIST method before LA-SCB testing. In this method, the moisture-conditioning was done in two phases, namely adhesion phase and pressurization phase. In the adhesion phase, samples were submerged in water in the MIST chamber. Water temperature was then raised to 60°C and maintained for 20 hours to affect the adhesion properties of the samples. In the pressurization phase, samples were subjected to 280 kPa pressure for 3,500 cycles. The pressure was generated by inflating a bladder located in the MIST chamber using an air piston. After the pressurization phase, water was drained, and samples were taken out of the chamber for further testing.

5.3.4 Test Methods

5.3.4.1 Hamburg Wheel Tracking (HWT) Test

The rutting and moisture-induced damage potentials of the associated mixes were evaluated using the HWT test following the AASHTO T 324 test method (AASHTO, 2014b). Samples with a diameter of 150 mm and a height of 60 mm were compacted using an SGC. Two sets of samples from each mix were tested to ensure repeatability. The tests were conducted by submerging asphalt mix samples in a temperature-controlled water bath at 50°C. A load of 705 N was applied on the samples using a reciprocating steel wheel with a wheel pass frequency of 52 passes/minute. Tests were conducted until the samples reached a rut depth of 20 mm or 20,000 wheel passes. The rutting and stripping potentials of the mixes were evaluated based on the

conventional method by plotting rut depth vs wheel passes. For this purpose, the post compaction deformation and creep slope were determined to evaluate the rutting potential of the mixes. The rut depth at 1,000 wheel passes was used as the post-compaction point as suggested by Yildirim and Kennedy (2002). After post compaction point, the linear creep region of the rut curve indicates plastic flow of the samples during the HWT test. The creep potential was evaluated by determining the creep slope (i.e. rut depth per wheel pass in the creep region). The moisture-induced damage potential was assessed by determining the stripping slope and *SIP* of the mixes from the HWT test results. The *SIP* was considered as the inflection point where rut curve changed from the creep region to the stripping region. The stripping slope is the rate of change in rut depth in the stripping region.

In addition to the conventional method, a new method known as TAMU method, proposed by Yin et al. (Yin et al., 2014), was used and the results were compared with the *SIP* results. According to this method, visco-plastic strain and stripping strain were separated from the rut depth. A parameter, called stripping number (LC_{SN}), was used to determine the maximum number of load cycles an asphalt mix can resist in the HWT test before the occurrence of adhesive fracture. Also, the rut depth accumulation resulting from stripping was quantified using a parameter called stripping life (LC_{ST}). The LC_{ST} was determined as the number of wheel passes required to produce a stripping strain of 12.5 mm. The visco-plastic strain increment ($\Delta\varepsilon_{10,000}^{vp}$), which was defined as the slope of the visco-plastic strain at 10,000 wheel passes, was used to quantify the resistance to rutting. Further details of the procedure are given by Yin et al. (2014).

5.3.4.2 Indirect Tensile Strength (ITS) Test

The TSR value of a mix was determined by conducting the indirect tensile strength (ITS) test on dry and moisture-conditioned specimens following the AASHTO T 283 test method (AASHTO, 2014a). For this purpose, specimens having a diameter of 150 mm and a height of 95 mm were compacted using an SGC. As mentioned in the previous section, a single cycle of freeze-thaw conditioning following the AASHTO T 283 method (AASHTO, 2014a) was used to induce the moisture damage. The *TSR* value was then determined using Equation (5.1). Another parameter, called toughness index (*TI*) ratio, which is the ratio of the toughness indices of the moisture-conditioned and the dry specimen, was used as a new mechanistic parameter for quantifying moisture-induced damage potential. This approach is based on the fracture mechanics principle and accounts for the post-peak behavior of asphalt mixes, unlike TSR (Kim et al., 2012). The *TI* was calculated from the ITS test results using Equation (5.2). The *TI* value of an ideal brittle material with no post-peak load-carrying capacity is zero, whereas the *TI* value should be 1 for an elastic perfectly plastic material with no loss in load-carrying capacity after peak load (Shu et al., 2008; Huang et al., 2010). Several researchers (Mull et al., 2002; Wu et al., 2005; Li and Marasteanu, 2010; Kim et al., 2012; Mohammad et al., 2016; Ozer et al., 2016b; Saeidi and Aghayan, 2016) have used a tensile strain of 3% as a terminal strain for dry specimens. In this study, the TI values were calculated up to a tensile strain of 4% as the moisture-conditioned specimens did not reach peak strength at 3% strain.

$$TSR = \frac{ITS\ of\ Moisture{-}conditioned\ Specimens\ (ITS_{wet})}{ITS\ of\ Dry{-}conditioned\ Specimens\ (ITS_{dry})} \qquad (5.1)$$

$$TI = \frac{A_\varepsilon - A_p}{\varepsilon - \varepsilon_p} \quad (5.2)$$

where,

ε = strain corresponding to 4% tensile strain,

ε_p = strain corresponding to peak strength,

A_ε = area under normalized stress-strain curve up to 4% tensile strain (ε),

A_p = area under normalized stress-strain curve up to peak strength (ε_p).

5.3.4.3 Louisiana Semi-Circular Bend (LA-SCB) test

The semi-circular specimens of 150 mm in diameter, 75 mm in height, and 50 mm in thickness were prepared for conducting LA-SCB test. For this purpose, samples with a diameter of 150 mm and height of 120 mm were prepared using an SGC. The samples were then divided into two subsets. One subset was kept at 25°C while the other subset was moisture-conditioned using the MIST method mentioned in the previous section. Then the specimens were cut as per the abovementioned shapes, and notches (25.4, 31.8 and 38 mm depth) were made for LA-SCB testing. Three replicates were tested for each notch depth. The LA-SCB tests were performed at 25°C by applying a monotonically increasing load at a rate of 0.5 mm/min until failure. The results of the SCB tests were analyzed by calculating the critical energy release rate or J-integral (J_c). The J-integral was calculated by plotting the areas under the load-deformation curves until peak loads observed for each specimen against the notch depths. The J-integral was calculated using Equation (5.3) in which *dU/da* was obtained from the slope of the strain energy vs notch depth plot. The mechanistic basis of J-integral from SCB testing is discussed by Wu et al. (2005).

$$J_c = -(\frac{1}{b})\frac{dU}{da} \quad (5.3)$$

where,

J_c = critical strain energy release rate,

b = width of the specimen,

U = strain energy to failure,

a = notch depth of the specimen.

The *J_c ratio* was calculated by dividing the J-integral value of a MIST-conditioned by the corresponding value of the dry specimen using Equation (5.4).

$$J_c \text{ ratio} = \frac{J_c \text{ of MIST-conditioned Specimens } (J_{c-Mist})}{J_c \text{ of Dry-conditioned Specimens } (J_{c-dry})} \quad (5.4)$$

5.4 RESULTS AND DISCUSSIONS

5.4.1 HWT Results

5.4.1.1 Conventional method

Figure 5.2 presents the rut depths vs. number of wheel passes obtained from HWT tests for all five mixes. The rut depths in Figure 5.2 represent the average of two sets of samples. Table 5.2 presents the rutting parameters for all mixes determined by the conventional method. From Figure 5.2, the rut depths at 10,000 and 20,000 wheel passes for Mix-1-None (control mix) were 2.8 and 14.9 mm, respectively. A *SIP* was observed at 11,500 wheel passes for Mix-1-None, indicating a potential for moisture-induced damage. The creep and stripping slope for Mix-1-None occurred at 4,120 and 880 passes/mm, respectively.

The effect of WMA additive was observed by comparing the rutting parameters of Mix-1-None and Mix-2-WMA. From Figure 5.2, the rut limit (20 mm) of Mix-2-

WMA was reached around 13,000 passes. At 10,000 passes, Mix-2-WMA exhibited a rut depth of 11.5 mm which was higher than that of Mix-1-None (2.81 mm) at the same number of wheel passes. Also, the number of wheel passes required for 1 mm deformation at the creep and the stripping phases were lower for Mix-2-WMA than Mix-1-None. Therefore, it can be concluded that the mix containing WMA is expected to exhibit a higher rutting and moisture-induced damage than the control mix. These findings were consistent with the results reported by previous studies (Prowell et al., 2007; Ghabchi et al., 2013).

The rut depths for the mix containing ASA (Mix-3-ASA) were lower than those measured for the control mix (Mix-1-None), indicating an improvement in rutting resistance. For example, the rut depth after 10,000 and 20,000 wheel passes for Mix-3-ASA were 2.4 mm and 9.8 mm, respectively. The addition of ASA reduced the creep slope as well. Furthermore, the stripping inflection point for Mix-3-ASA occurred at 13,700 loading cycle, the highest among all mixes. Therefore, the addition of ASA is expected to reduce the moisture-induced damage potential of mixes, which is consistent with the findings of the previous studies (Wasiuddin et al., 2007c; Arabani and Hamedi, 2014; Abuawad et al., 2015).

The effect of the addition of PPA on moisture-induced damage and rutting potential of asphalt mix (Mix-4-PPA) can be observed from Figure 5.2 and Table 5.2. The addition of PPA made the mix more susceptible to moisture-induced damage and rutting. The *SIP* for Mix-4-PPA occurred at 5,500 loading cycles with a stripping slope of 850 passes/mm. However, the post- compaction deformation for Mix-4-PPA was lower than the control mix indicating a higher rutting resistance at the initial stage. With

an increase in wheel passes, the Mix-4-PPA specimens were damaged due to moisture and exhibited higher rut depths than the control mix. A similar increase in rutting and moisture-induced damage potential with a PPA-modified binder was reported in previous studies (Orange et al., 2004; Fee et al., 2010; Al-Qadi et al., 2014). The mix containing 20% RAP (Mix-5-RAP) exhibited a higher moisture susceptibility than the control mix. The Mix-5-RAP specimens exhibited a stripping inflection point at a lower number of wheel passes (around 9,000 passes) than the control mix. However, the stripping slope was similar to that of the control mix.

5.4.1.2 TAMU method

Yin et al. (2014) proposed two parameters, namely LC_{SN} and LC_{ST} for evaluating moisture-induced damage potential of asphalt mixes. Mixes with higher LC_{SN} values are expected to be less susceptible to moisture-induced damage than those having lower LC_{SN} values. Table 5.2 presents the LC_{SN} values for the tested mixes. Based on Table 5.2, among all mixes, Mix-4-PPA exhibited the lowest LC_{SN} value (131 passes) indicating a higher potential for moisture-induced damage. On the other hand, the mix containing ASA exhibited the highest LC_{SN} (3,312 passes) compared to the control mix (1,228 passes).

According to Yin et al. (2014), LC_{ST} value represents the moisture-induced damage potential of a mix after it passes the stripping number (LC_{SN}). From Table 5.2, the LC_{ST} values for Mix-1-None, Mix-2-WMA, Mix-3-ASA, Mix-4-PPA and Mix-5-RAP were 18,019, 10,482, 18,402, 17,203 and 16,160, respectively. Based on the LC_{ST} values, the control (Mix-1-None) and the mix containing ASA (Mix-3-ASA) exhibited a higher resistance to moisture-induced damage than the one containing WMA additive

(Mix-2-WMA). Also, the mix containing PPA-modified binder and RAP exhibited a lower LC_{ST} value compared to that of the control mix.

A higher value of $\Delta\varepsilon_{10,000}^{vp}$ for a mix represents a better rutting resistance than that with a lower $\Delta\varepsilon_{10,000}^{vp}$value. Based on Table 5.2, the mix containing ASA (Mix-3-ASA) exhibited a higher $\Delta\varepsilon_{10,000}^{vp}$value than other mixes and is expected to have the highest rutting resistance among all mixes. The lowest rutting resistance was observed in the mix containing PPA-modified binder (Mix-4-PPA). Also, Mix-2-WMA exhibited a lower resistance to rutting than the control mix.

5.4.2 Indirect Tensile Strength (ITS) Test

5.4.2.1 Tensile strength ratio (TSR)

The indirect tensile strength (ITS) values of the dry and moisture-conditioned specimens and *TSR* values of all five mixes are presented in Figure 5.3(a). The ITS value presented in Figure 5.3(a) is the average of three replicates. From Figure 5.3(a), ITS values of the dry-conditioned (ITS_{dry}) specimens for Mix-1-None, Mix-2-WMA and Mix-3-ASA were 638 kPa, 599 kPa and 621 kPa, respectively. Therefore, the addition of WMA additive and ASA reduced the ITS_{dry} by approximately 6% and 3%, respectively. However, the ITS_{wet} value increased with the addition of WMA additive and ASA by approximately 19% and 32%, respectively, compared to the control mix. As a result, the *TSR* value increased from 0.73 (Mix-1-None) to 0.93 for Mix-2-WMA. Also, approximately no reduction in tensile strength (TSR= 0.99) was observed with the addition of ASA (Figure 5.3(a)). Similar increase in *TSR* as well as reduction in moisture susceptibility with the addition of ASA was reported by LaCroix et al. (2016).

The ITS_{dry} and ITS_{wet} values of Mix-4-PPA were 878 kPa and 639 kPa, respectively, whereas the same for the control mix were 638 kPa and 463 kPa, respectively. Also, significantly higher ITS_{dry} and ITS_{wet} values were observed for Mix-5-RAP compared to control mix. Therefore, an increase in the tensile strength of a mix is expected with the addition of PPA and RAP. Although the incorporation of PPA in the mix increased both the ITS_{dry} and ITS_{wet}, the *TSR* value (0.73) did not satisfy the specification requirement (TSR<0.80). Therefore, a higher moisture susceptibility is expected for PPA-modified mix. A similar trend of increasing moisture susceptibility with the addition of PPA was reported by several studies (Orange et al., 2004; Fee et al., 2010; Abuawad et al., 2015). From Figure 5.3(a), the incorporation of RAP in the mix resulted in a *TSR* value less than 0.80, indicating a reduction in the resistance to moisture-induced damage.

5.4.2.2 Toughness Index (TI) Ratio

Figure 5.3(b) presents the average TI values of asphalt mixes under dry (TI_{dry}) and moisture conditioning (TI_{wet}) states. The moisture-conditioned specimens exhibited an increase in their plastic behavior compared to dry specimens for all mixes. For example, the TI_{dry} value for the control mix was 0.78 which increased to 0.98 after moisture conditioning. In dry conditions, the addition of WMA additive to the mix (Mix-2-WMA) resulted in an increase in plastic behavior. However, additions of ASA, PPA and RAP caused reductions in the *TI* value indicating reductions in plastic behavior of mixes. A reduction in the *TI* value with the addition of RAP was reported by several researchers (Shu et al., 2008; Huang et al., 2010). The mix with PPA (Mix-4-PPA) exhibited the highest reduction (approximately 20%) in the *TI* value than the control mix. No significant effect on the TI_{wet} value was observed for Mix-2-WMA and

Mix-3-ASA. However, the addition of PPA and RAP exhibited approximately 7 and 11% reduction on the TI_{wet} value, respectively. Based on the *TI ratio* (TI_{wet}/TI_{dry}) (Figure 5.3(b)), it was evident that the changes in the *TI* values for Mix-3-ASA and Mix-4-PPA were higher than that in Mix-1-None, Mix-2-WMA and Mix-5-RAP. As an increase in the *TI* value indicates an increase in plastic behavior, mixes with high *TI ratios* are expected to perform worse after the initiation of crack. Therefore, Mix-4-PPA is expected to exhibit the lowest resistance to moisture-induced damage compared to other mixes.

5.4.3 Louisiana Semi-Circular Bend (LA-SCB) Test

The LA-SCB tests were used to characterize the fracture properties of asphalt mixes by determining their J-integral (J_c) values. The J-integral values of the dry ($J_{c\text{-}dry}$) and MIST-conditioned ($J_{c\text{-}MIST}$) specimens for all mixes are presented in Figure 5.4. For this purpose, three replicates were tested at each notch depths. The average of the three specimens was used to calculate J_c at each condition. From Figure 5.4, the addition of ASA reduced the fracture resistance in dry-condition specimens. However, no significant change in fracture resistance occurred for Mix-2-WMA and Mix-4-PPA under dry condition. Among all mixes, specimens with RAP (Mix-5-RAP) exhibited the highest J_c value at both dry and MIST conditioning. A higher amount of binder (5.5%) present in Mix-5-RAP might be responsible for the increased J_c value. However, the $J_{c\text{-}MIST}$ values varied significantly from the $J_{c\text{-}Dry}$ values for all mixes. The J_c *ratio* of Mix-1-None through Mix-5-RAP were found to be 0.60, 0.92, 1.07, 0.61 and 0.74, respectively. The J_c *ratio* of 1.07 (higher than 1.00) for Mix-3-ASA may be due to the softening of binder during MIST conditioning. Based on the J_c *ratio,* significant

reduction in moisture susceptibility is expected for mixes with WMA additive, ASA and RAP. However, the mix with PPA exhibited similar moisture-induced damage potential as the control mix.

5.4.4 Surface Free Energy Method

The moisture-induced damage potential of asphalt mixes with different additives were evaluated using the SFE parameters. According to the SFE method, the adhesion between binder and aggregate is a function of the surface free energies of both these materials. The total SFE (Γ^{Total}) of a material consists of a non-polar Lifshitz-van der Waals component (Γ^{LW}) and a polar acid-base component (Γ^{AB}). Van Oss et al. (1988) further divided the polar acid-base component into a monopolar acidic component (Γ^{+}) and a monopolar basic component (Γ^{-}) using Equation (5.5).

$$\Gamma^{Total} = \Gamma^{LW} + \Gamma^{AB} = \Gamma^{LW} + 2\sqrt{(\Gamma^{+}\Gamma^{-})} \qquad (5.5)$$

The surface free energy components of the binder blends and aggregates used in the asphalt mixes were determined in a previous study (Ali et al., 2020) conducted by the authors. Therefore, only brief descriptions of the test methods and results are presented in the following section.

The surface free energy components of the PG 64-22 binder with different additives were determined using the dynamic Wilhelmy plate (DWP) test. For this purpose, WMA additive (0.5% by weight of neat binder), ASA (0.5% by weight of neat binder), PPA (1.5% by weight of neat binder) and RAP (20% by weight of total binder) were blended with the PG 64-22 binder. Binder blends were prepared using a high shear mixer operating at a speed of 1,000 rpm for 45 minutes at 155°C temperature. The contact angles of the binder blends with five probe liquids of known SFE components,

namely water, glycerol, formamide, diiodomethane and ethylene glycol were measured. The SFE components of the binder blends were calculated from the contact angle of the binder-probe liquid interface and SFE components of the probe liquids. The detail of the DWP test method and the SFE components of the binder blends are reported in a previous study (Ali et al., 2020).

The universal sorption device (USD) test was used to determine the vapor sorption isotherms as well as the SFE components of the aggregate used in mixes. For convenience of this study, the effect of sand was assumed insignificant on the calculation of SFE energy parameters as it consisted only 15% of the total aggregate. The USD test was conducted with three probe vapors, namely water, methyl propyl ketone (MPK), and toluene. The temperature of the test was kept constant at 25°C. The adsorption isotherms were determined by varying the relative pressure from 0.05 to 1.00. The adsorption isotherms obtained from the USD test were then used to calculate the equilibrium spreading pressure (π_e) of each vapor on the aggregate surface. The SFE components of the aggregate were determined from the equilibrium spreading pressures (π_e). The details of the USD test method and the SFE components of the aggregate can be found in a previous publication by the authors (Ali et al., 2020).

The SFE components of the binder blends (*A*) and aggregate (*S*) were combined to determine the work of adhesion (W_{AS}) and work of debonding (W_{ASW}^{wet}) of the binder-aggregate system in presence of water (*W*) and energy ratio (ER_1) using Equations (5.6), (5.7) and (5.8), respectively.

$$W_{AS} = 2\sqrt{(\Gamma_A^{LW}\Gamma_S^{LW})} + 2\sqrt{(\Gamma_A^{+}\Gamma_S^{-})} + 2\sqrt{(\Gamma_A^{-}\Gamma_S^{+})} \qquad (5.6)$$

$$W_{ASW}^{wet} = 2\sqrt{(\Gamma_A^{LW}\Gamma_S^{LW})} - 2\sqrt{(\Gamma_W^{LW}\Gamma_S^{LW})} - 2\sqrt{(\Gamma_A^{LW}\Gamma_W^{LW})} + 2\Gamma_W^{LW} - 2\sqrt{\Gamma_W^{+}}\left(\sqrt{\Gamma_S^{-}} + \sqrt{\Gamma_A^{-}} - \sqrt{\Gamma_W^{-}}\right) - 2\sqrt{\Gamma_W^{-}}\left(\sqrt{\Gamma_S^{+}} + \sqrt{\Gamma_A^{+}} - \sqrt{\Gamma_W^{+}}\right) + 2\sqrt{(\Gamma_A^{+}\Gamma_S^{-})} + 2\sqrt{(\Gamma_A^{-}\Gamma_S^{+})} \quad (5.7)$$

$$ER_1 = \left|\frac{W_{AS}}{W_{ASW}^{wet}}\right| \quad (5.8)$$

Figure 5.5 presents the W_{AS}, W_{ASW}^{wet} *and* ER_1 values between the aggregates and PG 64-22 binder with different additives. The W_{AS} between the binder-aggregate system corresponds to the formation of cracking at the interface between the binder and aggregate under vacuum. It is desirable to have a high value of W_{AS} to produce a durable mix with higher resistance to moisture-induced damage (Bhasin, 2007). From Figure 5.5, the addition of WMA, ASA, RAP and PPA increased the W_{AS} for the binder-aggregate system indicating better bond strength than the binder without any additive. Among all additives, the addition of RAP exhibited the highest increase in the W_{AS} (approximately 5% increase). It is important to determine the reduction in the W_{AS} of a binder-aggregate system in presence of a third medium such as water. The tendency of the binder to strip from the aggregate surface can be quantified with the W_{ASW}^{wet} value. A smaller magnitude of the W_{ASW}^{wet} is desirable as a higher value would indicate a thermodynamic potential for moisture-induced damage (Bhasin, 2007). From Figure 5.5, the addition of WMA additive reduced the magnitude of the $|W_{ASW}^{wet}|$, indicating an increase in the resistance to moisture susceptibility. A similar trend was observed with the addition of ASA and RAP. However, the addition of PPA resulted in an increase in the magnitude of $|W_{ASW}^{wet}|$, hence, an increase in the moisture-induced damage potential of the mix. The ER_1 represents the combined effects of the W_{AS} and W_{ASW}^{wet} as a single parameter. According to Bhasin (2007), the ER_1 can screen mixes based on their

susceptibility to moisture-induced damage. The ER_1 of the aggregate and PG 64-22 with no additives was 0.99. The addition of WMA, ASA and RAP increased and PPA reduced the ER_1 value compared to the control binder-aggregate system. Therefore, use of WMA, ASA and RAP are expected to reduce moisture susceptibility of the binder-aggregate system. However, PPA modification of PG 64-22 binder may result in an increase of moisture susceptibility with rhyolite aggregate.

5.4.5 Comparison of Different Parameters

Table 5.3 presents the ranking of asphalt mixes using different parameters. From Table 5.3, both the conventional (*SIP*) and TAMU (LC_{SN}) methods provided very similar ranking of the asphalt mixes with respect to moisture-induced damage. The mix with PPA (Mix-4-PPA) showed the lowest *SIP* value among all mixes, followed by mixes with WMA (Mix-2-WMA), RAP (Mix-5-RAP), control (Mix-1-None) and ASA (Mix-3-ASA). In case of the LC_{SN}, Mix-5-RAP performed better than Mix-1-None. From Table 5.3, variation in ranking of the asphalt mixes was observed for the *TSR* and the *TI ratio* values obtained from the ITS test. Based on the *TSR*, Mix-3-ASA exhibited the highest and Mix-5-RAP exhibited the lowest resistance to moisture susceptibility. The Mix-2-WMA, Mix-1-None and Mix-4-PPA were ranked as second, third and fourth, respectively. However, *TI ratio* ranked the mixes as Mix-2-WMA, Mix-5-RAP, Mix-1-None, Mix-3-ASA and Mix-4-PPA from the lowest to the highest level of moisture susceptibility. The variation was expected as the *TSR* and *TI ratio*s represent the behavior of a mix at the peak load and after the peak load, respectively. In case of the J_c *ratio* and *TSR*, mixes with WMA (Mix-2-WMA), ASA (Mix-3-ASA) and PPA (Mix-4-PPA) exhibited similar ranks with regard to the moisture-induced damage

potential. However, Mix-1-None and Mix-5-RAP were ranked as third and fifth with respect to the *TSR*, whereas, ranked as fifth and third according to the J_c *ratio*, respectively. Although both the J_c and *TI* values are indicators of fracture performance of a mix, the ranking of the mixes from the J_c *ratio* were not consistent with the TI ratio. According to Kim et al. (Kim et al., 2012), the J_c value represents the pre-peak fracture energy whereas *TI* is related to the post-peak fracture energy. Also, the HWT and TSR ranked mixes differently. In all cases, mixes with ASA and PPA exhibited the highest and the lowest resistance to moisture-induced damage among all mixes, respectively. Based on the HWT parameters, Mix-2-WMA had a high moisture-induced damage potential. However, from the TSR results, the addition of WMA additive to the mix resulted in a reduction in the moisture susceptibility. Therefore, effects of different additives on the moisture-induced damage resistance of mixes are dependent on the evaluation mechanism.

In this study, attempts were made to determine the relationship between the laboratory performance-based parameters and the SFE parameters. The correlations of the *SIP*, LC_{SN}, *TSR*, *TI ratio and* J_c *ratio* with the energy ratio (ER_1) are presented in Figures 5.6 (a), (b), (c), (d) and (e), respectively. From Figures 5.6(a) and 6(b), no significant correlations of the *SIP* and LC_{SN} with the ER_1 could be observed for asphalt mixes with PG 64-22 binder blends and rhyolite aggregate. However, an improved correlation ($R^2 = 0.60$) was observed for the LC_{SN} vs *ER1* when Mix-3-ASA was excluded from the comparison. The Mix-3-ASA exhibited a higher resistance to moisture-induced damage from the HWT test and resulted in a higher value of LC_{SN} compared to other mixes. From the ITS test, the *TSR* exhibited a poor correlation with

the ER_1 (R^2 = 0.01) (Figure 5.6(c)). The poor correlation likely resulted from the difference in the mechanisms *TSR* and ER_1 address. Maximum strengths of a mix after drying and moisture conditioning is considered in the *TSR* parameter, whereas, W_{AS} and W_{ASW}^{wet} that are determined using the SFE components of binder and aggregate are considered in ER_1. However, the *TI ratio* exhibited the strongest correlation with ER_1 among all parameters considered in this study with a R^2 value of 0.64 (Figure 5.6(d)). Also, the slope of the linear trend line between the *TI ratio* vs ER_1 plot was observed to be negative indicating a need to define a maximum value of the *TI ratio* to evaluate moisture-induced damage potential of asphalt mixes. Considering the limited scope of the present study, the maximum allowable limit of the *TI ratio* will be addressed in future. From Figure 5.6(e), the J_c *ratio* exhibited a better correlation with the ER_1 than *TSR* with a R^2 value of 0.13. Therefore, it can be concluded that the J_c *ratio* from LA-SCB (with MIST conditioning) has the potential for use as an indicator of moisture-induced damage of asphalt mixes. However, future studies with a larger dataset are required for a better understanding of the J_c *ratio* for evaluating moisture-induced damage potential of asphalt mixes.

5.5 CONCLUSIONS

In this study, the effects of the addition of different additives on the moisture susceptibility of asphalt mixes were evaluated using laboratory performance tests, namely the HWT, ITS and SCB and the SFE method. A new method of data analysis, known as the TAMU method, was used for evaluating the moisture-induced damage potential from the HWT test. The moisture-induced damage potentials of the asphalt mixes were also evaluated using the *TSR* and *TI ratio* by conducting ITS test on dry-

and moisture-conditioned samples. A new parameter, called the J_c *ratio* based on the LA-SCB test for evaluating the moisture-induced damage potential was introduced. All the conventional and unconventional performance-based parameters were compared with the SFE parameters. Based on the results and discussions presented in the preceding sections, the following conclusions can be drawn:

i. The SFE method exhibited an increase in the ER_1 parameter with the addition of WMA, ASA and RAP to the binder-aggregate system indicating a reduction in susceptibility to moisture. However, the incorporation of PPA into asphalt mixes may increase the potential for moisture-induced damage.

ii. From the HWT test, mixes with WMA additive exhibited a higher susceptibility to rutting and moisture-induced damage following the PPA-modified mix. However, the addition of ASA improved the resistance to rutting and moisture-induced damage of the mix based on both the conventional and the TAMU method. However, the stripping number from the TAMU method showed a better correlation with the ER_1 indicating a higher potential to identify moisture-induced damage susceptible mixes.

iii. Based on the HWT and *TSR*, asphalt mixes with ASA are expected to exhibit reduced susceptibility to rutting and moisture. The addition of PPA increased the susceptibility to moisture-induced damage although the tensile strength was higher than the other mixes for both dry and moisture-conditioned samples. The TI results indicated that the moisture conditioning process increased the plastic behavior in all mixes. Also, *TI ratio* exhibited a good correlation with the SFE parameter.

iv. The LA-SCB test with MIST conditioning exhibited the potential for use as a laboratory performance test for screening of asphalt mixes in the mix design phase. However, further studies are needed to validate the J_c *ratio* as an alternative to the current moisture-induced damage parameter.

The findings of this study are expected to help enhance the understanding of moisture susceptibility of asphalt mixes. The correlations between different laboratory-based performance parameters and ER_1 were developed based on limited asphalt mix test results (one type of aggregate with one type of binder and different additives). Future studies are needed to evaluate these relationships with a larger dataset consisting of different binder-aggregate combinations. Considering the limited scope of the present study, future studies are needed to determine correlations between and among the HWT, ITS and LA-SCB parameters with field moisture-induced damage performance.

Table 5.1 Test Matrix for Laboratory Performance Tests on Asphalt Mixes

Mix ID	NMAS (mm)	Binder Type	Additive/ RAP	Amount (%)	Number of Samples				
					HWT	ITS		LA- SCB	
					Submerged	Wet	Dry	Dry	MIST
Mix-1-None	12.5	PG 64-22	--	--	2	3	3	9*	9*
Mix-2-WMA	12.5	PG 64-22	WMA	0.5	2	3	3	9*	9*
Mix-3-ASA	12.5	PG 64-22	ASA	0.5	2	3	3	9*	9*
Mix-4-PPA	12.5	PG 64-22	PPA	1.5	2	3	3	9*	9*
Mix-5-RAP	12.5	PG 64-22	RAP	20	2	3	3	9*	9*

*3 samples were tested at each notch depth

Table 5.2 Different Parameters Obtained from HWT Test

AASHTO Method				
Mix ID	Post-compaction (mm)	Creep slope (Passes/mm)	Stripping Inflection Point (*SIP*)	Stripping Slope (Passes/mm)
Mix-1-None	1.11	4,120	11,500	880
Mix-2-WMA	1.56	1,714	5,800	500
Mix-3-ASA	0.97	5,426	13,700	930
Mix-4-PPA	0.95	3,204	5,500	850
Mix-5-RAP	1.03	2,421	9,000	895
TAMU Method				
Mix ID	$\Delta\varepsilon_{10,000}^{vp}$	**LC_{SN}**		**LC_{ST}**
Mix-1-None	3.91E-06	1,228		18,019
Mix-2-WMA	9.32E-06	867		10,482
Mix-3-ASA	1.93E-06	3,312		18,402
Mix-4-PPA	3.17E-05	131		17,203
Mix-5-RAP	3.52E-06	1,776		16,160

Table 5.3 Ranking of Asphalt Mixes based on Different Laboratory-based Performance Parameters

Mix ID	HWT Test		ITS Test		LA-SCB Test
	SIP	LC_{SN}	*TSR*	*TI ratio*	J_c *ratio*
Mix-1-None	2	3	3	3	5
Mix-2-WMA	4	4	2	1	2
Mix-3-ASA	1	1	1	4	1
Mix-4-PPA	5	5	4	5	4
Mix-5-RAP	3	2	5	2	3

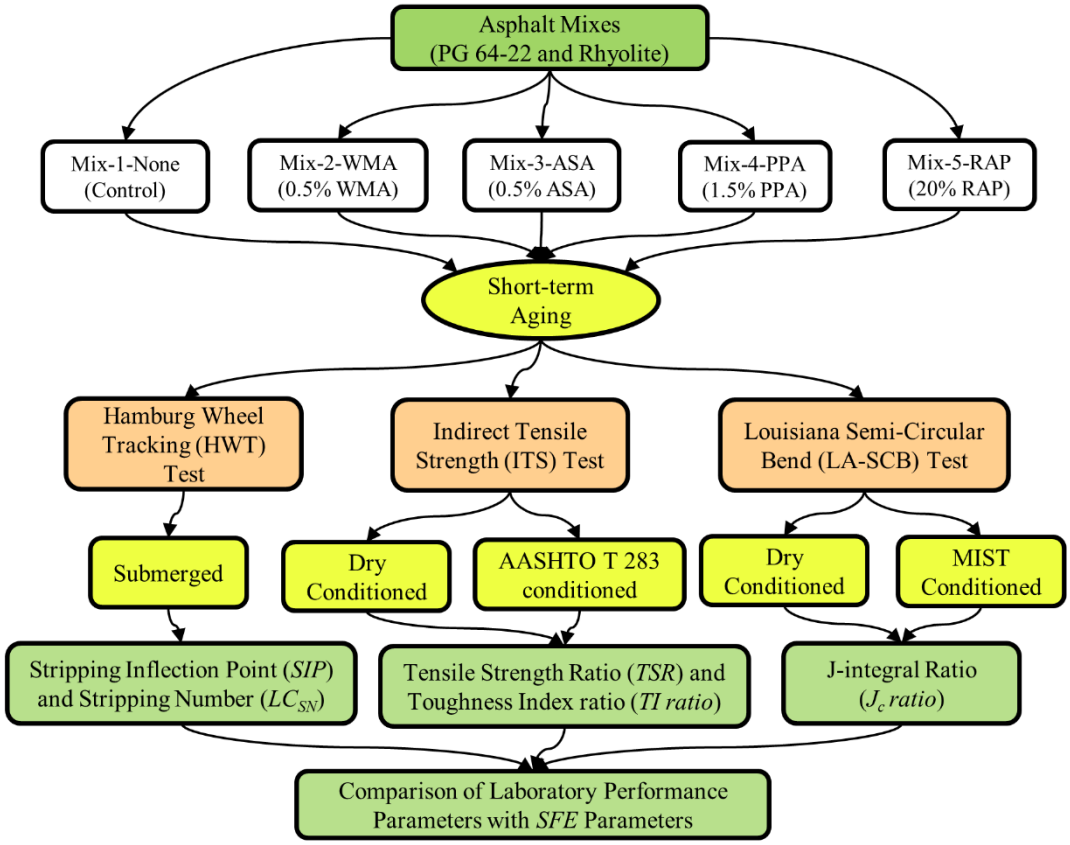

Figure 5.1 Workflow diagram for the study

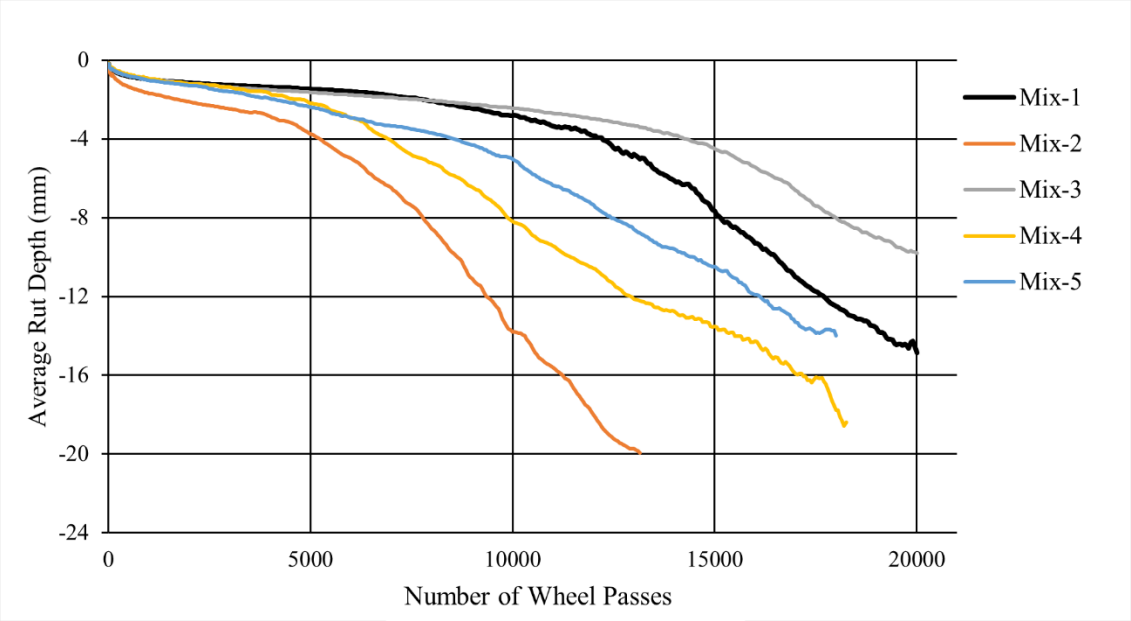

Figure 5.2 Rut depths vs. wheel passes from HWT test

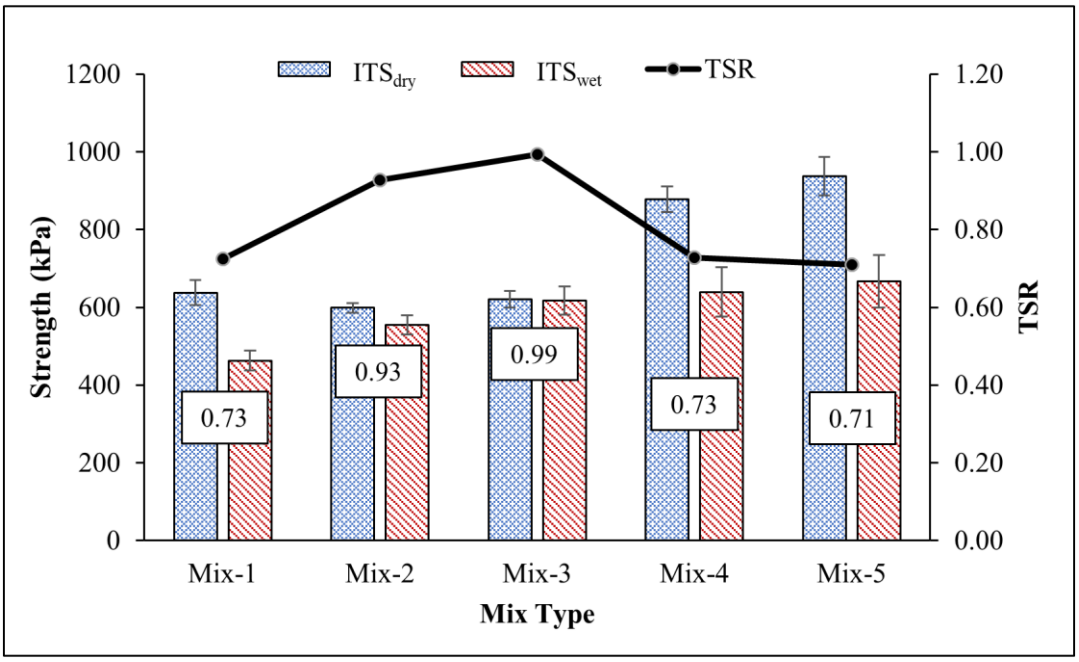

(a)

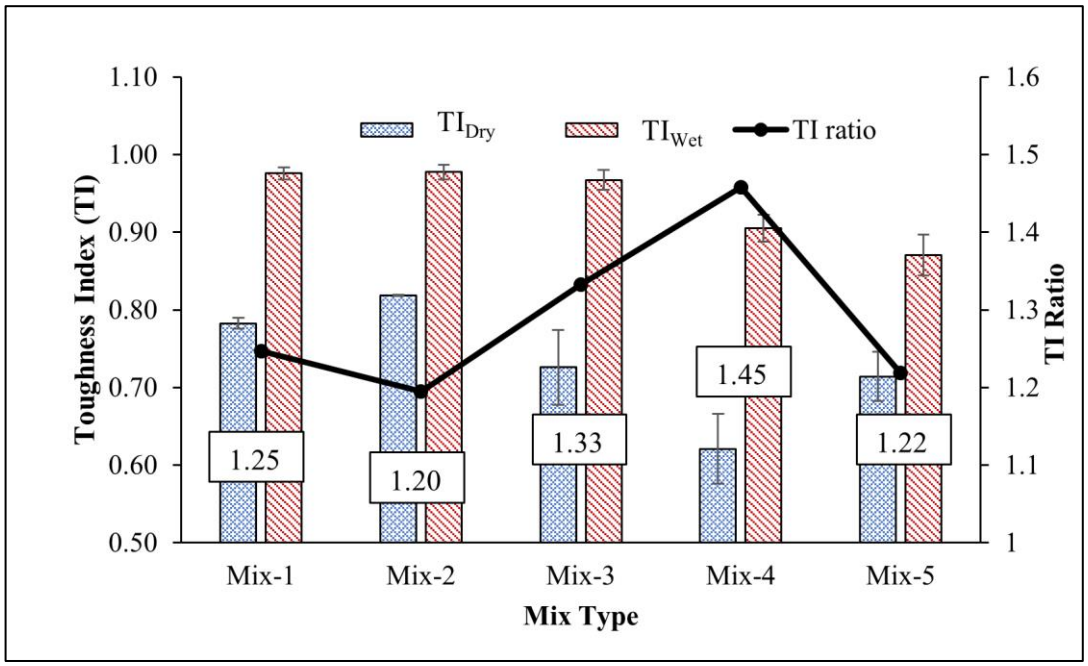

(b)

Figure 5.3 (a) Indirect tensile strength (*ITS$_{dry}$* and *ITS$_{wet}$*) and *TSR* values; (b) toughness index (*TI$_{dry}$* and *TI$_{wet}$*) and *TI ratios* of asphalt mixes from ITS test

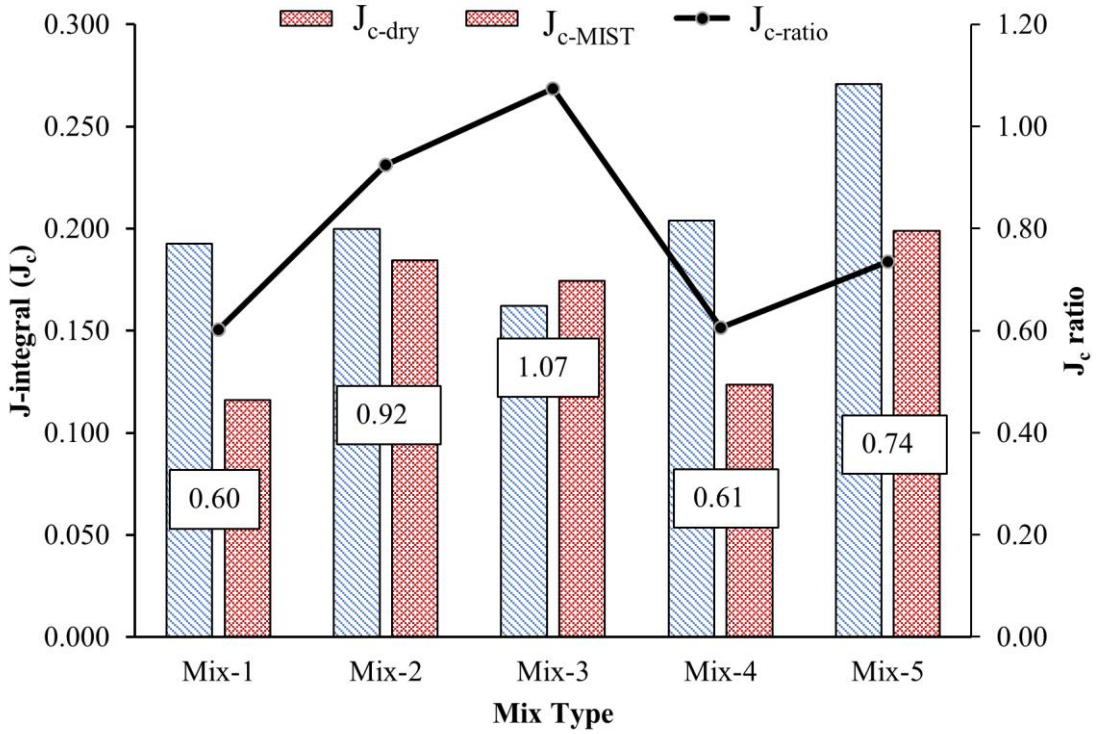

Figure 5.4 $J_{c\text{-}dry}$ and $J_{c\text{-}MIST}$ values and J_c *ratio* of asphalt mixes from LA-SCB test

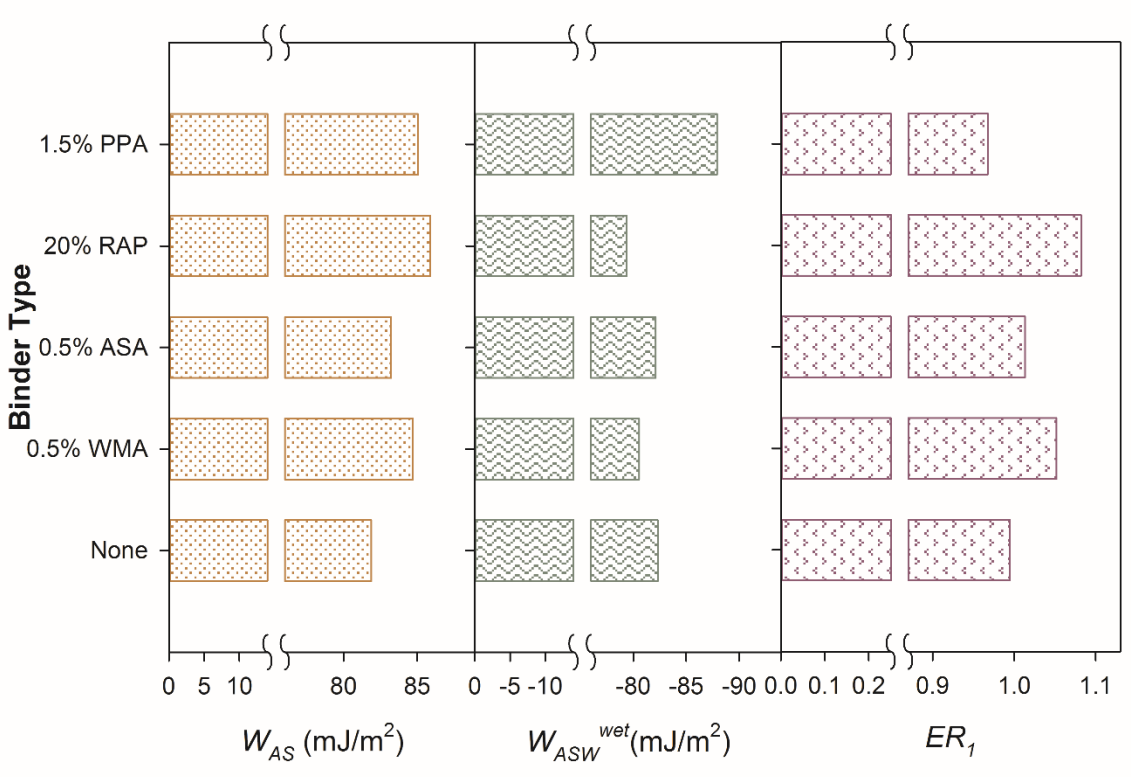

Figure 5.5 Work of adhesion (W_{AS}), work of debonding (W_{ASW}^{wet}) and energy ratio (ER_1) of binder blends with rhyolite aggregate

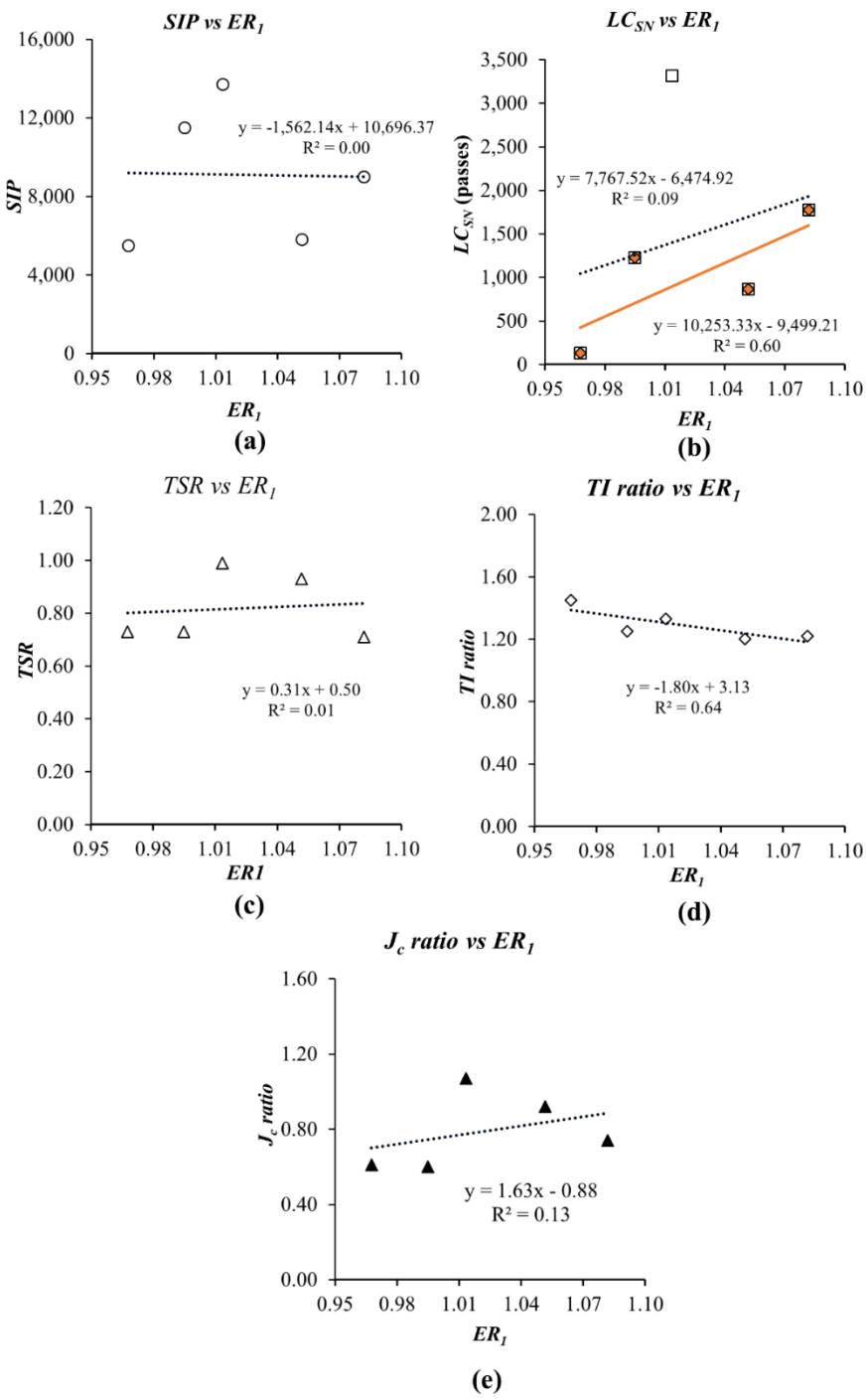

Figure 5.6 Comparison of different laboratory performance parameters with SFE parameter; (a) *SIP vs ER₁*, (b) *LC$_{SN}$ vs ER₁*; (c)*TSR vs ER₁*; (d) *TI ratio vs ER₁* and (e) *J$_c$ ratio vs ER₁*

CHAPTER

6

CONCLUSIONS AND RECOMMENDATIONS

6.1 CONCLUSIONS

In this study, the effects of additives, aggregate types and aging on the moisture-induced damage potential of asphalt mixes were studied by using the thermodynamic approach, chemical analysis and laboratory-based performance tests. In Chapter 2, attempts were made to understand the differences in the surface free energy estimation of binders using different methods, namely the GvOC, Owens-Wendt, Wu and Neumann methods. Also, the effect of probe liquid sets on the calculation of SFE components by the GvOC, Owens-Wendt and Wu method was evaluated. Furthermore, attempts were made to identify the probe liquid sets that produce consistent energy parameters for a binder-aggregate system. In Chapter 3, chemical and thermodynamic properties of asphalt binder and aggregates were used to evaluate the compatibility of binder-aggregate system. The FTIR test was used to characterize the functional groups of the binder blends. The XRF test was used to determine the elemental compositions of both binders and aggregates. The SFE components of the binder blends and aggregates were determined using the dynamic Wilhelmy plate and the universal sorption device test. Effects of aggregate types, aging and additives on the moisture-induced damage potential were identified by investigating the changes in chemical and thermodynamic properties. In Chapter 4, the effect of aging on the moisture-induced damage performance of the binder-aggregate system was assessed by evaluating the changes in

the energy parameters from the SFE method. In addition, the moisture-induced damage potentials of short-term and long-term aged asphalt mixes were evaluated using the *TSR* and the G_f *ratio* parameters. Correlations between the moisture-induced damage performance parameters from laboratory performance tests and the SFE method were also investigated. In Chapter 5, the effects of the addition of different additives on the moisture susceptibility of asphalt mixes were evaluated using laboratory performance tests, namely the HWT, ITS and SCB tests. A new method of data analysis, known as the TAMU method, was used for evaluating the moisture-induced damage potential from the HWT test. The moisture-induced damage potentials of the asphalt mixes were also evaluated using the *TSR* and *TI ratio* by conducting ITS test on dry- and moisture-conditioned specimens. A new parameter, called the J_c *ratio* based on the LA-SCB test for evaluating the moisture-induced damage potential was introduced. The conventional and unconventional performance-based parameters were compared with the SFE parameters. The important findings from this study are listed below:

i. Different SFE estimation methods were found to characterize binders differently. The differences in the SFE components resulting from the assumptions and mathematical formulations used by different methods were responsible for different characterization of binders. The differences in the SFE were reflected in the energy parameters of the binder-aggregate system as well.
ii. The WGFDE, WGDE and WFDE probe liquid sets were found to provide consistent energy parameters for the GvOC method. Similar probe liquid sets are expected to produce consistent energy parameters for the OW method as well. In

case of the Wu method, the WGFDE, WFGD and WFED probe liquid sets can be used to obtain consistent SFE of binders.

iii. Among different component-based approaches, only the GvOC method was found to characterize asphalt mixes similar to the Neumann method.

iv. The results of the SFE method indicated that the properties of aggregates have significantly higher influence on the moisture-induced damage potential of a mix than the properties of binder.

v. Based on the chemical analysis and the surface free energy method, the rhyolite (R1) and limestone (L1 and L3) aggregates are expected to exhibit good resistance to moisture-induced damage when used in a mix. The test results indicated poor moisture-induced damage resistance for L2 limestone and G1 granite aggregate.

vi. The analyses of FTIR spectra were found to provide valuable information on the functional groups present in the binders. Also, the FTIR test was able to detect the additives and modifiers used in binders.

vii. A general increasing trend of the carbonyl and sulfoxide functionalities for binders with short and long-term aging was observed from the FTIR analyses. The increase in these functional groups may produce water soluble bonds at the interface making it susceptible to moisture.

viii. Asphalt mixes, in general, were found to become more prone to moisture-induced damage with long-term aging. Significant changes in the SFE components, *ITS* and G_f values were observed due to the thermal degradation of the constituents of binder and additives.

ix. From SFE method and chemical analysis, the addition of WMA and ASA are expected to reduce moisture susceptibility of asphalt mix. Similar improvements were also observed from the *TSR* and G_f *ratio* parameters. The presence of amine group in both WMA and ASA is expected to enhance bonding between binder and aggregate.

x. The use of 20% RAP is expected to improve the resistance to moisture-induced damage. However, the performance of the binder blend with RAP may deteriorate with aging.

xi. In general (except L2 aggregate), PPA modification increased the potential for moisture-induced damage of a binder-aggregate system. From laboratory-based performance test, the mix containing PPA was found to exhibit the lowest *TSR* values among all mixes indicating the highest susceptibility to moisture-induced damage.

xii. The stripping number (LC_{SN}) from the HWT test showed a better correlation with the ER_1 indicating a higher potential to identify moisture-induced damage susceptible mixes.

xiii. The *TI* results indicated that the moisture conditioning process increased the plastic behavior in all mixes. Also, *TI ratio* exhibited a good correlation with the SFE parameter.

xiv. The G_f *ratio* from IL-SCB and J_c *ratio* from LA-SCB test exhibited the potential for use as a laboratory performance test for screening of asphalt mixes in the mix design phase.

6.2 RECOMMENDATIONS

Considering the limited scope of this study, future studies are recommended to address the following issues:

i. The moisture-induced damage potential of asphalt mixes produced with aggregates from sources different than the ones used in the current study can vary depending on their mineralogical and surface compositions. Therefore, future studies should address moisture-induced damage evaluation of other aggregates and selection of binder-aggregate combinations.

ii. In the current study, performance of asphalt mixes was evaluated for one type of aggregate (rhyolite). Therefore, future studies involving other types of aggregates such as limestone, granite and dolomite may be conducted to obtain a better understanding of additives and aging for different binder-aggregate combinations.

iii. The correlations between different laboratory-based performance parameters and ER_1 were developed based on a relatively small dataset. Future studies may evaluate these relationships with a larger dataset consisting of different binder-aggregate combinations.

iv. In the present study, standard test methods and loading rates were used to conduct the laboratory-performance tests. Future studies may consider the effects of loading rate and displacement on the evaluation of moisture-induced damage potential of asphalt mixes.

v. The surface chemistry related to the adsorption and desorption of binders with different additives on the surface of different aggregates needs further investigation.

vi. The study was limited to 20% RAP. The effect of the addition of higher amounts of RAP (> 20%) to the moisture-induced damage potential of asphalt mixes should be investigated.

vii. In this study, the roughness of the binder surface was not considered in the calculation of contact angle with probe liquids. Effect of roughness of binder surface may be addressed in future studies.

viii. In this study, the influence of filler was considered insignificant in the calculation of moisture-induced damage of a binder-aggregate system. Future study is needed to quantify the SFE components of fillers and its contribution to the calculations of adhesive bond of a binder-aggregate system.

ix. Considering the limited scope of the present study, future studies are needed to determine correlations between and among the HWT, ITS and SCB parameters with field moisture-induced damage performance.

x. The present study was limited to laboratory test-based assessment of moisture-induced damage potential of asphalt mixes. Correlations between field performance and laboratory assessment may be pursued in future studies.

REFERENCES

AASHTO, 2013. ASTM D7870: Standard practice for moisture conditioning compacted asphalt mixture specimens by using hydrostatic pore pressure. West Conshohocken, PA: ASTM International.

AASHTO, 2014a. AASHTO T 283: Standard Method of Test for Resistance of Compacted Asphalt Mixtures to Moisture-induced Damage. Washington, DC: American Association of State Highway and Transportation Officials.

AASHTO, 2014b. AASHTO T 324: Standard Method of Test for Hamburg Wheel-track Testing of Compacted Asphalt Mixtures Washington, DC: American Association of State Highway and Transportation Officials.

AASHTO, 2015a. AASHTO R 30: Standard Practice for Mixture Conditioning of Hot Mix Asphalt (HMA). Washington, D.C.: American Association of State Highway and Transportation Officials.

AASHTO, 2015b. AASHTO T 312: Standard Method of Test for Preparing and Determining the Density of Asphalt Mixture Specimens by Means of the Superpave Gyratory Compactor. Washington, D.C.: American Association of State Highway and Transportation Officials.

AASHTO, 2016. AASHTO R 28: Standard Practice for Accelerated Aging of Asphalt Binder Using a Pressurized Aging Vessel (PAV) Washington, D.C.: American Association of State Highway and Transportation Officials.

AASHTO, 2017. AASHTO T 240: Standard Method of Test for Effect of Heat and Air on a Moving Film of Asphalt Binder (Rolling Thin-Film Oven Test)

Washington, D.C.: American Association of State Highway and Transportation Officials.

AASHTO, 2018. AASHTO TP 124: Standard Method of Test for Determining the Fracture Potential of Asphalt Mixtures Using the Flexibility Index Test (FIT). Washington, D.C.: American Association of State Highway and Transportation Officials.

Abo-Qudais, S. and Al-Shweily, H. 2007. Effect of aggregate properties on asphalt mixtures stripping and creep behavior. *Construction and Building Materials,* 21(9), 1886-1898.

Abuawad, I. M., Al-Qadi, I. L. and Trepanier, J. S. 2015. Mitigation of Moisture Damage in Asphalt Concrete: Testing Techniques and Additives/Modifiers Effectiveness. *Construction and Building Materials,* 84, 437-443.

Aguiar-Moya, J. P., Salazar-Delgado, J., Baldi-Sevilla, A., Leiva-Villacorta, F. and Loria-Salazar, L. 2015. Effect of aging on adhesion properties of asphalt mixtures with the use of bitumen bond strength and surface energy measurement tests. *Transportation Research Record,* 2505(1), 57-65.

Airey, G. D. 2003. Rheological properties of styrene butadiene styrene polymer modified road bitumens☆. *Fuel,* 82(14), 1709-1719.

Aksoy, A., Şamlioglu, K., Tayfur, S. and Özen, H. 2005. Effects of various additives on the moisture damage sensitivity of asphalt mixtures. *Construction and Building Materials,* 19(1), 11-18.

Al-Qadi, I. L., Abauwad, I. M., Dhasmana, H. and Coenen, A. R., 2014. *Effects of Various Asphalt Binder Additives/Modifiers on Moisture-Susceptible Asphaltic Mixtures.* Illinois Center for Transportation, 0197-9191.

Al-Qadi, I. L., Aurangzeb, Q., Carpenter, S. H., Pine, W. J. and Trepanier, J., 2012. *Impact of high RAP contents on structural and performance properties of asphalt mixtures.* Illinois: Illinois Center for Transportation, Research Report FHWA-ICT-12-002.

Al-Qadi, I. L., Fini, E. H., Masson, J.-F. and McGhee, K. M. 2008. Effect of bituminous material rheology on adhesion. *Transportation Research Record,* 2044(1), 96-104.

Al-Qadi, I. L., Ozer, H., Lambros, J., El Khatib, A., Singhvi, P., Khan, T., Rivera-Perez, J. and Doll, B., 2015. *Testing Protocols to Ensure Performance of High Asphalt Binder Replacement Mixes Using RAP and RAS.* Illinois Center for Transportation/Illinois Department of Transportation, 0197-9191.

Ali, S. A., Ghabchi, R., Zaman, M. and Bulut, R., 2019. *Development of a SFE Database for Screening of Mixes for Moisture Damage in Oklahoma.*

Ali, S. A., Zaman, M., Ghabchi, R., Rahman, M. A., Ghos, S. and Rani, S. 2020. Effect of Additives and Aging on Moisture-induced Damage Potential of Asphalt Mixes using Surface Free Energy and Laboratory-based Performance Tests. *Int. J. of Pave. Eng.*, 1-12.

Alvarez, A. E., Ovalles, E. and Caro, S. 2012a. Assessment of the effect of mineral filler on asphalt–aggregate interfaces based on thermodynamic properties. *Construction and Building Materials,* 28(1), 599-606.

Alvarez, A. E., Ovalles, E. and Epps Martin, A. 2012b. Comparison of asphalt rubber-aggregate and polymer modified asphalt–aggregate systems in terms of surface free energy and energy indices. *Construction and Building Materials*, 35, 385-392.

Arabani, M. and Hamedi, G. H. 2010. Using the Surface Free Energy Method to Evaluate the Effects of Polymeric Aggregate Treatment on Moisture Damage in Hot-Mix Asphalt. *Journal of Materials in Civil Engineering*, 23(6), 802-811.

Arabani, M. and Hamedi, G. H. 2014. Using the Surface Free Energy Method to Evaluate the Effects of Polymeric Aggregate Treatment on Moisture Damage in Hot-Mix Asphalt. *International Journal of Pavement Engineering*, 15(1), 66-78.

Arabani, M., Roshani, H. and Hamedi, G. H. 2011. Estimating moisture sensitivity of warm mix asphalt modified with zycosoil as an antistrip agent using surface free energy method. *Journal of Materials in Civil Engineering*, 24(7), 889-897.

Arafat, S., Noor, L., Wasiuddin, N. M. and Salomon, D. 2020. Development of a Test Method to Measure RAP Percentage in Asphalt Mixes in the Field Using a Handheld FT-IR Spectrometer. *Journal of Materials in Civil Engineering*, 32(12), 04020352.

Arnold, T. S., Needham, S. and Youtcheff Jr, J. 2009. Use of phosphoric acid as a modifier for hot-mix asphalt. *Transportation Research Circular E-C160, Polyphosphoric Acid Modification of Asphalt Binders*, 40-51.

ASTM, 2013. ASTM D7870: Standard Practice for Moisture Conditioning Compacted Asphalt Mixture Specimens by Using Hydrostatic Pore Pressure. West Conshohocken, Pennsylvania: ASTM International.

Bagampadde, U., Isacsson, U. and Kiggundu, B. 2006. Impact of Bitumen and Aggregate Composition on Stripping in Bituminous Mixtures. *Materials and structures,* 39(3), 303-315.

Baldi-Sevilla, A., Montero, M. L., Aguiar-Moya, J. P., Loria-Salazar, L. G. and Bhasin, A. 2017. Influence of bitumen and aggregate polarity on interfacial adhesion. *Road Materials and Pavement Design,* 18(sup2), 304-317.

Baumgardner, G. L. 2010. Why and how of polyphosphoric acid modification–an industry perspective. *Journal of the Association of Asphalt Paving Technologists,* 79.

Baumgardner, G. L., Masson, J., Hardee, J. R., Menapace, A. M. and Williams, A. G. 2005. Polyphosphoric acid modified asphalt: proposed mechanisms. *Journal of the Association of Asphalt Paving Technologists,* 74, 283-305.

Behnood, A. and Gharehveran, M. M. 2019. Morphology, rheology, and physical properties of polymer-modified asphalt binders. *European Polymer Journal,* 112, 766-791.

Bhasin, A., 2007. *Development of Methods to Quantify Bitumen-Aggregate Adhesion and Loss of Adhesion Due to Water.* Texas A&M University.

Bhasin, A., Howson, J., Masad, E., Little, D. and Lytton, R. 2007a. Effect of Modification Processes on Bond Energy of Asphalt Binders. *Transportation Research Record: Journal of the Transportation Research Board,* (1998), 29-37.

Bhasin, A., Little, D., Vasconcelos, K. and Masad, E. 2007b. Surface Free Energy to Identify Moisture Sensitivity of Materials for Asphalt Mixes. *Transportation Research Record: Journal of the Transportation Research Board,* (2001), 37-45.

Bhasin, A. and Little, D. N., 2006. *Characterizing Surface Properties of Aggregates Used in Hot Mix Asphalt.*

Bhasin, A. and Little, D. N. 2007. Characterization of aggregate surface energy using the universal sorption device. *Journal of Materials in Civil Engineering,* 19(8), 634-641.

Bhasin, A., Masad, E., Little, D. and Lytton, R. 2006. Limits on Adhesive Bond Energy for Improved Resistance of Hot-Mix Asphalt to Moisture Damage. *Transportation Research Record: Journal of the Transportation Research Board,* (1970), 3-13.

Bonemazzi, F., Braga, V., Corrieri, R., Giavarini, C. and Sartori, F. 1996. Characteristics of polymers and polymer-modified binders. *Transportation Research Record,* 1535(1), 36-47.

Buddhala, A., Hossain, Z., Wasiuddin, N. M., Zaman, M. and Edgar, A. 2011. Effects of an Amine Anti-stripping Agent on Moisture Susceptibility of Sasobit and Aspha-min Mixes by Surface Free Energy Analysis. *Journal of Testing and Evaluation,* 40(1), 91-99.

Caro, S., Masad, E., Bhasin, A. and Little, D. N. 2008a. Moisture Susceptibility of Asphalt Mixtures, Part 1: Mechanisms. *International Journal of Pavement Engineering,* 9(2), 81-98.

Caro, S., Masad, E., Bhasin, A. and Little, D. N. 2008b. Moisture Susceptibility of Asphalt Mixtures, Part 2: Characterisation and Modelling. *International Journal of Pavement Engineering,* 9(2), 99-114.

Chibowski, E. and Perea-Carpio, R. 2002. Problems of contact angle and solid surface free energy determination. *Advances in Colloid and Interface Science,* 98(2), 245-264.

Cooper III, S. B., Mohammad, L. N., Kabir, S. and King Jr, W. 2014. Balanced asphalt mixture design through specification modification: Louisiana's experience. *Transportation Research Record,* 2447(1), 92-100.

Cooper Jr, S. B., Cooper III, S. B., Mohammad, L. N. and Elseifi, M. A. 2016. Development of a Predictive Model Based on an Artificial Neural Network for the Semicircular Bend Test. *Transportation Research Record: Journal of the Transportation Research Board,* (2576), 83-90.

Copeland, A. R., Youtcheff, J. and Shenoy, A. 2007. Moisture sensitivity of modified asphalt binders: factors influencing bond strength. *Transportation Research Record,* 1998(1), 18-28.

Cui, S., Blackman, B. R., Kinloch, A. J. and Taylor, A. C. 2014. Durability of asphalt mixtures: Effect of aggregate type and adhesion promoters. *International Journal of Adhesion and Adhesives,* 54, 100-111.

Curtis, C., Lytton, R. and Brannan, C. 1992. Influence of aggregate chemistry on the adsorption and desorption of asphalt. *Transportation Research Record,* (1362).

Curtis, C. W., Ensley, K. and Epps, J., 1993. *Fundamental properties of asphalt-aggregate interactions including adhesion and absorption (SHRP-A-341).* Washington, DC.

D'Angelo, J. A., Harm, E. E., Bartoszek, J. C., Baumgardner, G. L., Corrigan, M. R., Cowsert, J. E., Harman, T. P., Jamshidi, M., Jones, H. W. and Newcomb, D. E., 2008. *Warm-mix asphalt: European practice.*

D'Angelo, J. A. 2010. Effect of poly phosphoric acid on asphalt binder properties. *Journal of the Association of Asphalt Paving Technologists,* 79.

Della Volpe, C., Maniglio, D., Brugnara, M., Siboni, S. and Morra, M. 2004. The solid surface free energy calculation: I. In defense of the multicomponent approach. *Journal of colloid and interface science,* 271(2), 434-453.

Della Volpe, C. and Siboni, S. 2000. Acid–base surface free energies of solids and the definition of scales in the Good–van Oss–Chaudhury theory. *Journal of Adhesion Science and Technology,* 14(2), 235-272.

Doyle, J. D. and Howard, I. L. 2013. Rutting and moisture damage resistance of high reclaimed asphalt pavement warm mixed asphalt: loaded wheel tracking vs. conventional methods. *Road Materials and Pavement Design,* 14(sup2), 148-172.

Dupré, A. and Dupré, P., 1869. *Théorie mécanique de la chaleur.* Gauthier-Villars.

Esmaeili, N., Hamedi, G. H. and Khodadadi, M. 2019. Determination of the stripping process of asphalt mixtures and the effective mix design and SFE parameters on its different phases. *Construction and Building Materials,* 213, 167-181.

Fakhri, M., Ghanizadeh, A. R. and Omrani, H. 2013. Comparison of fatigue resistance of HMA and WMA mixtures modified by SBS. *Procedia-Social and Behavioral Sciences,* 104, 168-177.

Fee, D., Maldonado, R., Reinke, G. and Romagosa, H. 2010. Polyphosphoric acid modification of asphalt. *Transportation Research Record: Journal of the Transportation Research Board*, (2179), 49-57.

Fowkes, F. 1964. Attractive Forces at Interfaces, Ind. Eng. Chem. 56 (12), 40-52.

Fuerstenau, D., Diao, J. and Hanson, J. 1990. Estimation of the distribution of surface sites and contact angles on coal particles from film flotation data. *Energy & fuels*, 4(1), 34-37.

Ge, D., Chen, S., You, Z., Yang, X., Yao, H., Ye, M. and Yap, Y. K. 2019. Correlation of DSR results and FTIR's carbonyl and sulfoxide indexes: Effect of aging temperature on asphalt rheology. *Journal of Materials in Civil Engineering*, 31(7), 04019115.

Ge, D., Yan, K., You, L. and Wang, Z. 2017. Modification mechanism of asphalt modified with Sasobit and Polyphosphoric acid (PPA). *Construction and Building Materials*, 143, 419-428.

Ghabchi, R., 2014. *Laboratory Characterization of Recycled and Warm Mix Asphalt for Enhanced Pavement Applications.* Dissertation (Ph.D.). University of Oklahoma.

Ghabchi, R., Barman, M., Singh, D., Zaman, M. and Mubaraki, M. A. 2016. Comparison of Laboratory Performance of Asphalt Mixes Containing Different Proportions of RAS and RAP. *Construction and Building Materials*, 124, 343-351.

Ghabchi, R., Singh, D. and Zaman, M. 2014. Evaluation of Moisture Susceptibility of Asphalt Mixes Containing RAP and Different Types of Aggregates and Asphalt

Binders Using the Surface Free Energy Method. *Construction and Building Materials,* 73, 479-489.

Ghabchi, R., Singh, D. and Zaman, M. 2015. Laboratory Evaluation of Stiffness, Low-temperature Cracking, Rutting, Moisture Damage, and Fatigue Performance of WMA Mixes. *Road Materials and Pavement Design,* 16(2), 334-357.

Ghabchi, R., Singh, D., Zaman, M. and Tian, Q. 2013. Mechanistic Evaluation of the Effect of WMA Additives on Wettability and Moisture Susceptibility Properties of Asphalt Mixes. *Journal of Testing and Evaluation,* 41(6), 933-942.

Gorkem, C. and Sengoz, B. 2009. Predicting Stripping and Moisture Induced Damage of Asphalt Concrete Prepared with Polymer Modified Bitumen and Hydrated Lime. *Construction and Building Materials,* 23(6), 2227-2236.

Grundke, K., Bogumil, T., Gietzelt, T., Jacobasch, H.-J., Kwok, D. and Neumann, A., 1996. Wetting measurements on smooth, rough and porous solid surfaces. *Interfaces, Surfactants and Colloids in Engineering.* Springer, 58-68.

Guo, F., Pei, J., Zhang, J., Xue, B., Sun, G. and Li, R. 2020. Study on the adhesion property between asphalt binder and aggregate: A state-of-the-art review. *Construction and Building Materials,* 256, 119474.

Haider, S., Hafeez, I. and Ullah, R. 2020. Sustainable use of waste plastic modifiers to strengthen the adhesion properties of asphalt mixtures. *Construction and Building Materials,* 235, 117496.

Hartland, S., 2004. *Surface and interfacial tension: measurement, theory, and applications.* CRC Press.

Harvey, J. T. and Lu, Q. 2005. Investigation of Conditions for Moisture Damage in Asphalt Concrete and Appropriate Laboratory Test Methods.

Hefer, A. W., Bhasin, A. and Little, D. N. 2006. Bitumen Surface Energy Characterization Using a Contact Angle Approach. *Journal of Materials in Civil Engineering*, 18(6), 759-767.

Hefer, A. W., Little, D. N. and Lytton, R. L. 2005. A Synthesis of Theories and Mechanisms of Bitumen-Aggregate Adhesion Including Recent Advances in Quantifying the Effects of Water. *Journal of the Association of Asphalt Paving Technologists*, 74, 139-196.

Hesami, S., Roshani, H., Hamedi, G. H. and Azarhoosh, A. 2013. Evaluate the mechanism of the effect of hydrated lime on moisture damage of warm mix asphalt. *Construction and Building Materials*, 47, 935-941.

Hesp, S. A. and Shurvell, H. F. 2010. X-ray fluorescence detection of waste engine oil residue in asphalt and its effect on cracking in service. *International Journal of Pavement Engineering*, 11(6), 541-553.

Hesp, S. A. and Shurvell, H. F. 2013. Quality assurance testing of asphalt containing waste engine oil. *International Journal of Pavements*.

Hofko, B., Porot, L., Cannone, A. F., Poulikakos, L., Huber, L., Lu, X., Mollenhauer, K. and Grothe, H. 2018. FTIR spectral analysis of bituminous binders: reproducibility and impact of ageing temperature. *Materials and Structures*, 51(2), 1-16.

Holländer, A. 1995. On the selection of test liquids for the evaluation of acid-base properties of solid surfaces by contact angle goniometry. *J. Colloid Interface Sci.* , 169(2), 493-496.

Hossain, K., Karakas, A. and Hossain, Z. 2019. Effects of aging and rejuvenation on surface-free energy measurements and adhesion of asphalt mixtures. *Journal of Materials in Civil Engineering*, 31(7), 04019125.

Hossain, Z., Lewis, S., Zaman, M., Buddhala, A. and O'Rear, E. 2012. Evaluation for warm-mix additive-modified asphalt binders using spectroscopy techniques. *Journal of Materials in Civil Engineering*, 25(2), 149-159.

Howson, J., Masad, E. A., Bhasin, A., Branco, V. C., Arambula, E., Lytton, R. and Little, D. 2007. System for the evaluation of moisture damage using fundamental material properties. *The Texas A&M University System*.

Huang, B., Shu, X. and Vukosavljevic, D. 2010. Laboratory investigation of cracking resistance of hot-mix asphalt field mixtures containing screened reclaimed asphalt pavement. *Journal of Materials in Civil Engineering*, 23(11), 1535-1543.

Huang, S.-C. and Grimes, W. 2010. Influence of aging temperature on rheological and chemical properties of asphalt binders. *Transportation Research Record*, 2179(1), 39-48.

Huang, S.-C., Turner, T. F., Miknis, F. P. and Thomas, K. P. 2008. Long-term aging characteristics of polyphosphoric acid-modified asphalts. *Transportation Research Record*, 2051(1), 1-7.

Hurley, G. C. and Prowell, B. D. 2005. Evaluation of Sasobit for use in warm mix asphalt. *NCAT report,* 5(6), 1-27.

Hurley, G. C. and Prowell, B. D. 2006. Evaluation of potential processes for use in warm mix asphalt. *Journal of the Association of Asphalt Paving Technologists,* 75(4).

Isacsson, U. and Lu, X. 1995. Testing and appraisal of polymer modified road bitumens—state of the art. *Materials and Structures,* 28(3), 139-159.

Israelachvili, J. N. and Tabor, D. 1972. The calculation of van der Waals dispersion forces between macroscopic bodies. *Proceedings of the royal society of London. A. mathematical and physical sciences,* 331(1584), 39-55.

Jahromi, S. G. 2009. Estimation of resistance to moisture destruction in asphalt mixtures. *Construction and Building Materials,* 23(6), 2324-2331.

Johnson, D. R. and Freeman, R. B., 2002. *Rehabilitation techniques for stripped asphalt pavements.* Montana. Department of Transportation.

Johnson, K. L., Kendall, K. and Roberts, a. 1971. Surface energy and the contact of elastic solids. *Proceedings of the royal society of London. A. mathematical and physical sciences,* 324(1558), 301-313.

Kakar, M. R., Hamzah, M. O., Akhtar, M. N. and Woodward, D. 2016. Surface free energy and moisture susceptibility evaluation of asphalt binders modified with surfactant-based chemical additive. *Journal of cleaner production,* 112, 2342-2353.

Kalantar, Z. N., Karim, M. R. and Mahrez, A. 2012. A review of using waste and virgin polymer in pavement. *Construction and Building Materials,* 33, 55-62.

Kanitpong, K. and Bahia, H. 2005. Relating adhesion and cohesion of asphalts to the effect of moisture on laboratory performance of asphalt mixtures. *Transportation Research Record,* 1901(1), 33-43.

Khodaii, A., Khalifeh, V., Dehnad, M. and Hamedi, G. H. 2013. Evaluating the effect of zycosoil on moisture damage of hot-mix asphalt using the surface energy method. *Journal of Materials in Civil Engineering,* 26(2), 259-266.

Khodaii, A., Tehrani, H. K. and Haghshenas, H. 2012. Hydrated lime effect on moisture susceptibility of warm mix asphalt. *Construction and Building Materials,* 36, 165-170.

Kim, M., Mohammad, L. and Elseifi, M. 2012. Characterization of fracture properties of asphalt mixtures as measured by semicircular bend test and indirect tension test. *Transportation Research Record: Journal of the Transportation Research Board,* (2296), 115-124.

Kim, S., Park, J., Lee, S. and Kim, K. W. 2014. Performance of modified WMA Mixtures prepared using the same class pg binders of HMA mixtures. *Journal of Testing and Evaluation,* 42(2), 347-356.

Kim, S., Sholar, G., Byron, T. and Kim, J. 2009. Performance of polymer-modified asphalt mixture with reclaimed asphalt pavement. *Transportation Research Record: Journal of the Transportation Research Board,* (2126), 109-114.

Kringos, N., Scarpas, A., Copeland, A. and Youtcheff, J. 2008. Modelling of combined physical–mechanical moisture-induced damage in asphaltic mixes Part 2: moisture susceptibility parameters. *International Journal of Pavement Engineering,* 9(2), 129-151.

Kwok, D. Y. and Neumann, A. W. 1999. Contact angle measurement and contact angle interpretation. *Advances in colloid and interface science,* 81(3), 167-249.

Kwok, D. Y. H., 1998. *CONTACT ANGLES AND SURFACE EMRGETICS.* University of Toronto.

LaCroix, A., Regimand, A. and James, L. 2016. Proposed Approach for Evaluation of Cohesive and Adhesive Properties of Asphalt Mixtures for Determination of Moisture Sensitivity. *Transportation Research Record: Journal of the Transportation Research Board,* (2575), 61-69.

Lawrence, J. A. 2010. Self-Assembly and Chemical Patterning on Germanium (100).

Le Guern, M., Chailleux, E., Farcas, F., Dreessen, S. and Mabille, I. 2010. Physico-chemical analysis of five hard bitumens: Identification of chemical species and molecular organization before and after artificial aging. *Fuel,* 89(11), 3330-3339.

Li, D. and Neumann, A. 1990. A reformulation of the equation of state for interfacial tensions. *Journal of colloid and interface science,* 137(1), 304-307.

Li, D. and Neumann, A. 1992. Equation of state for interfacial tensions of solid-liquid systems. *Advances in Colloid and Interface Science,* 39, 299-345.

Li, X.-J. and Marasteanu, M. 2010. Using semi circular bending test to evaluate low temperature fracture resistance for asphalt concrete. *Experimental Mechanics,* 50(7), 867-876.

Little, D. N. and Bhasin, A., 2006. *Using surface energy measurements to select materials for asphalt pavement.*

Liu, F., Zhou, Z. and Wang, Y. 2019. Predict the rheological properties of aged asphalt binders using a universal kinetic model. *Construction and Building Materials,* 195, 283-291.

Liu, J., Yan, K., You, L., Ge, D. and Wang, Z. 2016. Laboratory performance of warm mix asphalt binder containing polyphosphoric acid. *Construction and Building Materials,* 106, 218-227.

Liu, Y., Apeagyei, A., Ahmad, N., Grenfell, J. and Airey, G. 2014. Examination of moisture sensitivity of aggregate–bitumen bonding strength using loose asphalt mixture and physico-chemical surface energy property tests. *International Journal of Pavement Engineering,* 15(7), 657-670.

Lu, X., Talon, Y. and Redelius, P., 406-001 Aging of Bituminous Binders–Laboratory Tests and Field Data. ed. *4th Eurasphalt Eurobitume Congress*, 2008, 1-12.

Luner, P. E. and Ohf, E. 2014. Surface free energies of cellulose ether films. *Contact Angle, Wettability and Adhesion, Volume 2,* 2, 299.

Luo, S., Tian, J., Liu, Z., Lu, Q., Zhong, K. and Yang, X. 2020. Rapid determination of styrene-butadiene-styrene (SBS) content in modified asphalt based on Fourier transform infrared (FTIR) spectrometer and linear regression analysis. *Measurement,* 151, 107204.

Mallick, R. B., Teto, M. R. and Mogawer, W. S., 2000. *Evaluation of use of manufactured waste asphalt shingles in hot mix asphalt.* Chelsea: University of Massachusettes.

Martin, J., Baumgardner, G. L. and Hanrahan, J. 2006. Polyphosphoric acid use in asphalt. *Asphalt,* 21(2).

Martin, K., Davison, R., Glover, C. and Bullin, J. 1990. Asphalt aging in Texas roads and test sections. *Transportation Research Record,* (1269).

Masad, E., Arambula, E., Ketcham, R., Abbas, A. and Martin, A. E. 2007. Nondestructive measurements of moisture transport in asphalt mixtures. *Asphalt Paving Technology-Proceedings,* 76, 919.

Masad, E. A., Zollinger, C., Bulut, R., Little, D. N. and Lytton, R. L. 2006. Characterization of HMA Moisture Damage Using Surface Energy and Fracture Properties (with Discussion). *Journal of the Association of Asphalt Paving Technologists,* 75.

McDaniel, R. S., Soleymani, H. and Shah, A. 2002. Use of reclaimed asphalt pavement (RAP) under Superpave specifications. *Washington, DC: Federal Highway Administration (FHWA/IN/JTRP-2002/6)*.

Mehrara, A. and Khodaii, A. 2013. A review of state of the art on stripping phenomenon in asphalt concrete. *Construction and Building Materials,* 38, 423-442.

Mirzababaei, P. 2016. Effect of Zycotherm on Moisture Susceptibility of Warm Mix Asphalt Mixtures Prepared with Different Aggregate Types and Gradations. *Construction and Building Materials,* 116, 403-412.

Moghadas Nejad, F., Hamedi, G. H. and Azarhoosh, A. 2012. Use of Surface Free Energy Method to Evaluate Effect of Hydrate Lime on Moisture Damage in Hot-Mix Asphalt. *Journal of Materials in Civil Engineering,* 25(8), 1119-1126.

Mohammad, L. N., Kim, M. and Challa, H., 2016. *Development of performance-based specifications for Louisiana asphalt mixtures.*

Mohammad, L. N., Negulescu, I. I., Wu, Z., Daranga, C., Daly, W. and Abadie, C. 2003. Investigation of the use of recycled polymer modified asphalt binder in asphalt concrete pavements (with discussion and closure). *Journal of the Association of Asphalt Paving Technologists*, 72.

Moraes, R., Velasquez, R. and Bahia, H. 2017. Using bond strength and surface energy to estimate moisture resistance of asphalt-aggregate systems. *Construction and Building Materials*, 130, 156-170.

Morrison, I. 1991. Does the phase rule for capillary systems really justify an equation of state for interfacial tensions? *Langmuir*, 7(8), 1833-1836.

Mothé, M. G., Leite, L. F. and Mothé, C. G. 2008. Thermal characterization of asphalt mixtures by TG/DTG, DTA and FTIR. *Journal of Thermal Analysis and Calorimetry*, 93(1), 105-109.

Mouillet, V., Lamontagne, J., Durrieu, F., Planche, J.-P. and Lapalu, L. 2008. Infrared microscopy investigation of oxidation and phase evolution in bitumen modified with polymers. *Fuel*, 87(7), 1270-1280.

Mull, M., Stuart, K. and Yehia, A. 2002. Fracture resistance characterization of chemically modified crumb rubber asphalt pavement. *Journal of Materials Science*, 37(3), 557-566.

Nazzal, M. D., Sargand, S. and Al-Rawashdeh, A. 2011. Evaluation of warm mix asphalt mixtures containing RAP using accelerated loading tests. *Journal of Testing and Evaluation*, 39(3), 305-312.

Neumann, A., Good, R., Hope, C. and Sejpal, M. 1974. An equation-of-state approach to determine surface tensions of low-energy solids from contact angles. *Journal of colloid and interface science,* 49(2), 291-304.

Nuñez, J. Y. M., Domingos, M. D. I. and Faxina, A. L. 2014. Susceptibility of low-density polyethylene and polyphosphoric acid-modified asphalt binders to rutting and fatigue cracking. *Construction and Building Materials,* 73, 509-514.

ODOT, 2009. 2009 standard specifications for highway construction. Oklahoma City, Oklahoma: Oklahoma Department of Transportation.

Orange, G., Martin, J.-V., Menapace, A., Hemsley, M. and Baumgardner, G. 2004. Rutting and Moisture Resistance of Asphalt Mixtures Containing Polymer and Polyphosphoric Acid Modified Bitumen. *Road Materials and Pavement Design,* 5(3), 323-354.

Othman, A. M. 2009. Effect of moisture-induced damage on fracture resistance of rubber-modified HMA mixtures. *Journal of Elastomers & Plastics,* 41(5), 401-414.

Owens, D. K. and Wendt, R. 1969. Estimation of the surface free energy of polymers. *Journal of applied polymer science,* 13(8), 1741-1747.

Ozer, H., Al-Qadi, I. L., Lambros, J., El-Khatib, A., Singhvi, P. and Doll, B. 2016a. Development of the fracture-based flexibility index for asphalt concrete cracking potential using modified semi-circle bending test parameters. *Construction and Building Materials,* 115, 390-401.

Ozer, H., Al-Qadi, I. L., Singhvi, P., Khan, T., Rivera-Perez, J. and El-Khatib, A. 2016b. Fracture characterization of asphalt mixtures with high recycled content

using Illinois semicircular bending test method and flexibility index. *Transportation Research Record: Journal of the Transportation Research Board,* (2575), 130-137.

Park, D.-W., Seo, W.-J., Kim, J. and Vo, H. V. 2017. Evaluation of moisture susceptibility of asphalt mixture using liquid anti-stripping agents. *Construction and Building Materials,* 144, 399-405.

Petersen, J. C. 2009. A review of the fundamentals of asphalt oxidation: chemical, physicochemical, physical property, and durability relationships. *Transportation Research Circular,* (E-C140).

Prowell, B., Hurley, G. and Crews, E. 2007. Field performance of warm-mix asphalt at national center for asphalt technology test track. *Transportation Research Record: Journal of the Transportation Research Board,* (1998), 96-102.

Qin, Q., Schabron, J. F., Boysen, R. B. and Farrar, M. J. 2014. Field aging effect on chemistry and rheology of asphalt binders and rheological predictions for field aging. *Fuel,* 121, 86-94.

Rani, S., 2019a. *Characterization of Rutting in Asphalt Pavements using Laboratory Testing.* Ph.D. Dissertation (Ph.D. Dissertation). University of Oklahoma, Norman.

Rani, S., 2019b. *Characterization of Rutting in Asphalt Pavements using Laboratory Testing.* Dissertation (Ph.D.). University of Oklahoma.

Rani, S., Ghabchi, R., Ali, S. A. and Zaman, M. 2020. Laboratory Characterization of Asphalt Binders Containing a Chemical-Based Warm Mix Asphalt Additive. *Journal of Testing and Evaluation,* 48(2).

Reinke, G. and Glidden, S. 2010. Analytical Procedures for Determining Phosphorus Content in Asphalt Binders and Impact of Aggregate on Quantitative Recovery of Phosphorus from Asphalt Binders. *Asphalt Paving Technology-Proceedings Association of Asphalt Technologists,* 79, 695.

Rudawska, A. and Jacniacka, E. 2018. Evaluating uncertainty of surface free energy measurement by the van Oss-Chaudhury-Good method. *International Journal of Adhesion and Adhesives,* 82, 139-145.

Rusanov, A. I. and Prokhorov, V. A., 1996. *Interfacial tensiometry.* Elsevier.

Saeidi, H. and Aghayan, I. 2016. Investigating the effects of aging and loading rate on low-temperature cracking resistance of core-based asphalt samples using semi-circular bending test. *Construction and Building Materials,* 126, 682-690.

Schuster, J. M., Schvezov, C. E. and Rosenberger, M. R., 2015. Influence of experimental variables on the measure of contact angle in metals using the sessile drop method. *International Congress of Science and Technology of Metallurgy and Materials, SAM - CONAMET 2013.*

Shu, X., Huang, B., Shrum, E. D. and Jia, X. 2012. Laboratory evaluation of moisture susceptibility of foamed warm mix asphalt containing high percentages of RAP. *Construction and Building Materials,* 35, 125-130.

Shu, X., Huang, B. and Vukosavljevic, D. 2008. Laboratory evaluation of fatigue characteristics of recycled asphalt mixture. *Construction and Building Materials,* 22(7), 1323-1330.

Singh, D. and Mishra, V. 2018. Different methods of selecting probe liquids to measure the surface free energy of asphalt binders. *Construction and Building Materials,* 175, 448-457.

Soleimani, A., Walsh, S. and Hesp, S. 2009. Asphalt cement loss tangent as surrogate performance indicator for control of thermal cracking. *Transportation Research Record: Journal of the Transportation Research Board,* (2126), 39-46.

Stuart, K. D., 1990. *Moisture damage in asphalt mixtures-a state-of-the-art report.*

Tan, Y. and Guo, M. 2013. Using surface free energy method to study the cohesion and adhesion of asphalt mastic. *Construction and Building Materials,* 47, 254-260.

Tarefder, R. A. and Ahmad, M. 2014. Evaluating the relationship between permeability and moisture damage of asphalt concrete pavements. *Journal of Materials in Civil Engineering,* 27(5), 04014172.

Tarefder, R. A. and Zaman, A. M. 2009. Nanoscale evaluation of moisture damage in polymer modified asphalts. *Journal of Materials in Civil Engineering,* 22(7), 714-725.

Tarrer, A. and Wagh, V., 1991. *The effect of the physical and chemical characteristics of the aggregate on bonding.* Strategic Highway Research Program, National Research Council Washington, DC ….

Tavana, H. and Neumann, A. 2007. Recent progress in the determination of solid surface tensions from contact angles. *Advances in colloid and interface science,* 132(1), 1-32.

Taylor, M. A. and Khosla, N. P., 1983. *Stripping of asphalt pavements: State of the art (discussion, closure).*

Tong, Y., Luo, R. and Lytton, R. L. 2015. Moisture and aging damage evaluation of asphalt mixtures using the repeated direct tensional test method. *International Journal of Pavement Engineering,* 16(5), 397-410.

Tunnicliff, D. G. and Root, R. E., Testing asphalt concrete for effectiveness of antistripping additives. ed. *Proceedings of the Association of Asphalt Paving Technologists,* 1983, 535-560.

Van Oss, C. J., Chaudhury, M. K. and Good, R. J. 1988. Interfacial Lifshitz-Van Der Waals and Polar Interactions in Macroscopic Systems. *Chemical Reviews,* 88(6), 927-941.

Vargas-Nordcbeck, A., Leiva-Villacorta, F., Aguiar-Moya, J. P. and Loria-Salazar, L. 2016. Evaluating moisture susceptibility of asphalt concrete mixtures through simple performance tests. *Transportation Research Record: Journal of the Transportation Research Board,* (2575), 70-78.

Vargha-Butler, E., Zubovits, T., Absolom, D., Neumann, A. and Hamza, H. 1985. Surface tension effects in the sedimentation of coal particles in various liquid mixtures. *Chemical engineering communications,* 33(5-6), 255-276.

Wasiuddin, N., Zaman, M. and O'Rear, E. 2008. Effect of Sasobit and Aspha-min on Wettability and Adhesion Between Asphalt Binders and Aggregates. *Transportation Research Record: Journal of the Transportation Research Board,* (2051), 80-89.

Wasiuddin, N. M., Fogle, C. M., Zaman, M. M. and Edgar, A. 2007a. Characterization of Thermal Degradation of Liquid Amine Anti-Strip Additives in Asphalt

Binders Due to RTFO and PAV-Aging. *Journal of Testing and Evaluation,* 35(4), 387-394.

Wasiuddin, N. M., Fogle, C. M., Zaman, M. M. and Edgar, A. 2007b. Characterization of Thermal Degradation of qa Liquid Amine Anti-Strip Additives in Asphalt qa Binders Due to RTFO and PAV-Aging. *Journal of Testing and Evaluation,* 35(4), 387-394.

Wasiuddin, N. M., Fogle, C. M., Zaman, M. M. and O'Rear, E. A. 2007c. Effect of Antistrip Additives on Surface Free Energy Characteristics of Asphalt Binders for Moisture-Induced Damage Potential. *Journal of Testing and Evaluation,* 35(1).

Wasiuddin, N. M., Zaman, M. M. and O'Rear, E. A. 2010. Polymeric Aggregate Treatment Using Styrene-Butadiene Rubber (SBR) for Moisture-Induced Damage Potential. *International Journal of Pavement Research & Technology,* 3(1).

Wei, J., Dong, F., Li, Y. and Zhang, Y. 2014. Relationship analysis between surface free energy and chemical composition of asphalt binder. *Construction and Building Materials,* 71, 116-123.

West, R., Rodezno, C., Julian, G., Prowell, B., Frank, B., Osborn, L. and Kriech, T. 2014. NCHRP Report 779: Field Performance of Warm Mix Asphalt Technologies. *Transportation Research Board of the National Academies, Washington, DC*.

Wu, S., Calculation of interfacial tension in polymer systems. ed. *Journal of Polymer Science Part C: Polymer Symposia*, 1971, 19-30.

Wu, S. 1973. Polar and nonpolar interactions in adhesion. *The Journal of Adhesion*, 5(1), 39-55.

Wu, Z., Mohammad, L. N., Wang, L. and Mull, M. A. 2005. Fracture resistance characterization of superpave mixtures using the semi-circular bending test. *Journal of ASTM International*, 2(3), 1-15.

Xiao, F., Amirkhanian, S. N. and Putman, B. J. 2010a. Evaluation of rutting resistance in warm-mix asphalts containing moist aggregate. *Transportation Research Record*, 2180(1), 75-84.

Xiao, F., Zhao, W., Gandhi, T. and Amirkhanian, S. N. 2010b. Influence of antistripping additives on moisture susceptibility of warm mix asphalt mixtures. *Journal of Materials in Civil Engineering*, 22(10), 1047-1055.

Yildirim, Y. and Kennedy, T. W., 2002. *Hamburg wheel tracking device results on plant and field cores produced mixtures.* Citeseer.

Yin, F., Arambula, E., Lytton, R., Martin, A. and Cucalon, L. 2014. Novel method for moisture susceptibility and rutting evaluation using Hamburg wheel tracking test. *Transportation Research Record: Journal of the Transportation Research Board*, (2446), 1-7.

Young, T. 1805. Analysis of Interfacial forces. *Philos. Trans. R. Soc. London*, 95, 65-69.

Yut, I., Bernier, A. and Zofka, A. 2015. Field applications of portable infrared spectroscopy to asphalt products. *Introduction to unmanned aircraft systems*, 127(5).

Żenkiewicz, M. 2006. New method of analysis of the surface free energy of polymeric materials calculated with Owens-Wendt and Neumann methods. *Polimery,* 51.

Żenkiewicz, M. 2007. Methods for the calculation of surface free energy of solids. *Journal of Achievements in Materials and Manufacturing Engineering,* 24(1), 137-145.

Zhang, D. 2020. An Equation-of-State approach to measure the surface free energy (SFE) of bituminous binders. *Measurement,* 158, 107715.

Zhang, D. and Liu, H. 2018. Proposed Approach for Determining Consistent Energy Parameters Based on the Surface Free Energy Theory. *Journal of Materials in Civil Engineering,* 30(11), 04018287.

Zhang, D. and Luo, R. 2019. Using the surface free energy (SFE) method to investigate the effects of additives on moisture susceptibility of asphalt mixtures. *International Journal of Adhesion and Adhesives,* 95, 102437.

Zhang, H., Chen, Z., Xu, G. and Shi, C. 2018. Evaluation of aging behaviors of asphalt binders through different rheological indices. *Fuel,* 221, 78-88.

Zhang, R., You, Z., Wang, H., Ye, M., Yap, Y. K. and Si, C. 2019. The impact of bio-oil as rejuvenator for aged asphalt binder. *Construction and Building Materials,* 196, 134-143.